EFFECTS OF CORROSION AND VEHICULAR IMPACT DAMAGE ON ULTIMATE CAPACITY OF STEEL BRIDGE BEAMS

By

AARON MICHAEL FINLEY

Bachelor of Science

Oklahoma State University

Stillwater, Oklahoma

2004

Submitted to the Faculty of the
Graduate College of the
Oklahoma State University
in partial fulfillment of
the requirements for
the degree of
MASTER OF SCIENCE
July, 2006

EFFECTS OF CORROSION AND VEHICULAR IMPACT

DAMAGE ON ULTIMATE CAPACITY

OF STEEL BRIDGE BEAMS

Thesis Approved:

Dr. Charles M. Bowen, Ph.D.
Thesis Adviser

Dr. Robert N. Emerson, Ph.D.

Dr. G. Steven Gipson, Ph.D.

Dr. A. Gordon Emslie, Ph.D.
Dean of the Graduate College

TABLE OF CONTENTS

LIST OF TABLES

LIST OF FIGURES

CHAPTER1: INTRODUCTION AND BACKGROUND

1.1 Introduction

According to the Federal Highway Administration, approximately one third of the nation's bridges are either structurally deficient or functionally obsolete. A factor contributing to the structural deficiency of steel bridge superstructures is damaged beams. Damage may take the form of section loss due to corrosion, or geometric distortion due to vehicular impact. These damage forms may cause reduced buckling capacity, elevated flexural stresses, and reduced ultimate moment capacity.

1.2 Background

The National Bridge Inventory 2003 report lists over 615,000 bridges. Approximately one third of these bridges are steel. Oklahoma contains over 23,000 bridges, 34% of which are made of steel (2000). Steel bridges are susceptible to damage that may result from corrosion and vehicular impact. Given the number of steel bridges throughout Oklahoma and the nation, the number of structurally deficient bridges in the nation, and the vulnerability of steel bridges to corrosion and impact damage, engineers could benefit from a greater understanding of the effects corrosion and impact damage have on the capacity of bridge members.

Corrosion is a commonly known problem with steel bridge members. Uniform corrosion may reduce the cross sectional dimensions of a girder evenly, in which case the load-carrying capacity of the girder is easily recalculated using the new dimensions of the reduced section. However, localized corrosion is also common, and may be severe enough to completely penetrate the girder web. Determination of girder capacity is more difficult with local corrosion as compared to uniform corrosion. Localized thinning of a girder and/or holes in the web will leave less area to sustain flexural and shear stresses. Also, the geometric properties (such as moment of inertia and radius of gyration) are altered, so the beam may have a greater propensity to buckle.

Although less common than corrosion damage, another issue affecting steel bridges is structural damage due to accidental impacts. This circumstance may occur when an over-height truck or equipment travels under an overpass. An example of such impact damage is shown in Figure 1.1, in which the bottom flange of a girder has been deformed by vehicular impact (2006).

Figure 1.1: Deformation of Flange Due to Impact, < http://www.steelstraightening.com/arizona.htm>

In the case of impact damage, the cross-sectional area of the girder may essentially remain unchanged, which means the ultimate moment capacity should be changed only slightly. However, the presence of a significant local deformation in the beam could adversely affect the girder's ability to resist buckling.

The Oklahoma Department of Transportation averages between 5 and 10 projects each year involving the repair of impacted bridges, while they average 10 to 20 projects a year involving the repair of corrosion damage (Allen 2004). Damaged bridge members are encountered on a regular basis. It is costly to close bridges, but if the damaged members retain enough capacity, closure may be unnecessary. The structural capacity of damaged members must be evaluated to determine if a bridge must be closed. Therefore, it would be useful to obtain a simple method for engineers to achieve a safe and acceptably accurate assessment of a damaged girder's remaining capacity. Bridge ratings may then

be adjusted or repairs conducted as necessary, so the public safety can be maintained without over-expenditure of time and money in the analysis and repair processes.

1.3 Objectives and Scope

The objectives of this research were to:

1. Determine the effects of various damage configurations on steel bridge members.
2. Possibly develop a simplified method (performed easily by hand or spreadsheet) to determine capacity of damaged members. The intent was to develop methods that would provide a quick yet accurate assessment of remaining capacity without requiring advanced computer analysis.

Damage examined includes scenarios likely caused by corrosion, such as holes of various sizes and locations in beam webs, and thinned sections of flanges. Web holes were studied to determine how they would affect flexural and shear stress distributions, as well as lateral torsional buckling capacity. Flange damage from corrosion was primarily examined to determine how lateral torsional buckling would be affected. Bearing capacity of beams with holes in webs and/or corrosion damaged flanges was not examined in this research, as it has been recently addressed in other work (Lindt and Ahlborn 2004). Lower flange and web deformation, such as might be caused be over-height vehicle impact, was also examined to determine its effect on flexural stress distribution and ultimate moment capacity.

1.4 Computer Simulation and Analysis

The analysis performed utilized ABAQUS 6.4.2, a non-linear finite element program. The research required more complex analysis (non-linear geometric and constitutive analysis, as well as elastic and inelastic buckling analysis) than other standard finite element packages (SAP, STAAD, etc.) are not capable of performing. ABAQUS also provides the user with more flexibility in modeling damaged members (such as a standard W-section with a section of web removed).

Several types of elements were examined and simple test cases were performed to determine the most appropriate type. The first elements utilized were linear, four-node constant stress tetrahedral elements, referred to by ABAQUS as C3D4 elements. These types of elements are generally acceptable for standard cases if the mesh is refined adequately. Test cases were run which modeled a W27x94 (discussed further in Chapter 3). The model was comprised of C3D4 elements approximately 2" on each side. When a point load was applied at midspan, a flexural stress distribution at quarterspan had an average error of approximately 1% throughout when compared to the theoretical distribution predicted by elementary beam theory (Timoshenko beam theory). (The flexural stress distribution was examined at quarterspan instead of midspan because the distribution may be slightly distorted immediately beneath a point load. This is a local phenomenon, and would not provide an adequate gauge of the model's overall accuracy).

However, the elastic buckling capacity predicted by finite element analysis was approximately 264% greater (192,224 lb vs. 52,750 lb) than the capacity predicted by

methods commonly used in the American Institute for Steel Construction design manual. The AISC methods are based on commonly derived elastic buckling expressions, found in Salmon and Johnson, 1996, and other texts. They calculate the critical moment, assuming a beam loaded with a uniformly distributed moment. To calculate the critical moment for other load configurations, the critical moment is multiplied by a scalar factor known as C_b. For a simply supported beam with a point load at midspan, Cb =1.32. For a uniformly distributed load, Cb=1.14. AISC methods also assume the load to be applied at the neutral axis of the beam. If the load is applied at the top flange, a destabilizing effect occurs which reduces the buckling capacity by approximately 1.4 (Galambos 1998). AISC methods are discussed further in Chapter 3. When a uniformly distributed load was applied to the top flange of the model, the buckling capacity predicted by finite element analysis was approximately 82% higher (462.1 lb/in vs. 253.1 lb/in.) than the capacity predicted by AISC methods.

Since the tetrahedral elements produced inaccurate buckling results, another element type was investigated. ABAQUS type B31 elements, which are first-order three-dimensional Timoshenko beams in space, were used for the next test model. When the W27x94 with a uniformly distributed load modeled with the beam element, the buckling capacity predicted by finite element analysis was only about 6% less (236.5 lb/in vs. 253.1 lb/in) than the capacity predicted by accepted theoretical results. Although the beam elements proved more accurate for simple buckling analyses, they were not useful for complex stress analyses because they do not allow localized modification of the beam geometry (such as the inclusion of impact damage or web holes).

The next element type tested was a four-node shell element referred to by ABAQUS as S4R. These are standard stress/displacement shell elements with reduced integration. They account for finite membrane strains and arbitrarily large rotations, and are typically suitable for large-strain analysis (2006). The W27x94 was modeled with square shell elements approximately 1.5" on each side and a point load was applied at midspan. A flexural stress distribution at quarterspan had approximately 1% average error throughout when compared to the theoretical distribution predicted by beam theory. For this same configuration, the finite element model predicted a buckling capacity about 6% less (49,769 lb vs. 52,750 lb) than the AISC results. Based on these results, shell elements were adopted for further tests because it was felt that they would yield results with acceptable accuracy. They also allowed beam models to be geometrically modified to simulate various forms of corrosion and impact damage. Figure 1.2 shows an example of a typical mesh used, which is 1" on a side. The beam shown is again a W27x94, 30' in length.

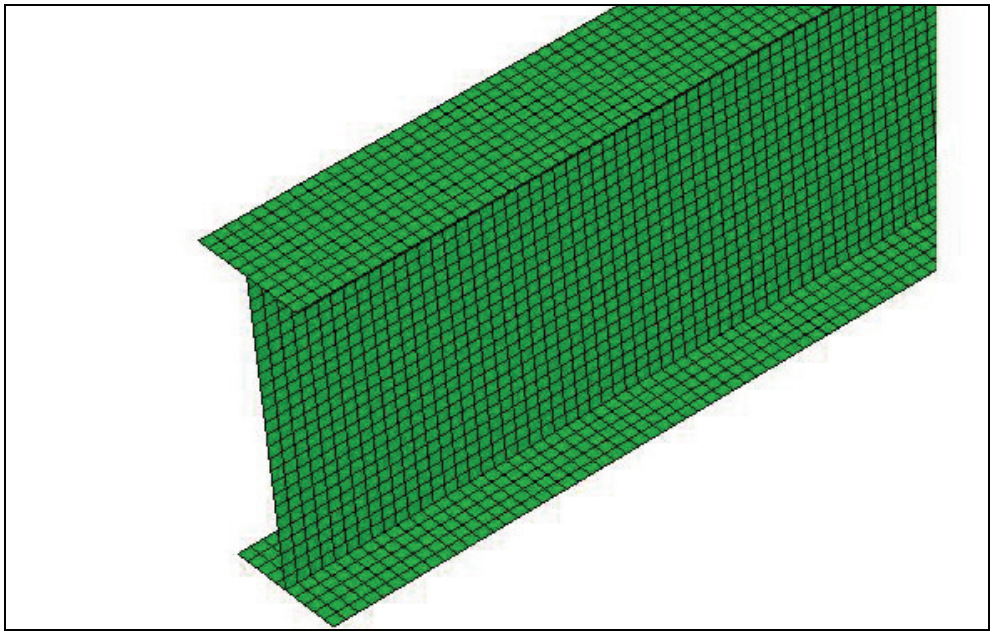

Figure 1.2: Typical 1" Shell Element Mesh

1.5 Hand Calculations

The research also examined methods which do not require advanced software. These calculations were primarily flexural stress calculations based on the Vierendeel procedure, which is more fully described in Section 3.2. The Vierendeel procedure is a means of predicting the flexural stress distributions on either side of a hole in a girder web. It can be done completely by hand, or programmed into a spreadsheet. Comparisons are made in Chapter 3 between Vierendeel and ABAQUS results to determine if simple hand procedures can accurately predict flexural stress distributions in the presence of web holes. In some cases, the Vierendeel procedure provides very good predictions for the magnitude and location of the maximum flexural stress. However, the accuracy of the method seems to be affected by specific beam geometry, making it hard to clearly state when the method should be used.

Ultimate moment capacity was also computed by hand (and in Excel spreadsheets). These calculations were performed for beams with web holes or thinned flanges. No new techniques were used; section properties were recalculated based on modified geometries. These calculations demonstrated clear trends which are more fully discussed in Chapter 5.

CHAPTER 2: LITERATURE REVIEW

The first step in this research was a review of relevant literature. Literature which provided means to simply calculate capacity of damaged members would be especially useful. These simply calculated results could then be compared to results acquired from more advanced analysis using finite elements. Although there were several papers dealing with corroded or impact damaged beams, few of them directly related with assessing the remaining flexural capacity of the beams. For example, Frangopol and Nakib's article titled "Effects of Damage and Redundancy on the Safety of Existing Bridges" (Frangopol and Nakib 1991) initially appeared to be closely related to the problem under consideration. However, the article opens with discussion of the fact that there is currently no method for quantifying structural redundancy levels in bridge systems, then an example bridge is analyzed using finite elements to demonstrate how accidental damage and corrosion damage would affect the redundancy of the structure. Unfortunately, the focus on redundancy does not translate into remaining flexural capacity, especially for individual bridge members.

Kayser and Nowak (Kayser and Nowak 1989) present analytical information on capacity loss as a result of corrosion in steel bridges. The effects of corrosion loss on bending, shearing, and bearing behaviors are all considered. For example, effects of corrosion on bending performance are demonstrated in a graph of percent remaining ultimate moment capacity vs. flange loss. However, the capacity loss is calculated based on the reduced

section properties which would result from uniform corrosion. A formula is provided for predicting the depth of corrosion penetration over time, but no other calculations or predictive formulae are provided. Conclusions focus on the fact that corrosion can lead to web buckling in bearing, and bearing stiffeners can create a more corrosion-tolerant structure. The material discussed clearly parallels the current project. However, uniform corrosion is the main focus, and localized corrosion is mentioned only briefly.

Shanafelt and Horn (Shanafelt and Horn 1984) provide a subsection titled "Strength of Damaged Member." This subsection merely states that during damage assessment "a complete evaluation of strength should be made." However, no further discussion is offered on how to best evaluate the strength of the damaged members. Informative material is also presented about when impacted members should or should not be straightened, yet this determination is not made on the basis of remaining capacity. A main point is that by measuring the curvature of a deformed member, it can be determined if the member has deformed plastically. If not, the member should not be straightened. When adjacent members which have deformed plastically are straightened, the elastically deformed member should straighten itself.

Darwin (Darwin 1990) presents information on the design of beams with web holes, such as might be necessary during construction for the placement ductwork or piping. Because the paper is written from a design standpoint, it assumes the engineer will have control over many details such as hole size and location, corner radius, and others. Though this will not be the case when analyzing beams that have web holes due to

corrosion, many of the items present are still adaptable to the current situation. For example, equations are provided for determining the ultimate moment capacity of a beam with a web hole. By using approximate dimensions so the corrosion hole is assumed rectangular, the given equations may be applicable. Also, multiple beam configurations are addressed, including bare steel members and composite beams with varying slab types.

Perhaps the most applicable piece of literature acquired was the report by Kulicki (Kulicki, Prucz et al. 1990). This was a comprehensive report dealing with topics from types and mechanisms of corrosion to how it affects many different elements of several bridge types. One portion discusses material loss and provides useful equations. A Vierendeel analysis is employed to analyze flexural stresses around a hole in a girder web. These equations allow one to compare hand calculated stresses with those generated by a finite element simulation, which proved to be especially valuable for the current project. The equations provide predictions for a wide variety of rectangular hole configurations and locations. Guidelines are given for transforming non-rectangular shapes into rectangles for analytical purposes, resulting in a very versatile predictive procedure.

Some articles reviewed were more pertinent to the finite element simulation aspect of the current project. Olsson conducted a study on steel channel columns used in industrial rack and shelving systems (Olsson, Sandberg et al. 1999). These columns are commonly subjected to impact damage (such as from fork lifts or trucks). Though the channel

sections have significantly different geometry from bridge members, the side impact damage is a similar scenario to over-height vehicle damage in bridge members. Thin-shell finite elements were used to model the channel geometry, simulate impact damage to the channels, then test the axial loading capacity. Finite element results were then confirmed with laboratory results. Although axially loaded columns are not directly relevant to the current research, this article provided an example of how finite elements could be used to handle situations such as vehicular impact damage. Based on Olsson's work, it appeared that using similar elements would allow accurate modeling of vehicular impact damage, and his laboratory verification helps confirm the validity of the procedure (especially encouraging, since the current project is not able to include laboratory testing).

Dinno and Birkemoe performed finite element analysis on plate girder web panels with patches of localized corrosion damage (Dinno and Birkemoe 1997). The panels were not entire girders, but were short sections. Dimensions varied from length being equal to depth, to length twice the depth. The work was primarily a parametric study to determine what variables cause the greatest decrease in strength (such as hole size, aspect ratio, vertical or diagonal shift from panel center). Rectangular holes were the primary focus, because results showed that rectangular holes had a greater influence on panel strength than holes of other shapes with the same area. This finding influenced the use of square and rectangular holes in the current research. Results showed that the extent of web thinning was the most sensitive parameter in strength loss. This fact was considered in the current research, when corrosion was modeled by holes in the web instead of thinned

sections. The sensitivity to thinning confirms the conservatism of using web holes. The ratio of corroded patch area to the entire panel area was also a significant parameter. General information on panel loading and model setup is provided, which makes this another good example of how finite element analysis software can be used to address the current project. Specific information on mesh size was not provided. Dinno and Birkemoe used the Ansys software and the type shell43 element, described as "a four-noded quadrilateral element that has large out-of-plane deflection and strain capabilities." This is similar to the ABAQUS S4R element used in the current research.

CHAPTER 3: LATERAL TORSIONAL BUCKLING OF CORROSION DAMAGED MEMBERS

One of the limit states analyzed during the research was elastic lateral torsional buckling. Beams with various forms of corrosion damage were analyzed for remaining lateral torsional buckling (LTB) capacity. Damage parameters included holes in the web, partial-width flange thinning for the full beam length, and full-width flange thinning for part of the beam length. Analyses initially focused on the capacity of the beam alone and later analyses included a composite slab.

3.1 Setup and Test Cases

A W27x94 was used as the standard test section. The majority of tests were run with the W27x94 because the 27" depth is representative of the most commonly used rolled shapes in Oklahoma Turnpike Authority bridges. Some tests were also run with a hypothetical plate girder section, with flange dimensions 18" x 1" and web dimensions 60" x 0.375." This section was created so results obtained with the W27x94 could be compared to a significantly different beam geometry. The plate girder section has flanges approximately twice as wide and twice as thick as the W27x94, while the girder web is almost twice as deep and about 25% thinner than the W27x94 web. For most tests, simply supported boundary conditions were applied at the bottom flange on both ends. Also, rotation was restrained for all nodes in the cross section at each end (see Figure

3.1). This set of boundary conditions is referred to in this thesis as the "standard" conditions for LTB tests. These boundary conditions were believed to closely match the boundary conditions for which theoretical lateral torsional buckling equations were derived. As shown in Table 3.1, finite element results using these boundary conditions closely matched accepted theoretical results.

Theoretical results were calculated with procedures used by Timoshenko (Timoshenko and Gere 1961). These procedures contain expressions for the critical load specific to each loading condition (point load at midspan and uniformly distributed load). The AISC Manual of Steel Construction (AISC 2001) results are from the commonly derived expression (Salmon and Johnson 1996) as well as other texts. This expression is for the critical moment, and is derived for constant moment along the beam's entire length. A scalar coefficient, C_b (AISC 2001) is introduced to modify the expression for cases of non-constant moment. The manual provides C_b values of 1.32 for a point load at midspan and 1.14 for a uniformly distributed load. Both Timoshenko and AISC Manual results are included. Although the Timoshenko procedure consistently yields slightly larger discrepancies from finite element results, it confirms the trends shown by the newer AISC methods.

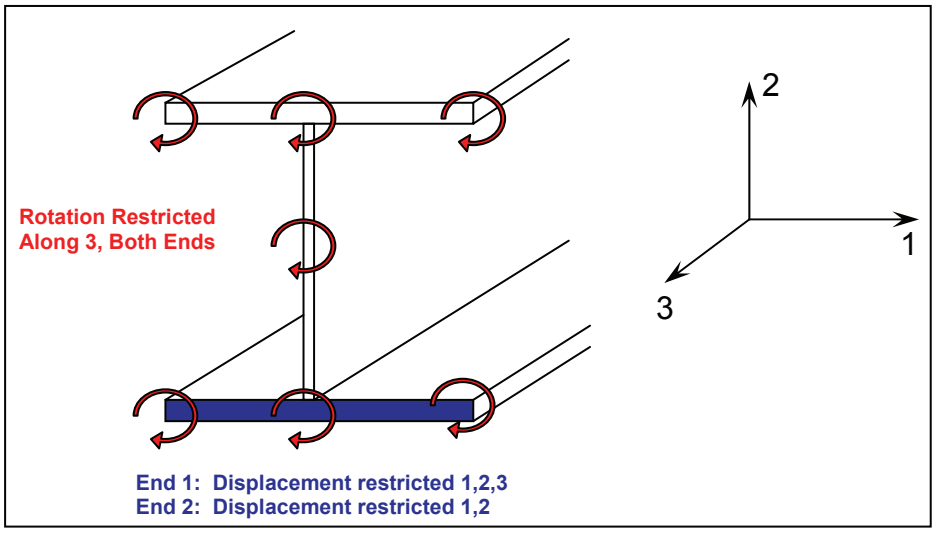

Figure 3.1: Standard Boundary Conditions

The following test cases were used to generate the critical loads (shown as q) in Table 3.1:

1) Simply supported W27x94, 30', uniformly distributed load applied at neutral axis.

2) Simply supported W27x94, 30', concentrated load at midspan, applied at neutral axis.

	Uniformly Dist. Load (Case 1)	Concentrated Load (Case 2)
q_{crit}, Finite Element	345.3 lb/in	70,306 lb
q_{crit}, Timoshenko*	357.1 lb/in	77,243 lb
q_{crit}, AISC **	354.3 lb/in	73,850 lb
% Error, Finite Element vs. Timoshenko	3.3%	9.0%
% Error, Finite Element vs. AISC	**2.5%**	**4.8%**

*(Timoshenko and Gere 1961)
**(AISC 2001)

Table 3.1: Test Cases with Standard Boundary Conditions, Load at Neutral Axis

However, beams in bridges are loaded along the top flange, not along the neutral axis. The test cases were run again with the load applied at the top flange and checked for agreement with theoretical results. Results are shown in Table 3.2.

	Uniformly Dist. Load (Case 1)	Concentrated Load (Case 2)
q_{crit}, Finite Element	245.6 lb/in	49,769 lb
q_{crit}, Timoshenko*	257.4 lb/in	51,410 lb
q_{crit}, modified AISC **	253.1 lb/in	52,750 lb
% Error, Finite Element vs. Timoshenko	4.6%	3.2%
% Error, Finite Element vs. modified AISC	**3.0%**	**5.7%**

*(Timoshenko and Gere 1961)
**(AISC 2001)

Table 3.2: Test Cases with Commonly Used Boundary Conditions, Load at Top Flange

Table 3.2 contains modified AISC results because the Timoshenko expressions include coefficients to account for top flange loading versus neutral axis loading, while the AISC expression assumes neutral axis loading. Another approach (Galambos 1998) modifies the C_b factor to compensate for loading other than the neutral axis. For top loading, Mcr is reduced by a factor of 1.4. The critical load decreases when applied at the top flange because it will produce a tipping effect that destabilizes the beam. Applying the load at the bottom flange would produce a stabilizing effect and increase the critical load by a factor of 1.4. Tables 3.1 and 3.2 show finite element results consistently within 3-5% of the theoretical results, which indicates a satisfactory model and boundary conditions have been established.

Although the standard boundary conditions mirror those used in Timoshenko's derivations, it was theorized that beams in bridges may be subject to slightly different conditions. The web may have nothing to restrain it, so it was decided to try test cases reflecting this. The modified boundary conditions applied simple supported conditions to the bottom flanges at the beam ends. Instead of restricting rotation throughout the cross section, lateral motion was restricted at the top flange/web intersection (see Figure 3.2). These boundary conditions were designed to model the lateral support provided by x-bracing (with no slab present).

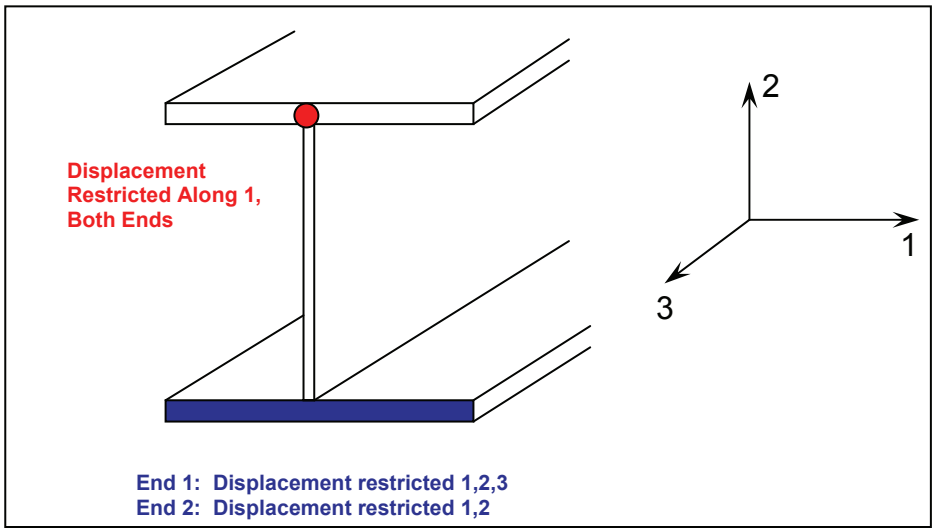

Figure 3.2: Modified Boundary Conditions

Since most tests would be run with loads at the top flange, the modified boundary conditions were checked against the test cases involving loads along the top flange. Results are shown in Table 3.3. As expected, the less restrictive boundary conditions produced slightly lower critical loads. The difference in results between the two sets of boundary conditions for both cases is less than 3%. Therefore, it was decided that the

results obtained with the standard boundary conditions would provide an acceptable model of beam behavior, even if actual beams did not have rotational constraints at the supports.

	Uniformly Dist. Load	Concentrated Load
q_{crit}, Original Bound. Cond.	245.6 lb/in	49,769 lb
q_{crit}, Modified Bound. Cond.	239.1 lb/in	48,670 lb
% Difference, Modified vs. Original	**2.5%**	**2.2%**

Table 3.2: Test Cases with Modified Boundary Conditions, Load at Top Flange

3.2 Holes in Web

The first type of beam damage analyzed was web damage due to corrosion. Corrosion damage often consists of localized thinned sections in the web. In severe cases, corrosion will completely penetrate the web. Figure 3.3 shows an example of corrosion which has fully penetrated a girder web (Kulicki, Prucz et al. 1990). It also appears that holes have been drilled to stop additional crack propagation.

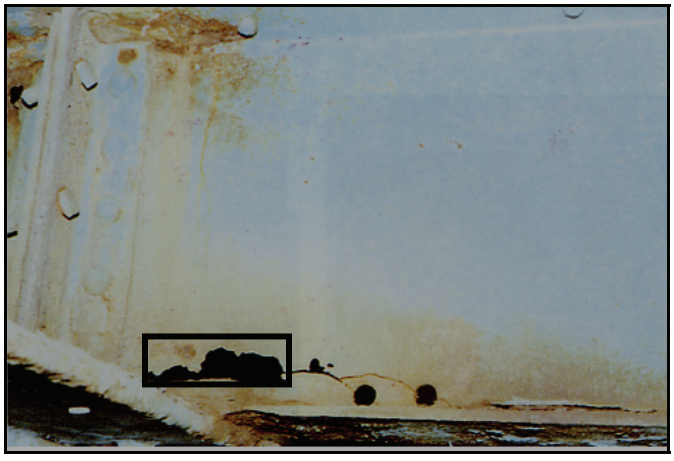

Figure 3.3: Photo of Corroded Web

All simulations conducted incorporated holes in the web instead of thinned sections, because this more severe damage case should provide conservative data which can be safely applied to thinned sections. Also, holes were modeled as square holes. The heavy rectangle drawn on Figure 3.3 demonstrates how the actual damage could be conservatively modeled by a rectangular hole. While square/rectangular holes may cause issues with stress concentrations at the corners, they are conservative in that corrosion holes will likely not have perfectly squared corners and stress concentrations will be less severe. If corners were rounded to eliminate or reduce the stress concentration issue, inspectors or engineers would have to determine whether or not holes in the field had corners which were sharper than those modeled here. Hence, it was felt square holes would conservatively approximate a worst-case scenario. Corrosion is most likely to attack a beam web at supports, where there might be a joint in the deck. It is also commonly seen just above the bottom flange, since the flange may retain moisture from precipitation and condensation. Flanges may also collect moisture during wet weather as vehicular traffic splashes water up onto bridge members. However, initial tests were conducted with holes vertically centered at midspan. This configuration provided a good starting point from which the model could easily be modified, and it was believed that placing the hole at midspan (where the moment is highest) would have the most detrimental affect on LTB capacity. Bearing-type failures such as web yielding or buckling were not analyzed, since those type failures were explored in other work (Lindt and Ahlborn 2004). The primary focus for this research was flexural failures. Two span members were not tested, because the highest flexural stresses will occur over the support. If a hole were introduced above the support, there would almost certainly be a

shear failure (see Table 3.4). Also, it is assumed that lateral bracing will be provided at a support and LTB cannot occur.

3.2.1: Hole Depth

The first series of tests utilized a W27x94, length 30', with standard boundary conditions. A concentrated load is applied at midspan, on the top flange. These tests investigate the affect on LTB capacity as hole depth increases. Several large holes were placed in the model, with depths from 12" (45% of total beam depth) to 22" (82% of total beam depth). Results are shown in Table 3.4. The plastic moment capacity (Mp) shown represents the highest theoretical moment capacity. Mp calculations were based on the modified cross-sectional geometry resulting from the presence of a hole. The losses in Mp and shear capacity are included to provide a perspective on the relative importance of LTB losses. It is possible that LTB capacity will never be the governing limit state. This is especially true for cases in which the compression flange is fully laterally restrained, such as simple span composite bridges.

Beam	Hole Length	Hole Depth	LTB Capacity	**% loss LTB Capacity**	% loss Mp	% loss Shear Capacity
W27x94, 30'	--	--	49769 lb	**--**	--	--
W27x94, 30'	12"	12"	49757 lb	**0.02%**	6.4%	44.6%
W27x94, 30'	12"	18"	49748 lb	**0.04%**	14.4%	66.9%
W27x94, 30'	12"	22"	49744 lb	**0.05%**	21.6%	81.8%
W27x94, 30'	36"	12"	49669 lb	**0.20%**	6.4%	44.6%
W27x94, 30'	36"	18"	49651 lb	**0.24%**	14.4%	66.9%
W27x94, 30'	36"	22"	49644 lb	**0.25%**	21.6%	81.8%

Table 3.3: LTB Capacity with Increasing Hole Depth

As shown in Table 3.4, as the depth of the holes increases there is a non-linear decrease in capacity. However, the last test in the series involves a hole with dimensions one-tenth the total beam length and 82% of the total beam depth, and capacity is reduced only 0.25%. A hole this large clearly presents other problems, such as the 21.6% loss in plastic moment capacity and the 82% loss in shear capacity. Therefore, it was decided that developing extensive plots of LTB capacity vs. hole depth would not be of significant value. It was also decided that if a vertically centered hole of 82% section depth did not significantly affect LTB capacity, then there was no need to investigate the effects of vertical hole location. The depth of holes in the web does not have a significant impact on LTB capacity.

3.2.2: Hole Length

The next series of tests investigated the affects of increasing hole length. Again the beam was a W27x94, length 30'. Boundary conditions were applied as shown in Figure 3.2. A concentrated load is applied at midspan, on the top flange. Results are shown in Table 3.5.

Beam	Hole Length	Hole Depth	Capacity	**% loss LTB cap.**	% loss Mp
W27x94, 30'	--	--	48670 lb	**--**	--
W27x94, 30'	12"	12"	48657 lb	**0.03%**	6.4%
W27x94, 30'	36"	12"	48569 lb	**0.21%**	6.4%
W27x94, 30'	60"	12"	48394 lb	**0.57%**	6.4%
W27x94, 30'	120"	12"	47628 lb	**2.14%**	6.4%

Table 3.4: LTB Capacity with Increasing Hole Length

As with variable hole depth, there is a non-linear decrease in capacity as hole size increases. However, the LTB capacity loss is very small. For the largest test case, the hole was 1/3 the entire member length, and 45% the entire member depth. Yet the LTB capacity was only reduced by approximately 2%. Plastic moment capacity reduction is still of greater concern than LTB capacity.

The first two series of LTB tests all utilized beams with a concentrated load at midspan. To further investigate LTB with web deterioration under a different loading configuration, two more tests were run with a uniformly distributed load. A 30' W27x94 with standard boundary conditions was used for the tests. Results are shown in Table 3.6.

Beam	Hole Length	Hole Depth	Capacity	**% loss LTB cap.**	% loss Mp
W27x94, 30'	--	--	245.62 lb/in	**--**	--
W27x94, 30'	12"	6"	245.59 lb/in	**0.01%**	1.6%
W27x94, 30'	36"	6"	245.27 lb/in	**0.14%**	1.6%

Table 3.5: LTB Capacity Under Uniformly Distributed Load

As with the concentrated loading configuration, LTB capacity is not significantly affected by the web holes. With only a 6" deep hole vertically centered in the member, the plastic moment capacity is only reduced 1.6%. Yet that is over 10 times higher than the loss in LTB capacity for the member with a 36" x 6" hole in the web.

Based on the results of several tests with varying hole dimensions, it was concluded that the presence of holes in beam webs does not significantly reduce lateral torsional buckling capacity.

3.3 Flange Thinning

Corrosion commonly affects the flanges of steel bridge members, because they retain moisture and debris. This retained moisture on the surface of the steel accelerates corrosion. It is not feasible to model every potential flange deterioration possibility, so to capture the effects of flange corrosion, tests were run with two basic configurations: thinning part of the flange width for the full beam length, and thinning the full width of the flange for part of the beam length. It was felt these two methods would provide sufficient data for analysis of numerous corroded flanges encountered in the field.

3.3.1: Full Length, Partial Width Flange Thinning

The first series of tests for flange corrosion used the standard W27x94 test section. Standard boundary conditions were applied, and a concentrated load was applied to the top flange at midspan. Tests on a 30' beam showed more significant losses than were obtained while testing web holes, so beams of 25' and 35' length were also tested to see how beam length affected sensitivity to damage. The damage was simulated by thinning the bottom flange to ½ its original thickness for varying widths along the full length of the beam. A typical view of the damaged cross section at the bottom flange is shown in Figure 3.4, and test results are given in Table 3.7.

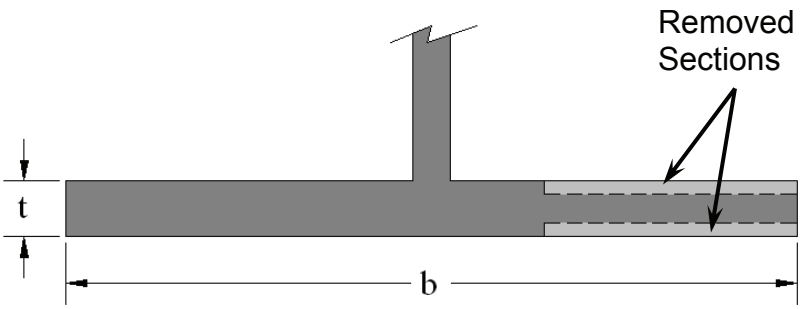

Figure 3.4: Full Length, Partial Width Flange Thinning

Beam	Damage Width	Capacity	**% loss LTB cap.**	% loss Mp
W27x94, 25’	--	76600 lb.	**--**	--
W27x94, 25’	0.125b	75777 lb.	**1.1%**	2.3%
W27x94, 25’	0.25b	74878 lb.	**2.2%**	4.6%
W27x94, 25’	0.375b	74032 lb.	**3.4%**	7.0%
W27x94, 25’	0.5b	73168 lb.	**4.5%**	9.6%
W27x94, 25’	b	69360 lb.	**9.5%**	20.4%
W27x94, 30’	--	49769 lb.	**--**	--
W27x94, 30’	0.125b	48973 lb.	**1.6%**	2.3%
W27x94, 30’	0.25b	48282 lb.	**3.0%**	4.6%
W27x94, 30’	0.375b	47611 lb.	**4.3%**	7.0%
W27x94, 30’	0.5b	46923 lb.	**5.7%**	9.6%
W27x94, 30’	b	44059 lb.	**11.5%**	20.4%
W27x94, 35’	--	34838 lb.	**--**	--
W27x94, 35’	0.125b	34327 lb.	**1.5%**	2.3%
W27x94, 35’	0.25b	33759 lb.	**3.1%**	4.6%
W27x94, 35’	0.375b	33219 lb.	**4.6%**	7.0%
W27x94, 35’	0.5b	32658 lb.	**6.3%**	9.6%
W27x94, 35’	b	30391 lb.	**12.8%**	20.4%

Table 3.6: LTB Capacity with Full Length, Partial Width Flange Thinning

These results are plotted in Figure 3.5. Since a longer beam will have a greater propensity to buckle than a shorter beam if all other variables are constant, it appears reasonable that the results show increasing sensitivity to damage with increasing beam length.

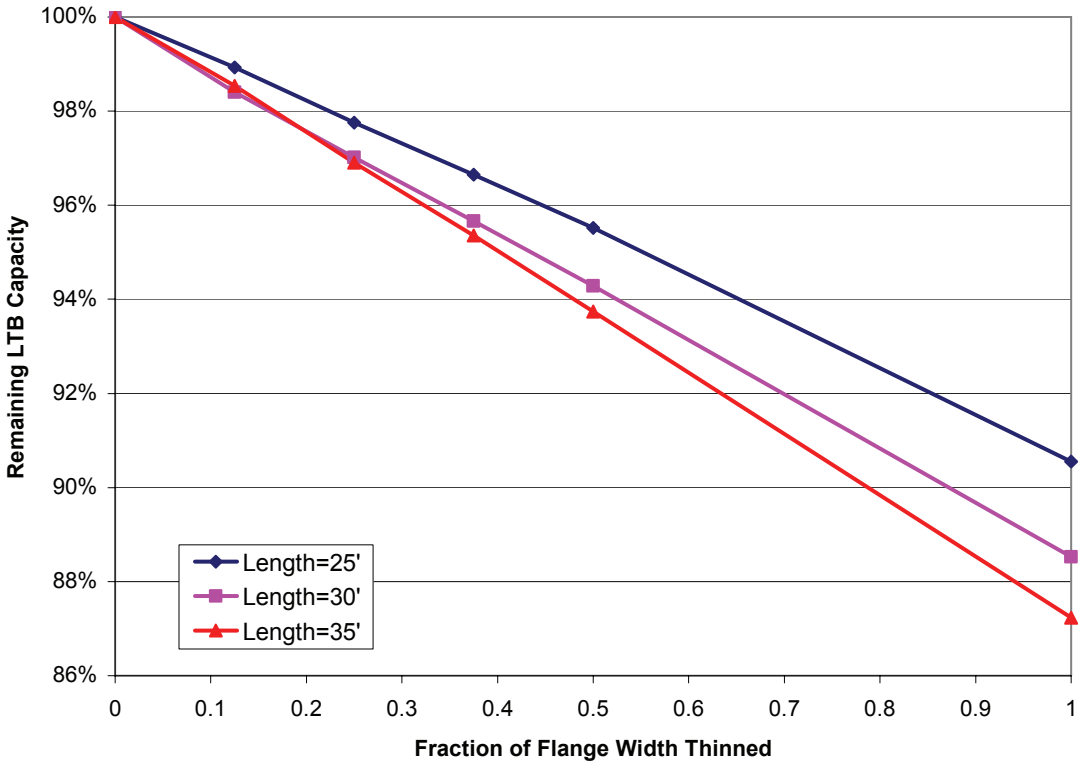

Figure 3.5: LTB Capacity for Three Beam Lengths, Full Length Partial Width Flange Damage

Flange thinning has significantly more effect on LTB capacity than holes in the web. As the damage width increases, capacity decreases linearly. However, examination of the results in Table 3.7 shows that LTB capacity may still not be the limiting criteria when the flange is thinned. Losses in plastic moment capacity are still higher than losses in LTB capacity.

3.3.2: Full Width, Partial Length Flange Thinning

The next series of flange thinning tests used a slightly different damage model. The flange was again thinned to ½ its original thickness. However, this was done for the full width of the flange for only a part of the beam length. The 30' W27x94 was used with standard boundary conditions. A 30' W18x50 with standard boundary conditions was also used, to see if a smaller beam would show more or less sensitivity to the flange damage. Beams were loaded with a concentrated load on the top flange at midspan. Results are shown in Table 3.8, and plotted in Figure 3.6.

Beam	Damage Length	Capacity	**% loss LTB cap.**	% loss Mp
W18x50, 30'	--	69.96 lb/in	**--**	--
W18x50, 30'	3'	69.73 lb/in	**0.33%**	21.9%
W18x50, 30'	7.5'	69.17 lb/in	**1.1%**	21.9%
W18x50, 30'	15'	66.79 lb/in	**4.5%**	21.9%
W18x50, 30'	22.5'	62.45 lb/in	**10.7%**	21.9%
W18x50, 30'	Full	58.32 lb/in	**16.6%**	21.9%
W27x94, 30'	--	245.62 lb/in	**--**	--
W27x94, 30'	3'	245.37 lb/in	**0.10%**	20.4%
W27x94, 30'	7.5'	244.06 lb/in	**0.64%**	20.4%
W27x94, 30'	15'	237.62 lb/in	**3.3%**	20.4%
W27x94, 30'	22.5'	226.74 lb/in	**7.7%**	20.4%
W27x94, 30'	Full	218.09 lb/in	**11.2%**	20.4%

Table 3.8: LTB Capacity with Full Width, Partial Length Flange Thinning

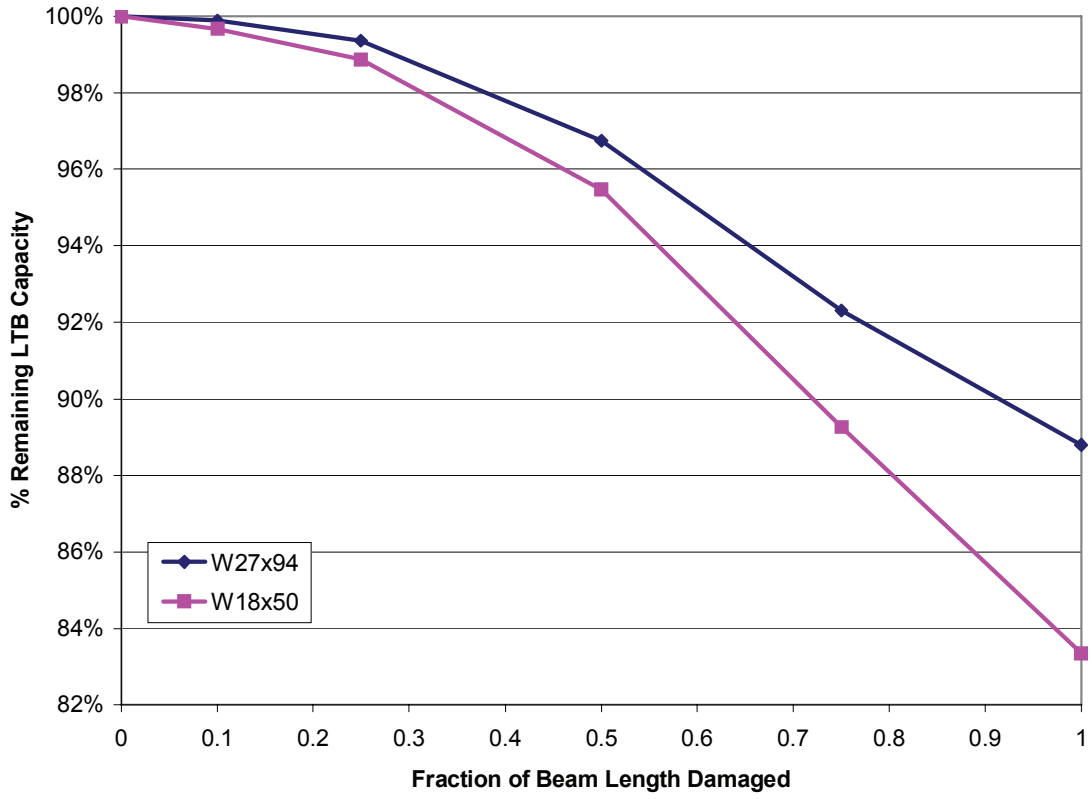

Figure 3.6: Remaining LTB Capacity vs. Length of Full-Width Damage

For full width damage, capacity decreases non-linearly with increasing damage length. The lighter beam section showed a greater sensitivity to the beam damage, both in terms of LTB capacity and plastic moment capacity. The greater sensitivity exhibited by the W18x50 is somewhat expected, because the lower flange of the W18x50 accounts for about 29% of the section's total cross sectional area. The lower flange of a W27x94 accounts for less cross sectional area, making up 27% of the total area.

3.3.3: Web Holes and Flange Damage

Two more tests were run on beams which were subject to holes in the web and flange damage. This was done to see if the presence of both damage types would compound the effects. The tests used the standard beam and boundary conditions, and a uniformly distributed load was applied at the top flange. Table 3.9 gives the results, and compares them to results for undamaged sections and sections subjected to only one damage type.

Beam	Flange Thinning	Hole Dimensions	$q_{crit.}$, lb/in	**% loss LTB cap.**	% loss Mp
W27x94, 30’	--	--	245.62	**--**	--
W27x94, 30’	--	12” x 6”	245.59	**0.01%**	1.6%
W27x94, 30’	½ orig. thickness, ½ flange width, full length	--	238.93	**2.72%**	9.6%
W27x94, 30’	½ original thickness, ½ flange width, full length	12” x 6”	238.96	**2.71%**	11.2%
W27x94, 30’	--	36” x 6”	245.27	**0.14%**	1.6%
W27x94, 30’	½ original thickness, ½ flange width, full length	--	238.93	**2.72%**	9.6%
W27x94, 30’	½ original thickness, ½ flange width, full length	36” x 6”	238.68	**2.83%**	11.2%

Table 3.9: LTB Capacity When Web Holes and Flange Thinning Both Present

The test incorporating a 12”x 6” hole and flange thinning seems to have produced a small numerical error, since it actually shows a slightly higher capacity than the beam with thinning only. However, when looking at the final results for both beams, it can be seen that the simultaneous presence of web holes and flange thinning does not compound the damage effects. Although not exact, it would be more accurate to say that the effects of the two damage types are approximately additive.

3.3.4: Two Continuous Spans: Full Length, Partial Width Flange Thinning

Although the majority of the bridges dealt with by the Oklahoma Turnpike Authority (OTA) are simple spans, some investigation was done for beams covering two continuous spans. Because web holes had such little impact on simple spans, they were not addressed for continuous spans. In addition to the standard section, a hypothetical plate girder was used for some of the tests. The plate girder had flange dimensions 18" x 1" and web dimensions 60" x 0.375." A plate girder was tested to again see how different sized sections would be affected by the same type of damage, and also to see if a thinner web would have a significant impact on the results. Both sections were subjected to a uniformly distributed load along the top flange and standard boundary conditions. Lengths given are for the total of both spans. Because the girder was roughly twice as deep as the rolled section, it was tested over a span twice as long as the rolled section. Test results are provided in Table 3.10 and are plotted in Figure 3.7.

Beam	Damage Width	Capacity	% loss LTB cap.	% loss Mp
W27x94, 60'	--	360.34 lb/in	--	--
W27x94, 60'	0.25b	347.95 lb/in	3.4%	4.6%
W27x94, 60'	0.5b	338.28 lb/in	6.1%	9.6%
W27x94, 60'	b	227.71 lb/in	36.8%	20.4%
Pl. Gird., 120'	--	253.52 lb/in	--	--
Pl. Gird., 120'	0.25b	242.53 lb/in	4.3%	5.0%
Pl. Gird., 120'	0.5b	235.96 lb/in	6.9%	10.5%
Pl. Gird., 120'	b	207.66 lb/in	18.1%	22.9%

Table 3.10: LTB Capacity for Two Continuous Spans, Full Length Partial Width Flange Thinning

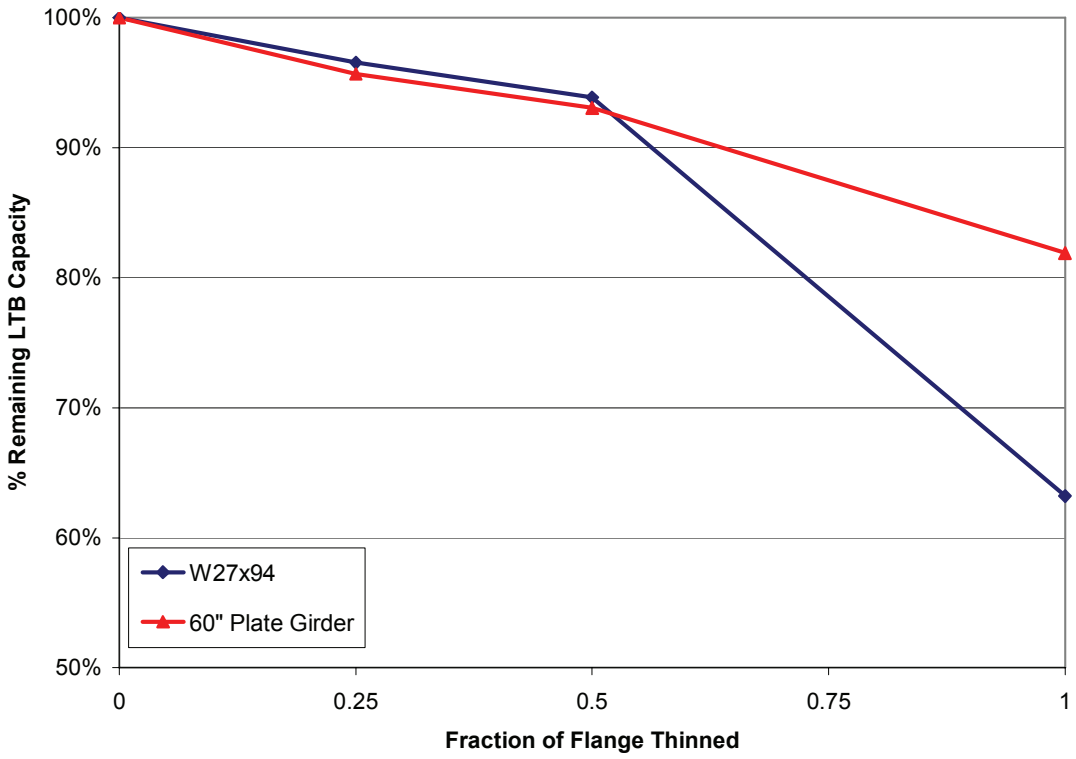

Figure 3.7: Remaining LTB Capacity vs. Width of Full Length Flange Thinning

Figure 3.7 shows that the two beams lost capacity at nearly the same rate until over half the flange width had been thinned. However, W27x94 clearly lost capacity much faster as damage exceeded half the flange width. Although plate girders were not tested at length, it is worth noting that they will likely retain their LTB capacity better than a rolled section would when subjected to flange thinning.

Web holes will have very little impact on lateral torsional buckling. Flange thinning has a more significant impact on lateral torsional buckling capacity, but neither damage type is likely to make LTB the governing limit state. Plastic moment capacity or shear capacity would likely be more critical.

CHAPTER 4: FLEXURAL STRESS DISTRIBUTION IN CORROSION-DAMAGED MEMBERS

Another major subject of investigation was flexural stress distribution in the presence of corrosion damage. Removing cross sectional area from a beam may affect the flexural stress distribution, because less material is available to resist the applied loads. Non-linear finite element analysis which assumed elastic perfectly-plastic behavior was used to model distressed members, and stress distributions were studied to determine whether corrosion damage could elevate stress to dangerous levels, perhaps causing yielding under lower loads than anticipated during the design of the member. Topics addressed in chapter 4 are summarized in Table 4.1.

Section	Analysis Set	Topic
4.1	--	Test cases, confirm finite element results match known theoretical results.
4.2	--	Demonstrate application of Vierendeel method.
4.3.1	1	Initial model, Vierendeel vs. finite element stress distributions at hole sides and center.
4.3.2	2	How does varying hole size affect the accuracy of the Vierendeel method.
4.3.3	3	Vierendeel applicability in no-shear locations (beams with multiple point loads).
4.3.4	4	Vierendeel applicability under distributed load.
4.3.5	5	How does beam geometry and h/t_w ratio affect the onset of stress shift.
4.3.6	--	In what circumstances will Vierendeel accurately predict the magnitude of the maximum flexural stress.
4.3.7	6	How does the flexural stress increase at the hole corner which is not the location of maximum stress.
4.3.8	7	How do the maximum stresses around vertically eccentric holes compare to the maximum stresses around vertically centered holes.

Table 4.1: Topics of Chapter 4

4.1 Setup and Test Cases

As with lateral torsional buckling, a W27x94 was used as the initial test section. Some tests were also run with the large plate girder section, with flange dimensions 18" x 1" and web dimensions 60" x 0.375." Simply supported boundary conditions were applied at the bottom flange on both ends. In order to verify the accuracy of the finite element model, simple test cases were run on undamaged beams and finite element results were compared to theoretical stress distributions.

4.1.1: Case 1, Concentrated Load

The first test case used a simply supported W27x94, 30', with a concentrated load applied to the top flange at midspan. Simply supported boundary conditions were applied at the bottom flange of the beam. See Figures 4.1 for boundary conditions. Flexural stress distributions over the depth of the cross section are shown in Figures 4.2 and 4.3.

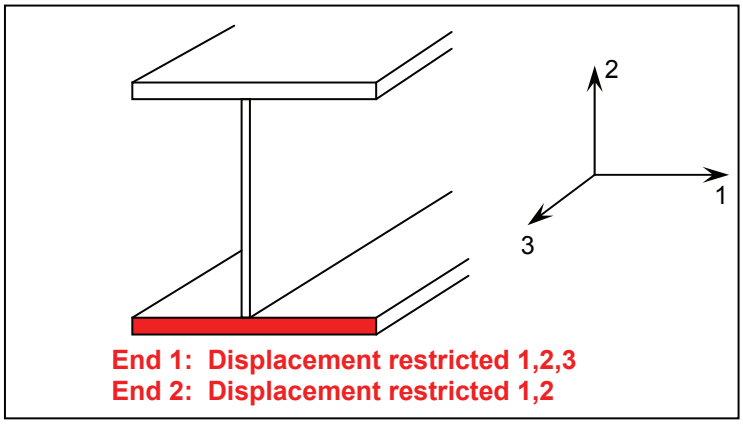

Figure 4.1: Test Case 1, Simply Supported Conditions at Bottom Flange

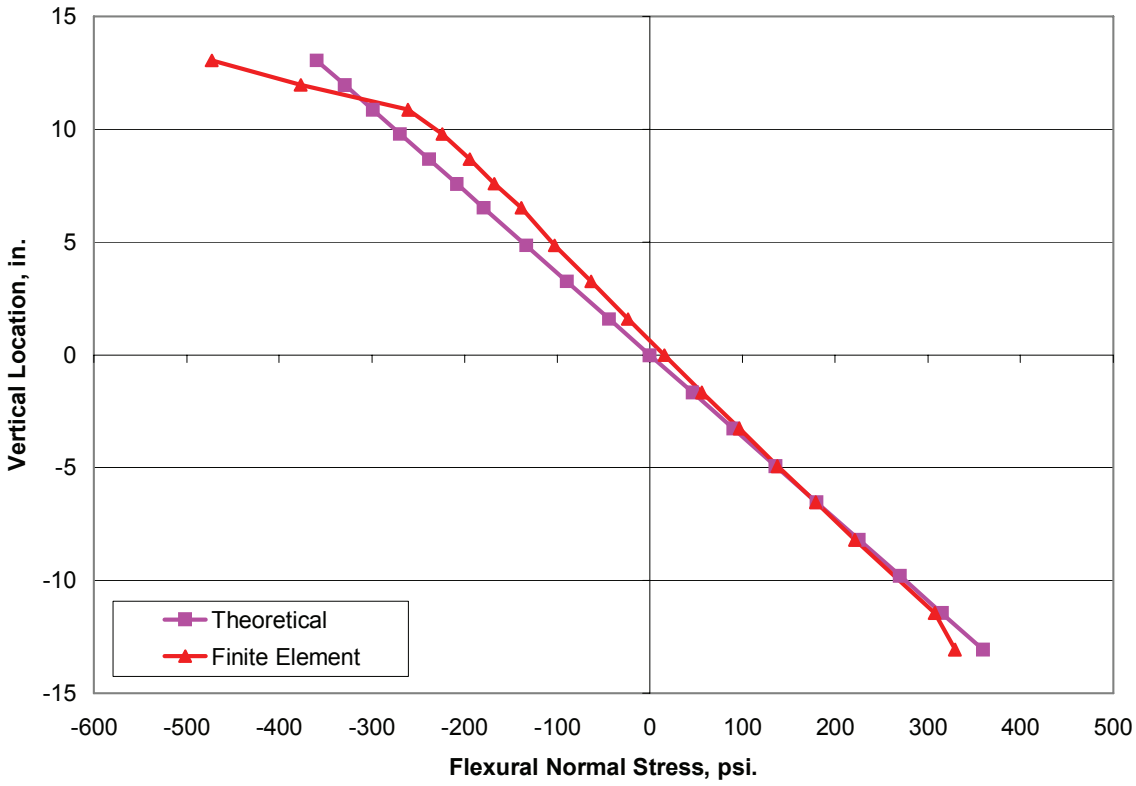

Figure 4.2: Flexural Stress Distribution, Test Case 1, Midspan

As shown in Figure 4.2, the stress distribution at midspan has a noticeable deviation from the theoretical stress distribution. The largest errors are present at the top of the beam directly beneath the point load, where finite element stresses are about 32% higher than the theoretical stresses. This may be the result of the point load in the finite element model, which places the entire load on one node, which is an infinitely small area. The increased stress could also be a result of contact stresses which are not accounted for in the theoretical model. For example, a stress element at the top of the beam subject to a vertical compressive load will try to expand horizontally as a result of Poisson's effect. The element will be unable to expand due to the flexural compression already present at the top of the beam, causing increased horizontal (flexural) compressive stress in the

element. (Much as a fully restrained steel bar would experience compressive stress if subjected to a temperature increase.) To investigate whether contact stresses were causing the errors, the stress distribution at quarterspan was also checked (see Figure 4.3 below). At quarterspan, the topmost point still has 9% error. However, almost all of the rest of the cross section has a 1% error. It was felt that the small aberration at the top flange was not significant, and that for the point loaded simply supported case, the finite element model yields satisfactory results. However, the stress distribution directly beneath a concentrated load will be affected by contact stresses and will not precisely match the theoretical stress distribution.

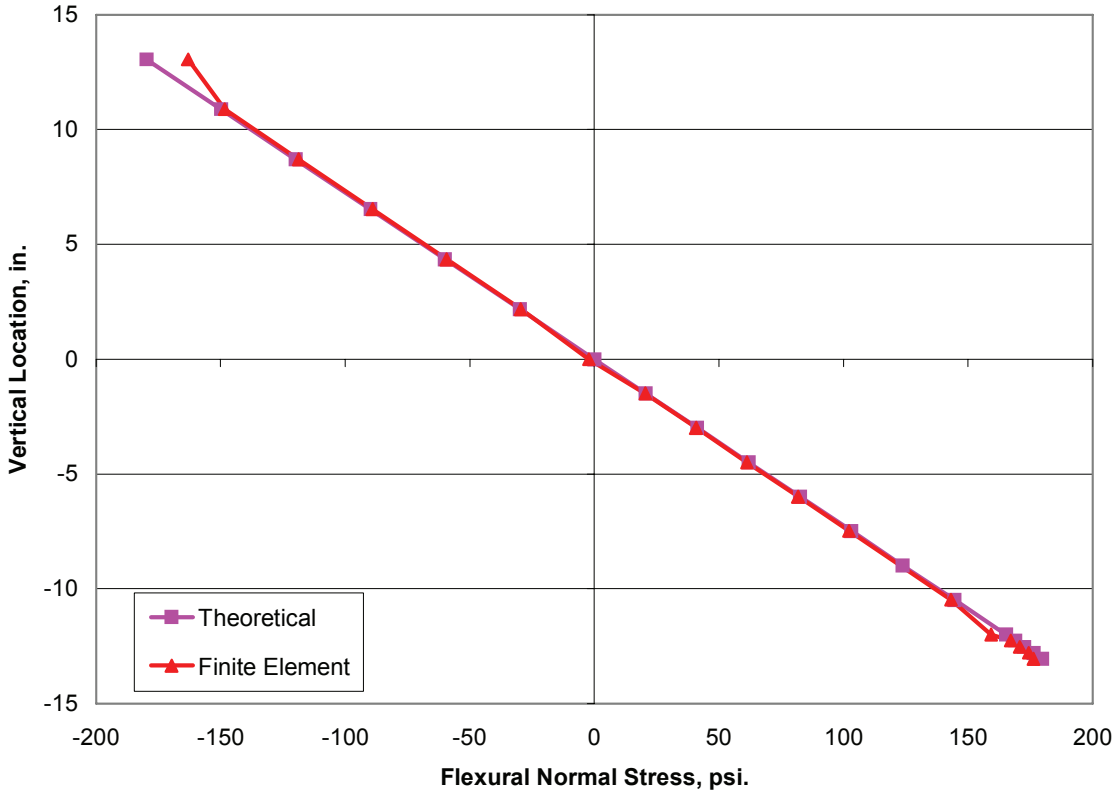

Figure 4.3: Flexural Stress Distribution, Test Case 1, Quarterspan

4.1.2: Case 2, Uniformly Distributed Load

The second test case used a W27x94, 30' long, with a 100 lb/in. uniformly distributed load applied along the top flange. Simply supported boundary conditions were applied at the bottom flange. The ABAQUS software has a "line load" loading function with units of force/length for beam elements, but it is not applicable for shell elements. In order to simulate the distributed load, a concentrated load was applied to every node along the centerline of the top flange. A 1" mesh was used, so a 100 lb. force was applied at every inch along the beam in order to approximate the 100lb/in distributed loading. Results are shown in Figure 4.4.

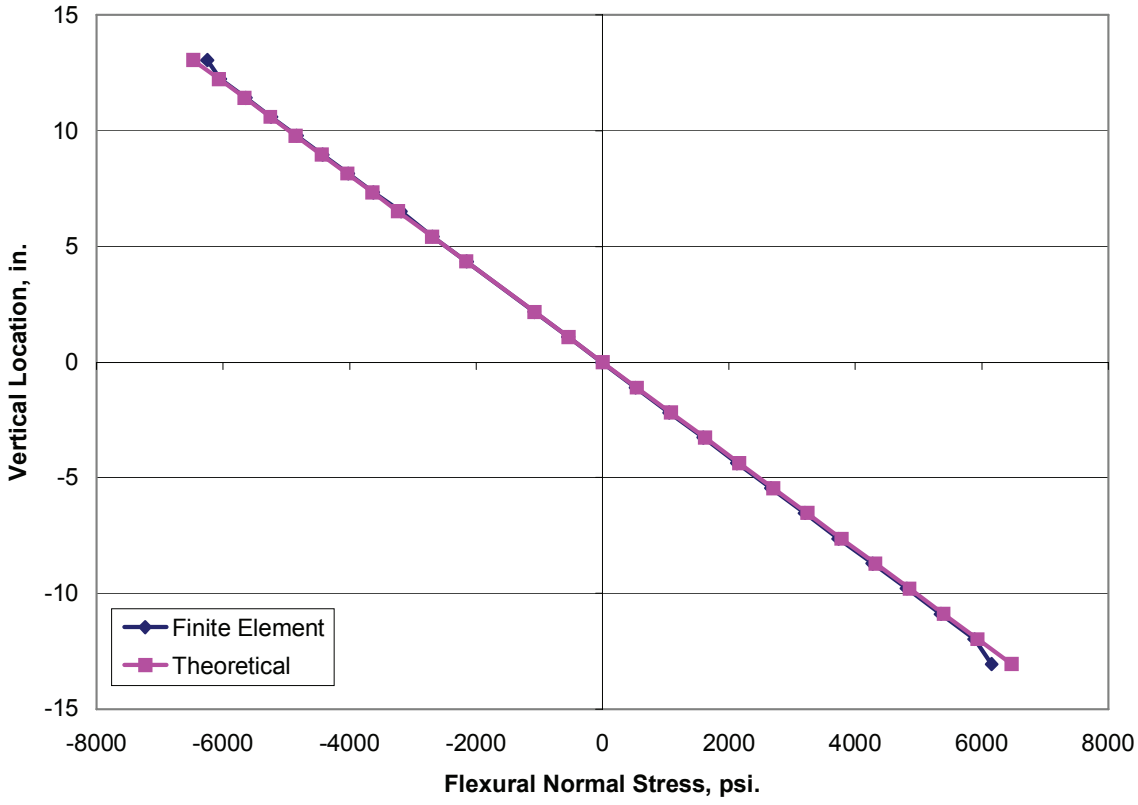

Figure 4.4: Flexural Stress Distribution, Test Case 2, Midspan

Figure 4.4 shows the flexural stress distribution at midspan. Here, the finite element results differ from theoretical by 3% and 5% at the top and bottom nodes, respectively. The average error for the rest of the nodes is less than 1%. It was felt this model yields satisfactory results for the simply supported, uniformly distributed load configuration. Applying many closely spaced concentrated loads is one way of approximating a uniformly distributed load. Test case 2 demonstrates that a reasonable degree of accuracy is obtained when the loads are spaced at 1" for this span (which is 0.28% of the span length). After observing the results of test cases 1 and 2, it was felt that the finite element results agreed with known theoretical results closely enough to validate the use of similar modeling techniques on future analyses.

4.2 Basic Vierendeel Analysis

A literature review found that an approximate hand method had been derived to predict the flexural stress distribution through the beam cross section when a hole is present. Simple "hand" calculation methods could be especially useful to engineers who might encounter damaged beams but do not have access to advanced analytical software. This method, the Vierendeel method (Bower 1966; Kulicki, Prucz et al. 1990), was investigated further. Several finite element tests were run to check the accuracy and applicability of the Vierendeel method.

The Vierendeel method is named for the Vierendeel truss. A Vierendeel truss consists of rigid upper and lower beams connected only by vertical members. These members are considered to be rigidly attached as opposed to most truss analyses which used pinned end connections. A beam with a hole in the web may be analyzed much like a Vierendeel

truss. The sections remaining above and below the hole are considered to be the upper and lower chords of the truss, while the areas at either end of the hole act as vertical truss members. Figure 4.5 shows the setup for a simple Vierendeel analysis with important parameters included.

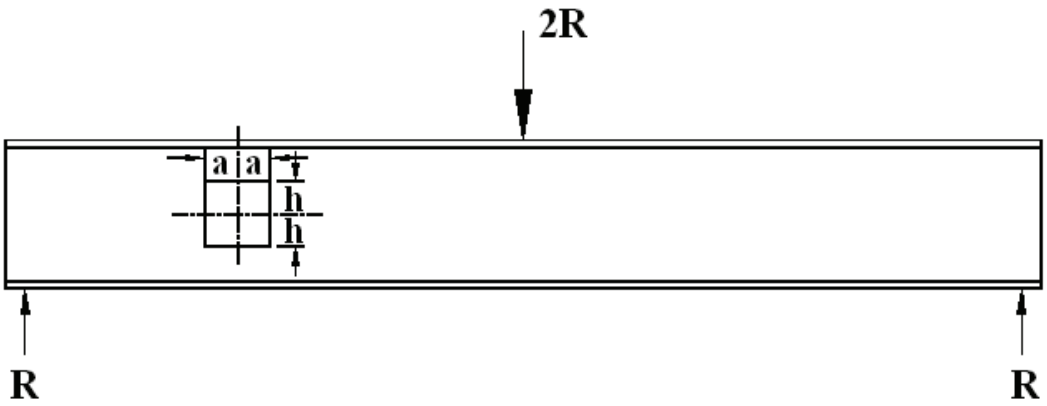

Figure 4.5: Basic Setup for Vierendeel Method (Bower, 1966)

The principal of the Vierendeel method is a simple extension of the basic flexural stress equation, $\sigma = \frac{M \cdot y}{I}$. The stress at a point above (or below) the hole is given by Equation 4.1:

$$\sigma_x = \pm \frac{V \cdot a \cdot y}{I_t} \pm \frac{M \cdot h}{I_n}$$

Equation 4.1

Equation 4.1 is composed of two terms; a component from the shear at the hole and a component from the global moment in the beam. When the a cross section of the beam at the hole edge is analyzed, a cut is taken through the center of the hole as shown in Figure

4.6. Figure 4.6 also shows the stress distributions caused by each component alone and the resulting stress distribution when the two components are added together.

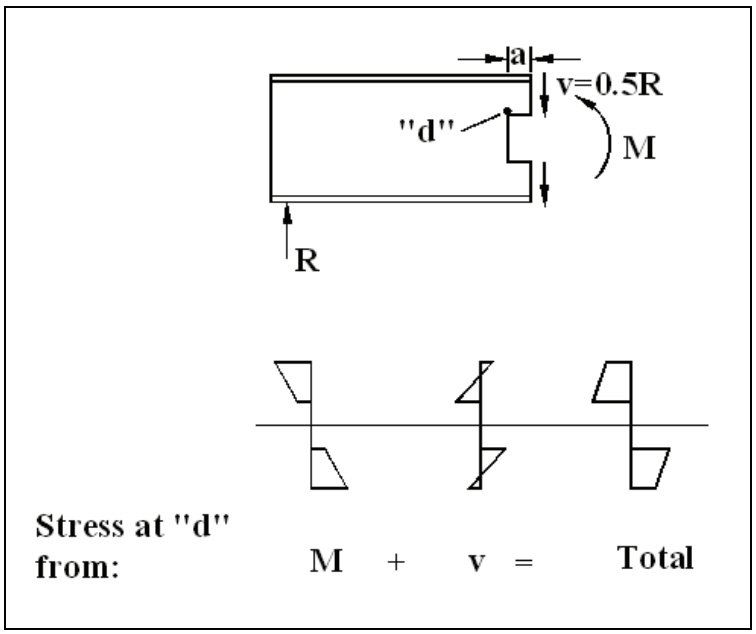

Figure 4.6: Stress Components of Vierendeel Method (Bower, 1966)

The first component of Equation 4.1 arises from the shear at the cut, but still takes the basic form of My/I. For the given beam (Figure 4.5) with a concentrated load of magnitude 2R at midspan, the end reaction is equal to R, and the shear anywhere between the end reaction and midspan is therefore R. The free body diagram in Figure 4.6 shows resulting shear on each remaining tee is 0.5R. For the point "d" shown in Figure 4.6 at the top left corner of the hole, the moment is equal to the resulting shear multiplied by the distance to point d, or V*a. The "I" value for this component is "$I_{t,}$" which is the moment of inertia of the remaining t-section above or below the hole. The "y" value is the distance from the centroid of the t-section to the point where the stress is being determined, as shown in Figure 4.7.

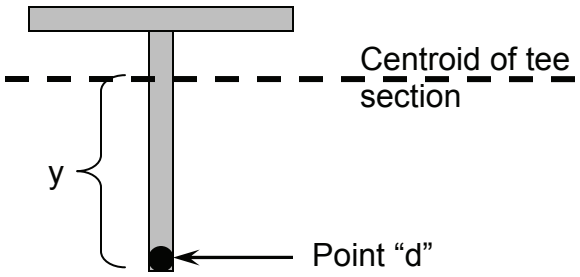

Figure 4.7: Cross Section of Top Tee Section

The second component of Equation 4.1 still takes the form of My/I, and it involves the moment on the gross beam section (for example, M=PL/4 at the center of a simply supported beam with a point load at midspan). Note that "M" is drawn in Figure 4.6 at the center of the hole for clarity, but is actually the moment *at the point where stress is being determined*. For the point d, it is the moment at the very edge of the hole. The "I" value for this component of Equation 4.1 is "$I_{n,}$" which is the moment of inertia for the net beam section (obtained from the gross cross-sectional area minus the cross-sectional area of the hole). The "y" value in this component is "h," which is the distance from the centroid of the gross cross section to the point where the stress is being determined. Therefore, the stress at point "d" shown in Figures 4.5 and 4.6 is given by $\sigma_x = -\frac{V \cdot a \cdot y}{I_t} - \frac{M \cdot h}{I_n}$. Both terms are negative because both moments (the beam moment and the shear-induced moment) cause point "d" to be in compression. Figure 4.6 shows the stress distributions resulting from each of the two components of Equation 4.1, as well as the final stress distribution resulting from their superposition (Bower, 1966). For clarification, an example calculation is provided in section 4.2.1.

Though the fundamental principles remain unchanged, the actual calculations become more complicated when the web hole is not vertically centered in the web. This is due to the fact that the shear is no longer carried proportionately (for example, if 1/3 of the remaining cross sectional area is in the top t-section, it cannot necessarily be assumed that 1/3 of the resulting shear is carried in the top section). Calculations to determine the shear distribution through the cross section are given in Kulicki, 1990.

An advantage of the Vierendeel method is that it can be performed without advanced software or a major time investment. It can be done by hand, or spreadsheets can be written to perform the calculations. Several examples of Vierendeel stress predictions were compared with finite element analysis, and these comparisons show that the Vierendeel stresses are conservative at the extreme fibers of the beam, and are often conservative next to the hole (this is not always the case, because sometimes the stress concentrations naturally present at a hole corner will outweigh the conservatism of the Vierendeel approach). A weakness of the procedure is that it cannot predict stress concentrations, which will be present at the edges and especially the corners of a hole. Examples of stress distributions generated by finite element analysis compared with those predicted by the Vierendeel analysis are given in section 4.2.1. The Vierendeel stress points were generated with an Excel spreadsheet. Note that "inside" hole edge refers to the edge of the hole nearest midspan, while "outside" refers to the edge of the hole nearest the end of the beam as illustrated in Figure 4.8.

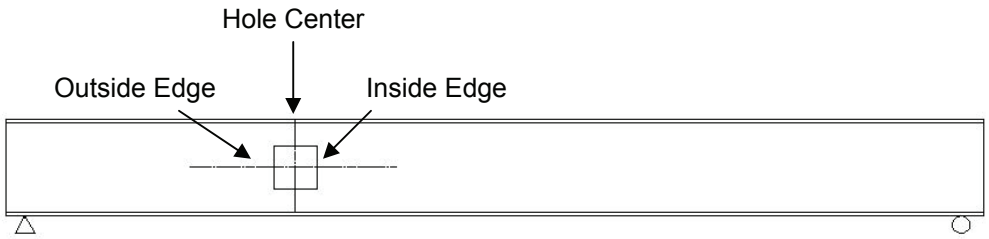

Figure 4.8: Inside Hole Edge, Outside Hole Edge, and Hole Center Notation

4.2.1: Example of finite element results vs. Vierendeel Calculations

Setup: W27x94, length = 30', with 12"x12" vertically centered hole in the web. Hole center is 7.5' from beam end. Beam is simply supported with 100 lb. point load at midspan. Results at the inside and outside hole edges are plotted in Figures 4.9 and 4.10.

The stress distributions from this model show that the Vierendeel analysis does predict a similar stress distribution to that generated by finite element analysis. There is some discrepancy between Vierendeel and finite element results, and in places the percentage error is significant. However, the Vierendeel analysis gives conservative results at the locations of highest stress. The stress distribution through the center of the hole is not shown. At the center of the hole, the Vierendeel stress was not conservative next to the hole. Yet it was conservative at the extreme fibers of the beam, where the stress was higher (the critical location). The stress that would be predicted by elementary beam theory if no hole were present, $\sigma = \frac{My}{I}$, is also plotted. Note that it provides a very poor match to the stress distribution obtained from finite element analysis; the location of the maximum stress is incorrect and the value is inaccurate.

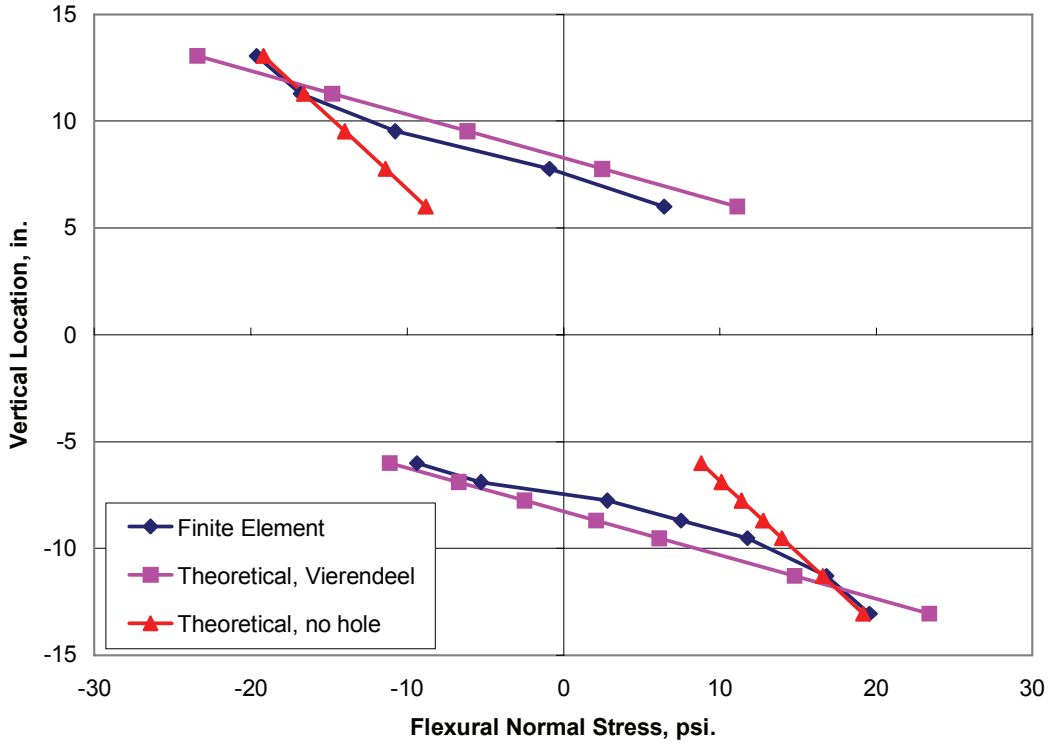

Figure 4.9: Example Flexural Stress Distribution, Inside Hole Edge

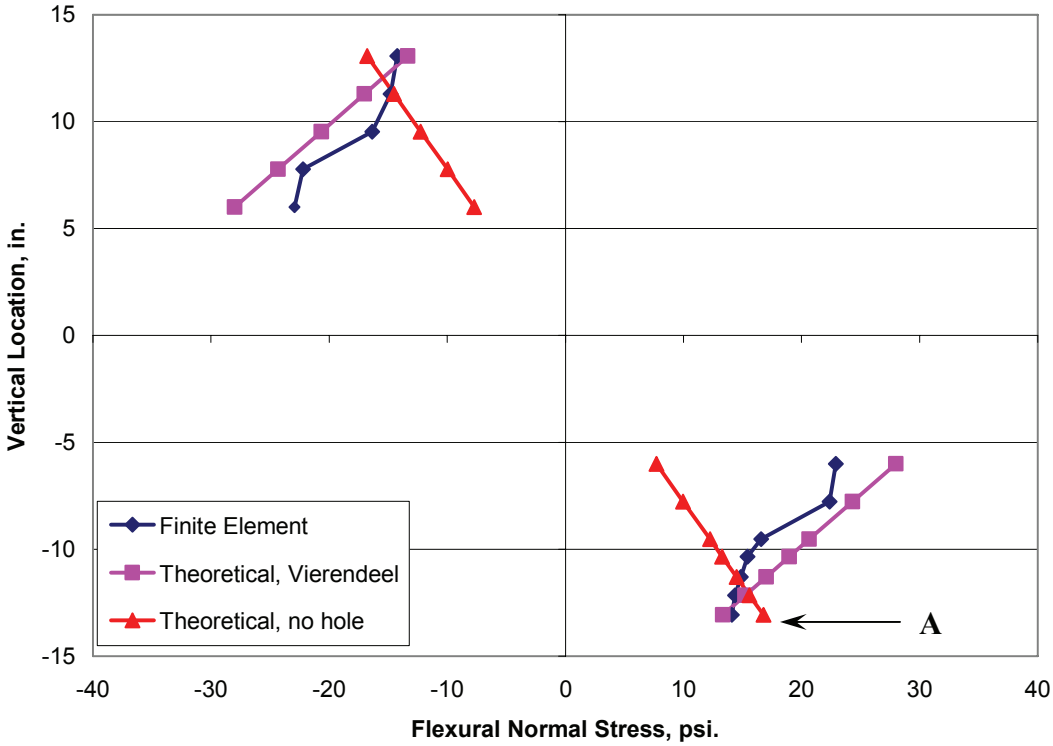

Figure 4.10: Example Flexural Stress Distribution, Outside Hole Edge

The following calculations demonstrate how the Vierendeel stress at point "A," indicated in Figure 4.10, was obtained. It may be helpful to refer to Figures 4.5 and 4.6.

4.2.2: Example Vierendeel Stress Calculations

Section: W27x94, 12"x12" hole, centered vertically 7.5' from end of beam (u = 7.5')

Load: Point load at midspan = 100 lb.

Because of the location of Point A, the flexural normal stress will be given by the expression:

$$\sigma_x = -\frac{V \cdot a \cdot y}{I_t} + \frac{M \cdot h}{I_n}$$

Now fill in the pieces of the equation:

I_g = 3270 in.^{4} (from AISC manual)

y_b = centroid of bottom t-section = 1.513 in. up from bottom surface

I_t = I for bottom t-section, = 44.28 in.^{4}

I_n = 3199.4 in.^{4} (= I_g-1/12(.49)(12)^3; .49 and 12 are the cross-sectional dimensions of a 12" hole in the web of a W27x94)

V= 25 lb. (from statics as shown in Figure 3.7)

a= 6"

y = distance between y_b and A. Point A vertically located 13.06" down from beam centerline, = 26.9/2 -13.06 = 0.39 in. up from bottom surface. The distance of 13.06" is a result of the mesh generated in ABAQUS; 26.9" is the actual depth of a W27x94.

=1.513-.39 = 1.123 in.

M = 50lb(7')(12"/1')= 4200 lb-in.

h = 13.06 in.

$$\sigma_x = -\frac{(25)(6)(1.123)}{44.28} + \frac{(4200)(13.06)}{3199.4} = -3.804 + 17.144 = \mathbf{13.34psi}$$

At the bottom extreme fiber at the outside hole edge (corresponding to point A in Figure 4.10), finite element methods yield a stress of 14.09 psi. The Vierendeel method predicts a flexural stress of 13.34 psi., which is about 5% less than the finite element result.

4.3 Simple Spans with Holes in Webs

4.3.1: Set 1—12"x 12" Vertically Centered Hole at Quarterspan, Concentrated Load at Midspan

The first stress analyses performed on damaged beams were done for simple spans with holes in the web. The first model used was the one presented in section 4.2.1., which involved a 12" x 12" hole placed in the web of a 30' W27x94 (results from this model are dealt with more fully here than in section 4.2). The hole depth was limited to 12" because reference material suggested that the Vierendeel method was most applicable to holes not exceeding half the web depth (Bower 1966). The hole center was located at the neutral axis, at quarterspan. A concentrated load of 100 lbs. was applied at midspan. Plots of stress distributions at the inside hole edge, hole center, and outside hole edge are shown in Figures 4.11, 4.12, and 4.13. The "Theoretical, no hole" plot is included to illustrate the distribution predicted by $\sigma = \frac{My}{I}$ if no hole is present. Throughout this

work, a “no hole” distribution was calculated using the moment of inertia of the gross section (as if no hole were present, hence the name). This was done as a means of comparing the finite element and Vierendeel methods, which attempt to compensate for the presence of a hole, with beam theory that does not attempt to compensate for the hole.

At the inside edge, the stress distribution predicted by the Vierendeel method matches the distribution well (see Figure 4.11). The Vierendeel stresses are conservative at all the maximum stress points.

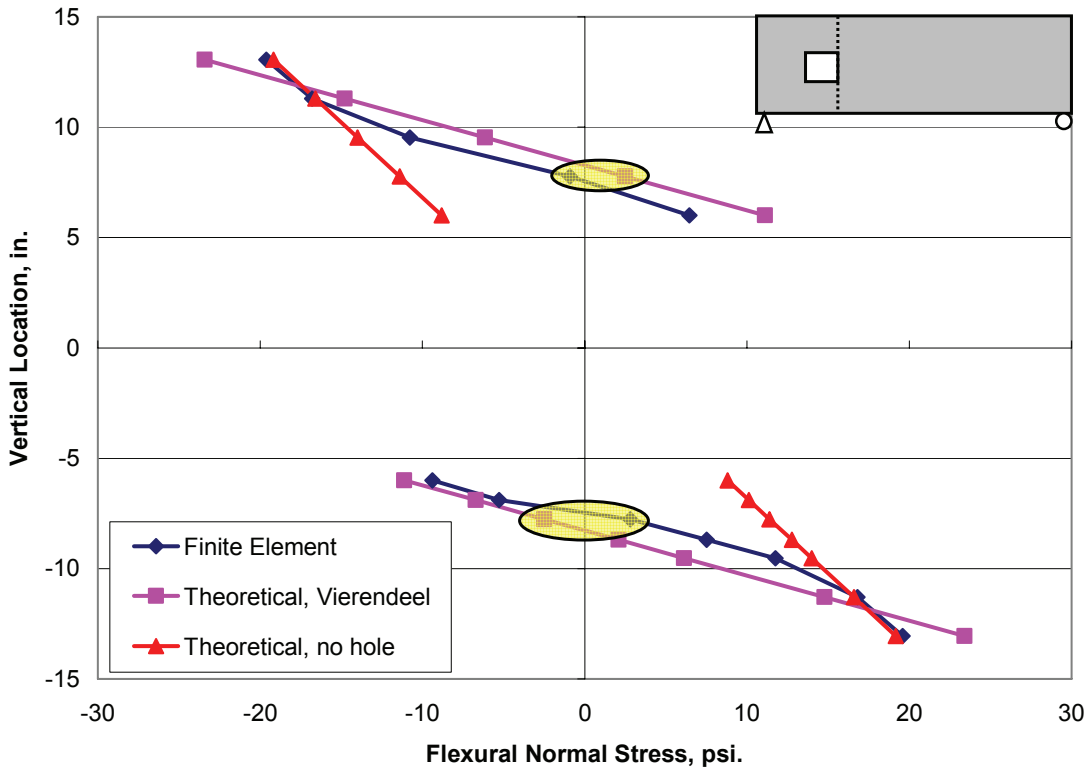

Figure 4.11: Flexural Stress Distribution at Inside Hole Edge

The average error is high at -50%, but the average error is somewhat misleading. At two points in the distribution, the Vierendeel and finite element stresses have opposite signs

(these locations are indicated by highlighted ellipses on Figure 4.11). These stress points caused very high errors which inflated the average error; if these two points are excluded the average error throughout the distribution is -3%. These locations also happen to be at the points where the magnitude of the stress is smallest. Therefore a high percentage difference between finite element and Vierendeel stresses reflects a small difference in the actual stress values (for example, at the vertical location +6 inches the finite element stress is -0.90 psi and the finite element stress is 2.48 psi, a difference of 3.38 psi).

At a cross section of the beam through the hole center (refer to Figure 4.8), the Vierendeel method again provides a close match with the finite element results (see Figure 4.12).

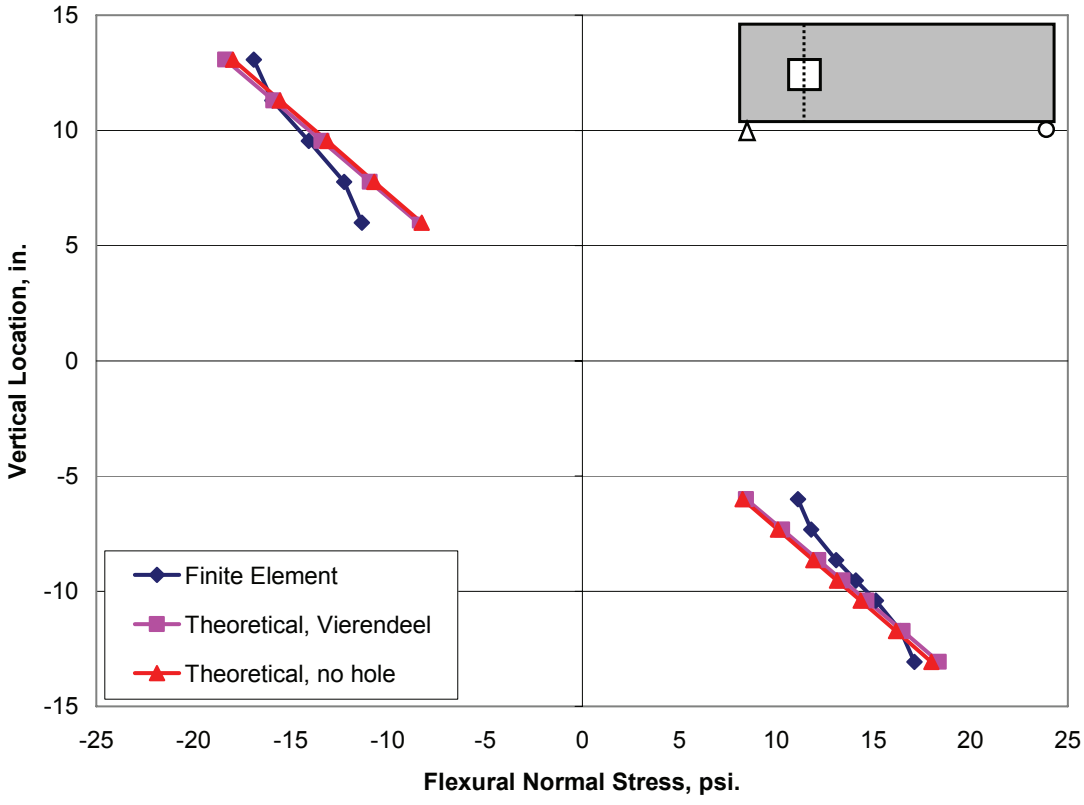

Figure 4.12: Flexural Stress Distribution at Hole Center

It should be noted that the Vierendeel stress distribution is nearly the same as the "no hole" distribution. Since the Vierendeel stress is derived from a cut taken at the center of the hole, the "a" term (the moment arm over which the shear force "V" acts) goes to zero. This eliminates the first term from the stress equation: $\sigma_x = \pm\frac{V \cdot \cancel{a} \cdot y}{I_t} \pm \frac{M \cdot h}{I_n}$. For a vertically centered hole, "h" is the same as "y" in the traditional flexural stress equation. The only difference is in the moments of inertia; since the net moment of inertia is slightly smaller than the gross moment of inertia the Vierendeel method will predict slightly higher stresses than if the hole had been ignored.

At the outside edge of the hole, the results are somewhat similar to those at the inside edge (see Figure 4.13). Although the shapes of the finite element and Vierendeel distributions are somewhat different, inspection of Figure 4.13 shows the Vierendeel method provides a better match with finite element results than would be obtained by ignoring the hole. The Vierendeel stress is conservative at the points of highest stress, which are next to the hole and not at the extreme fiber of the beam. At these locations, the Vierendeel stress is about 22% higher than the finite element stress, while the "no hole" theoretical stress is about 66% less than the finite element stress.

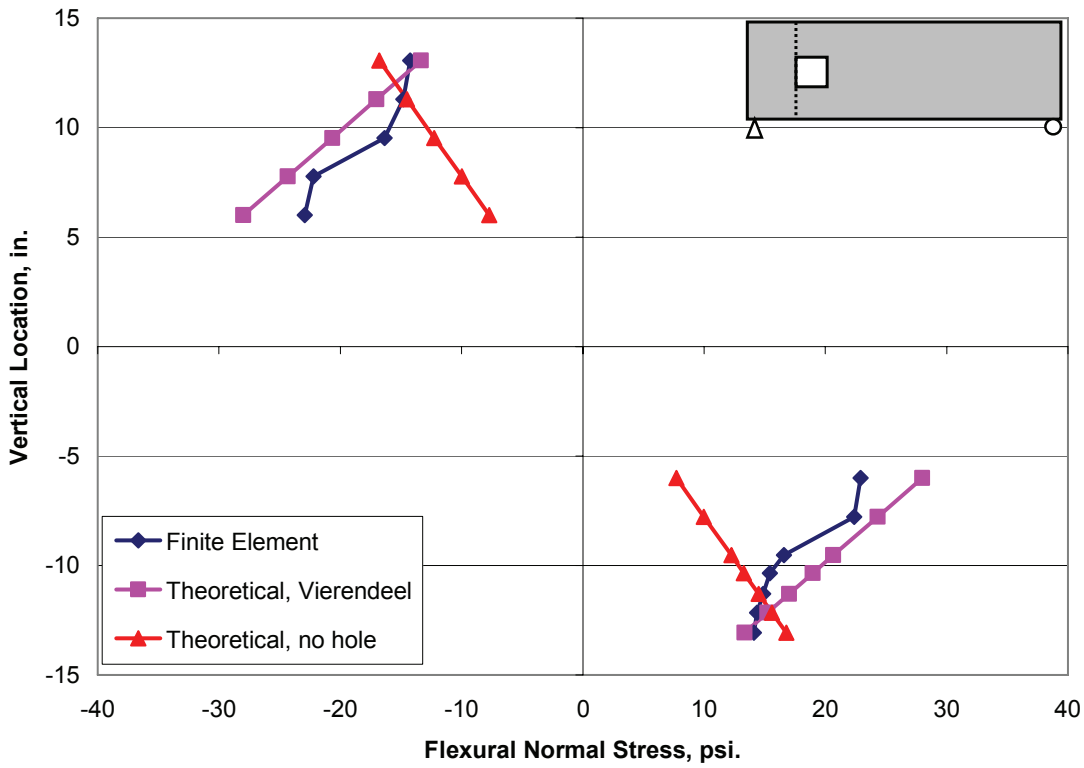

Figure 4.13: Flexural Stress Distribution at Outside Hole Edge

It should be noted that the previous analysis was run entirely within the elastic range, so the relatively small load used did not adversely affect results. Stresses will simply scale up in proportion to the load as long as no observed stresses are outside the elastic range (above 50 ksi).

Analysis set 1 indicated that the Vierendeel method had the potential to offer more accurate flexural stress distributions around web holes than beam theory could provide.

4.3.2: Set 2—Preliminary Investigation of Vierendeel Applicability vs. Hole Size, Holes at Quarterspan, Concentrated Load at Midspan

Analyses in Set 1 indicated that the Vierendeel method can provide accurate predictions of flexural stress distributions. Reference material indicated that the Vierendeel method was best used on holes which were less than half the member depth. Set 2 involved a series of models with varying hole sizes. The deep plate girder described in section 3.1 (flanges 18" x 1", web 60" x 0.375") was used, because the deeper web allowed a wide variety of hole depths to be modeled. Total member length was increased to 60', and the applied load was a concentrated load of 125,000 lb. applied on the top flange at midspan. The load and length were increased to subject the larger member to a greater moment. Holes were vertically centered at quarterspan, and were sized 10" x 10", 20" x 20", 30" x 30", and 40" x 40". The stress distributions at the inside hole edge, hole center, and outside hole edge are shown for all cases.

10" x 10" Hole

The first model used in Set 2 involved a 10" x 10" hole at quarterspan. The flexural stress distribution at the inside hole edge is shown in Figure 4.14.

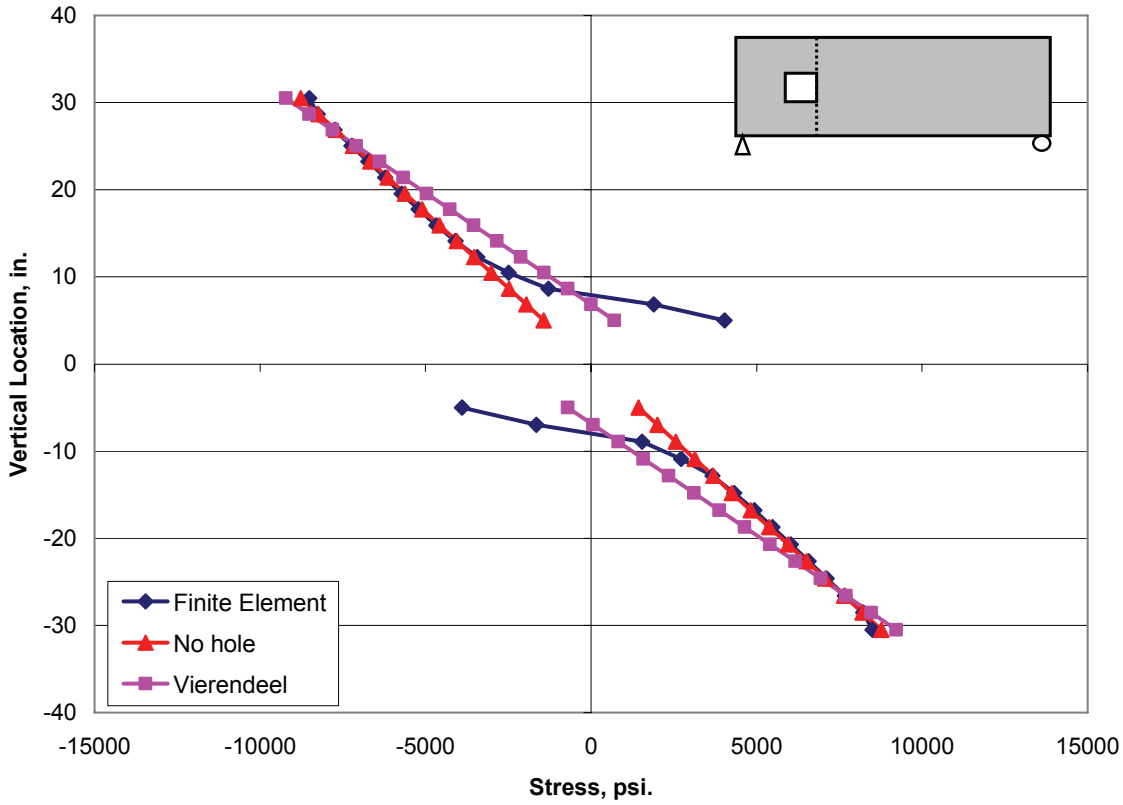

Figure 4.14: Flexural Stress Distribution at Inside Hole Edge, 10" x 10"

Through most of the member cross section except very near the hole, stresses predicted by elementary beam theory ignoring the hole provide a close match with finite element results. At the top and bottom edges of the hole, the stress shows a steep increase. This increase can be attributed to stress concentrations at the edge of the hole, which are not accounted for by the Vierendeel method or the elementary beam theory. Although the Vierendeel stresses at the top and bottom edges are closer to the finite element stress, the plot shows that the "no hole" distribution has a better overall match with finite element results. At the location of maximum stress, the beam theory stress differs from the finite element stress by 3.1%, while the Vierendeel stress differs from the finite element stress by 8.6%.

At the center of the hole, the finite element, Vierendeel, and "no hole" distributions are all nearly the same (see Figure 4.15).

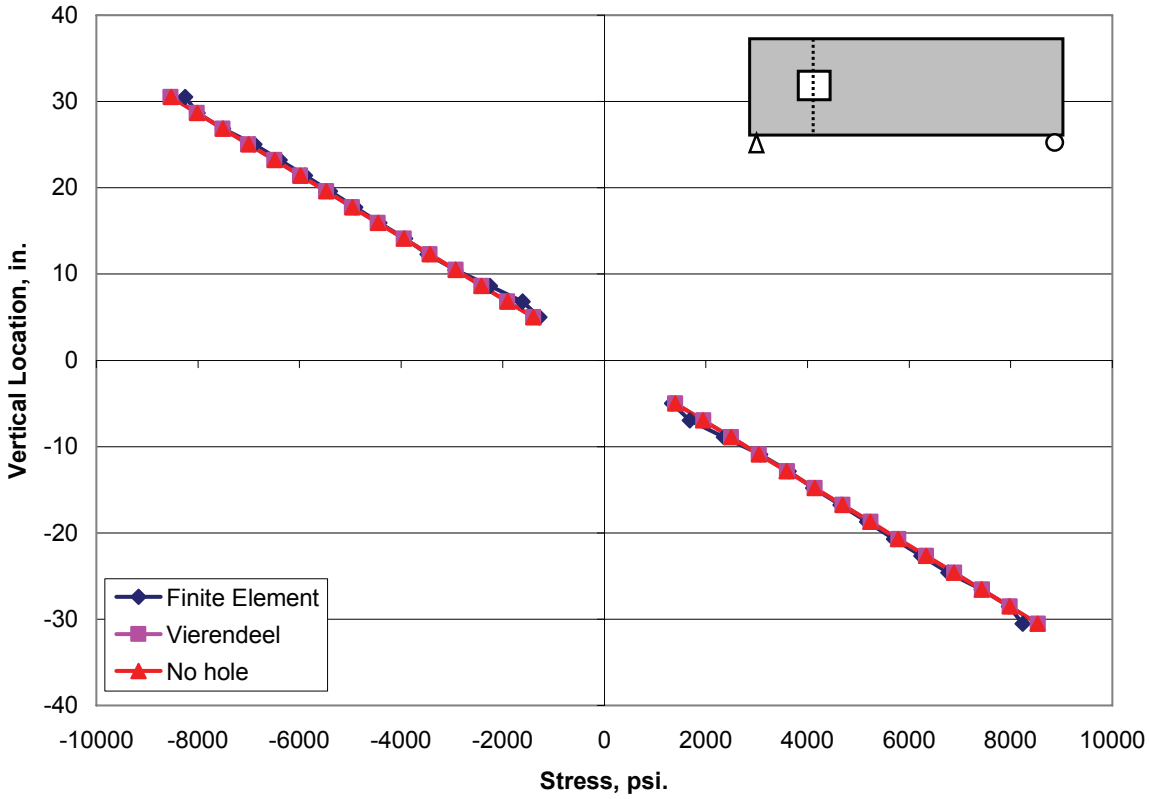

Figure 4.15: Flexural Stress Distribution at Hole Center, 10" x 10"

At the outside hole edge, the "no hole" distribution again matches finite element results for most of the cross section (see Figure 4.16).

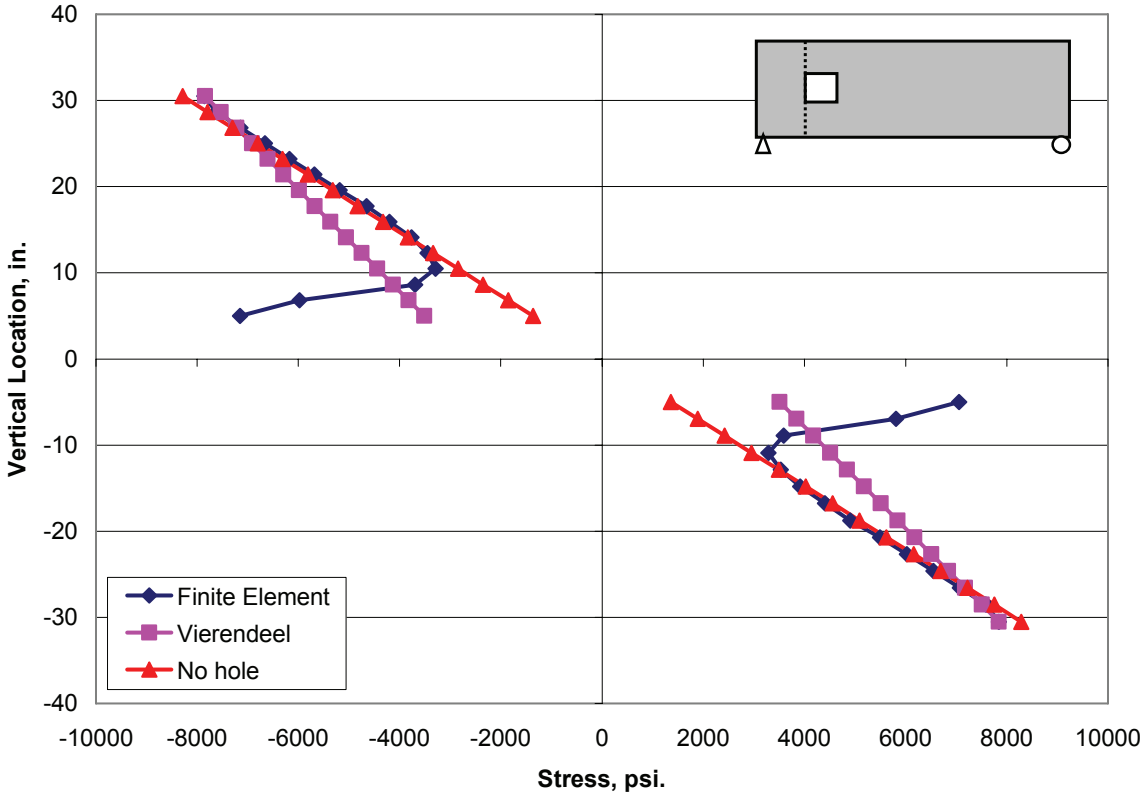

Figure 4.16: Flexural Stress Distribution at Outside Hole Edge, 10" x 10"

However, the deviations near the top and bottom of the hole due to stress concentrations are more emphasized. For the 10" x 10" hole (16% total member depth), the flexural stress distribution and the maximum flexural stress value are best predicted by the elementary beam method, $\sigma = My/I$, with the exception of stress concentrations occurring near the top and bottom hole edges. If a guideline with round numbers were to be used, it appears that for holes sized less than or equal to 15% of the total member depth, the flexural stress distribution is best calculated by ignoring the hole. (This will provide the best general distribution, but it would still be prudent to note the effects of stress concentrations around the hole.)

20” x 20” Hole

The next model used for Set 2 was identical to the first, but the hole size was increased to 20” x 20”. The flexural stress distribution at the inside hole edge is shown in Figure 4.17.

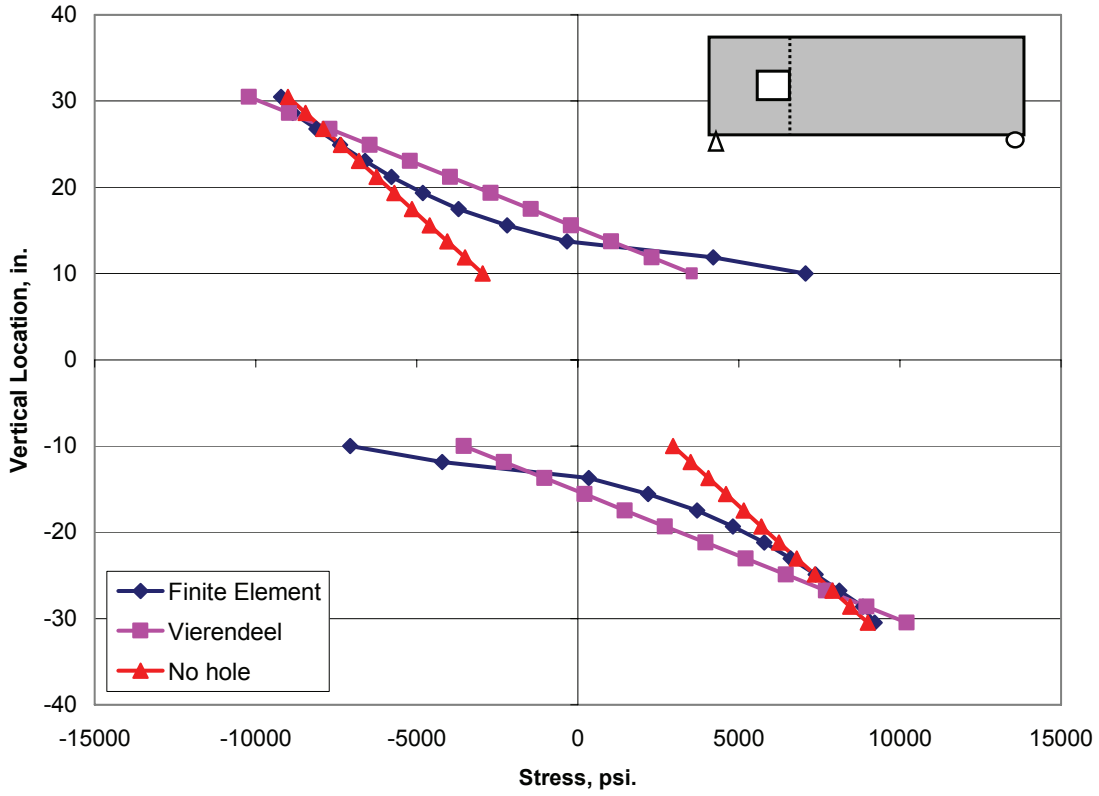

Figure 4.17: Flexural Stress Distribution at Inside Hole Edge, 20” x 20”

As demonstrated in Figure 4.17, increasing the hole size to 20” x 20” (32% total member depth) causes the results to deviate further from the “no hole” stress distribution, and the Vierendeel distribution showed a better correlation. At this point, neither method produces a very accurate prediction of the finite element results, but inspection of the plot shows the Vierendeel distribution matches slightly better than “no hole.” Although stress concentrations at the top and bottom of the hole cause higher stresses than the Vierendeel

method predicts, the Vierendeel method is still conservative at the top and bottom fiber of the beam, which is where the maximum stresses occur.

Figure 4.18 shows that for the 20" x 20" hole model, the stress distributions at the center of the hole all match quite well.

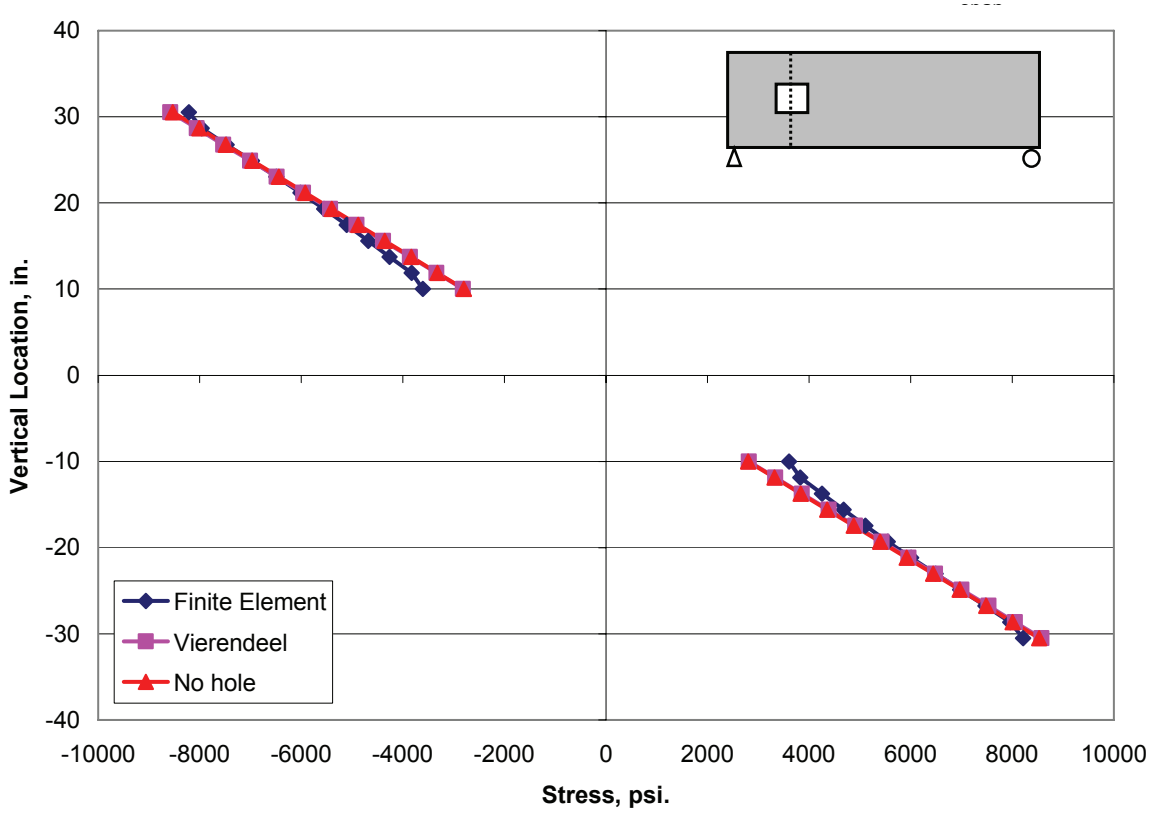

Figure 4.18: Flexural Stress Distribution at Hole Center, 20" x 20"

At the outside hole edge (see Figure 4.19), there is a wide variation in the distributions.

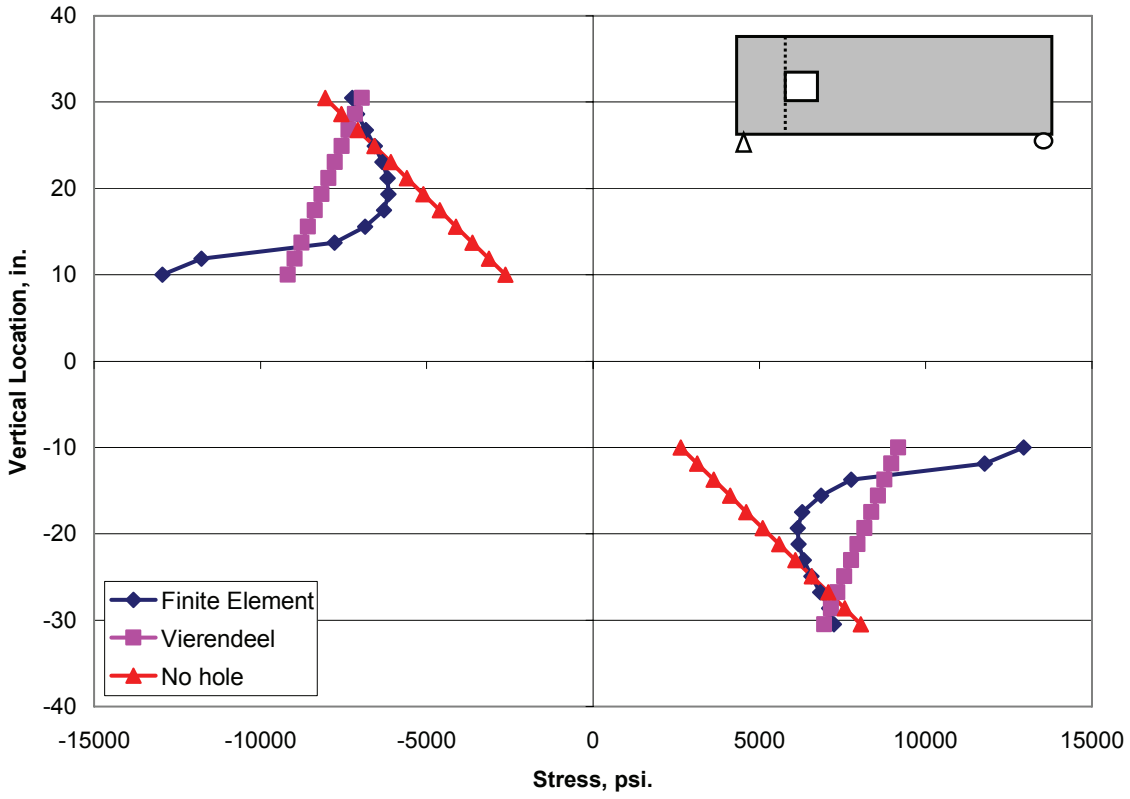

Figure 4.19: Flexural Stress Distribution at Outside Hole Edge, 20" x 20"

When compared to the outside edge distributions for the 10" x 10" model and the 30" x 30" model (discussed next), it is apparent that the 20" hole depth is in "transition"—ignoring the hole no longer provides a realistic stress distribution, but the Vierendeel method doesn't predict the distribution very well either. It is a similar situation to what is seen at the inside edge, but the difference between the stress distributions is more emphasized. The plot does show that the stress distribution is moving toward the Vierendeel distribution and away from the "no hole" distribution. For this hole depth, the maximum stress predicted by the Vierendeel method at the outside hole edge is about 29% less than the finite element stress. However, the Vierendeel method correctly predicts the location of the maximum stress (next to the top and bottom hole edges),

which would not occur with a "no hole" distribution. It should be noted that although the Vierendeel distribution does not match well for this hole depth, it comes closer to predicting the magnitude and location of maximum stresses at all cross sections than does the "no hole" distribution.

30" x 30" Hole

The third model incorporated in Set 2 had a 30" x 30" hole in the web; all other details were the same as the previous two models. The flexural stress distribution at the inside hole edge is shown in Figure 4.20.

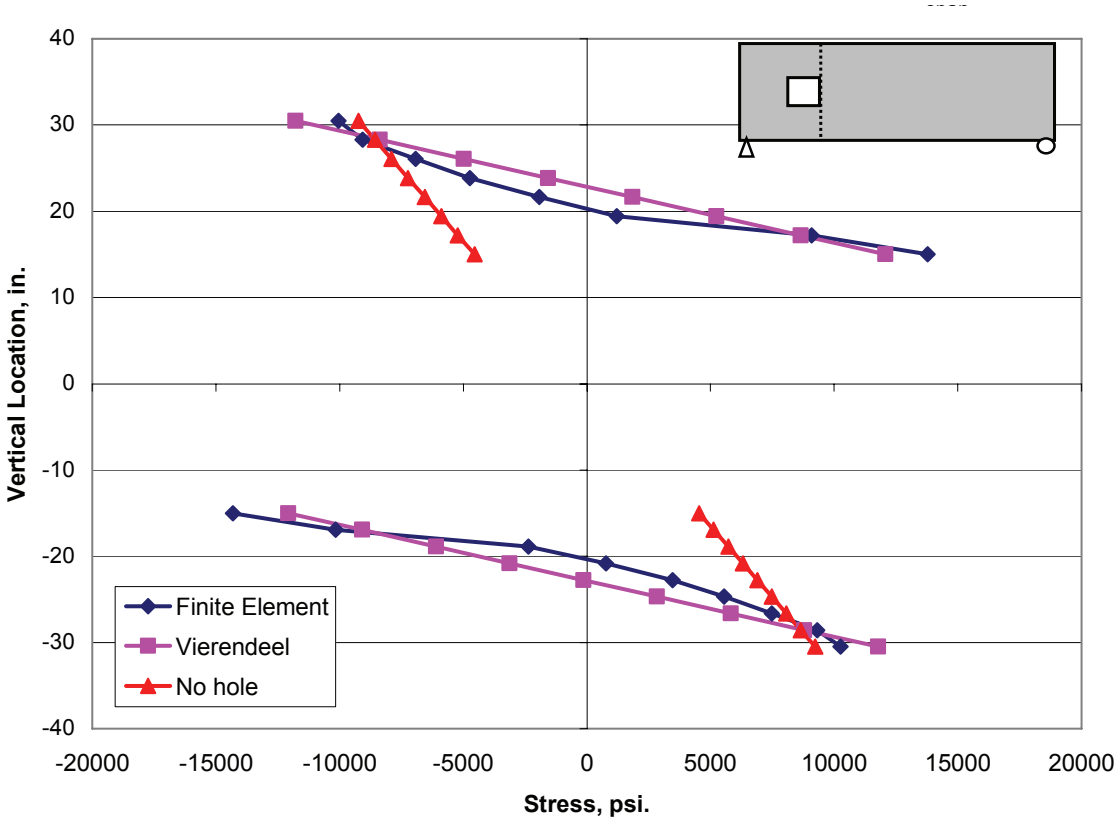

Figure 4.20: Flexural Stress Distribution at Inside Hole Edge, 30" x 30"

The plot in Figure 4.20 shows that for the 30” hole (48% of total member depth), the Vierendeel method clearly provides a better method of approximating the stress distribution than the “no hole” method at the inside edge. The Vierendeel method again correctly identifies the locations of maximum stress, but it is not conservative at these points (at the top and bottom hole edges). The Vierendeel stress at these points is approximately 17% lower than the finite element predicted stress.

Stress distributions at the hole center continue to match very closely, as shown in Figure 4.21.

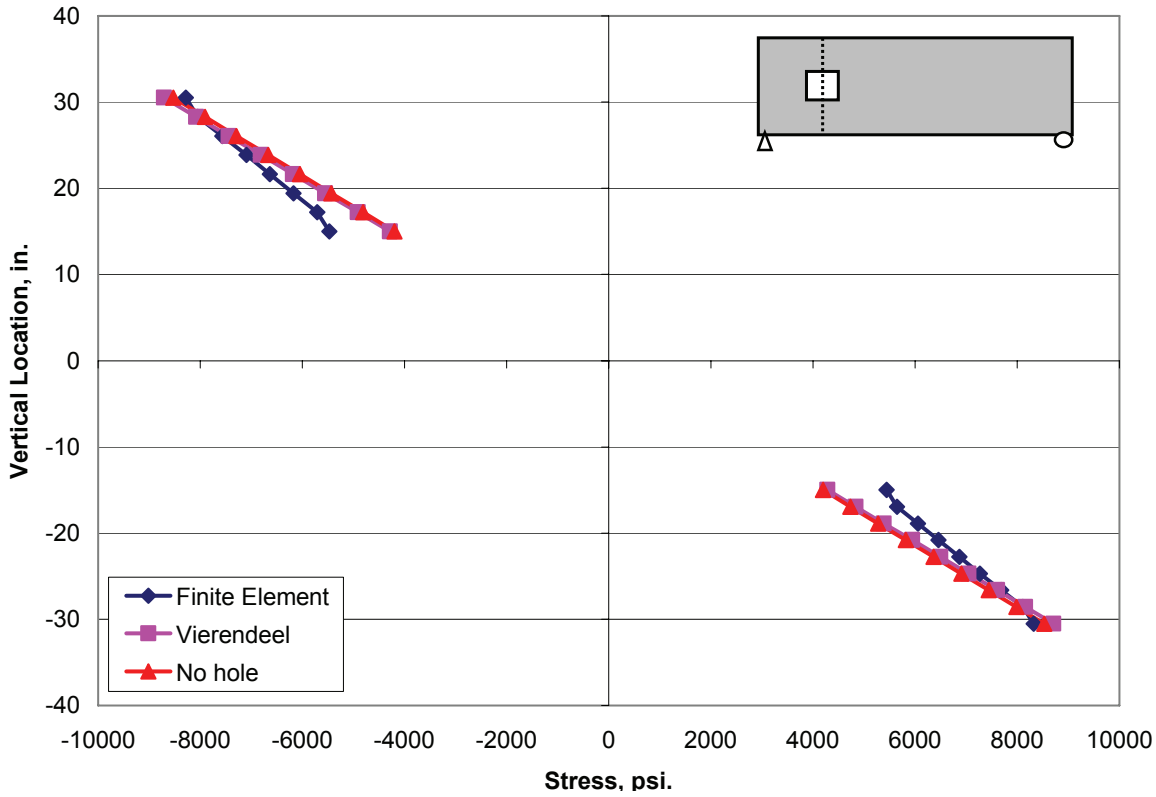

Figure 4.21: Flexural Stress Distribution at Hole Center, 30” x 30”

At the outside hole edge, the Vierendeel method provides a much closer match with finite element results than it did for the outside edge of the 20” hole (see Figure 4.22).

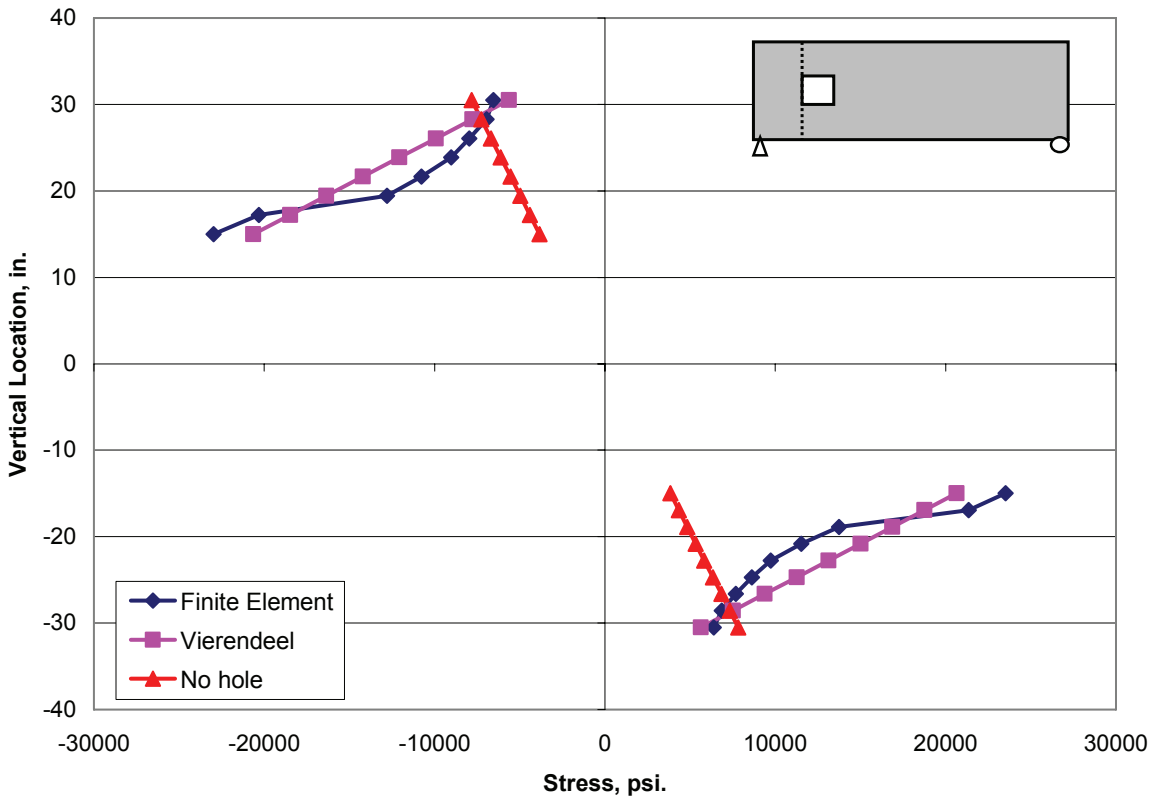

Figure 4.22: Flexural Stress Distribution at Outside Hole Edge, 30" x 30"

As with the inside edge, the Vierendeel results are not conservative at the maximum stress locations. The maximum Vierendeel stress is about 12% less than the maximum finite element stress. For the 30" hole, the Vierendeel method provides a good representation of the stress distribution, but does not conservatively predict maximum stress at the hole edges.

40" x 40" Hole

The final model used in Set 2 incorporated a 40" x 40" hole (65% of total member depth). The flexural stress distribution at the inside hole edge is shown in Figure 4.23.

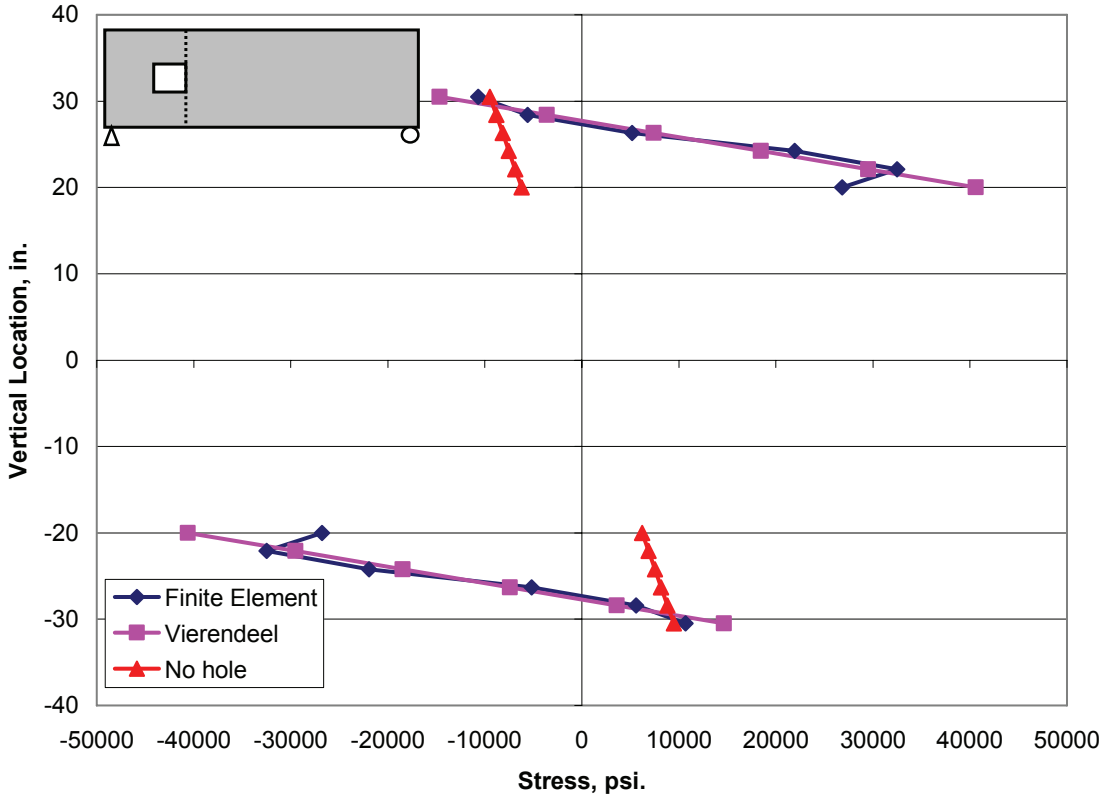

Figure 4.23: Flexural Stress Distribution at Inside Hole Edge, 40" x 40"

At the inside hole edge, the Vierendeel stress distribution provides a reasonable match with finite element results except for locations exactly at the top and bottom hole edges. In this case the Vierendeel method and finite element do not agree on the location of the maximum stress; finite element results show the maximum stress at the first node above/below the hole edge instead of exactly at the hole edge. However, the Vierendeel method is still conservative—the maximum Vierendeel stress is 16% higher than the maximum finite element stress.

At the center of the hole, the Vierendeel and "no hole" deviate from finite element results more than they have in the previous models. However, neither is significantly better than the other at matching finite element results; they still match each other very closely. Both are still conservative at the extreme fiber of the beam (location of maximum stress), as shown in Figure 4.24.

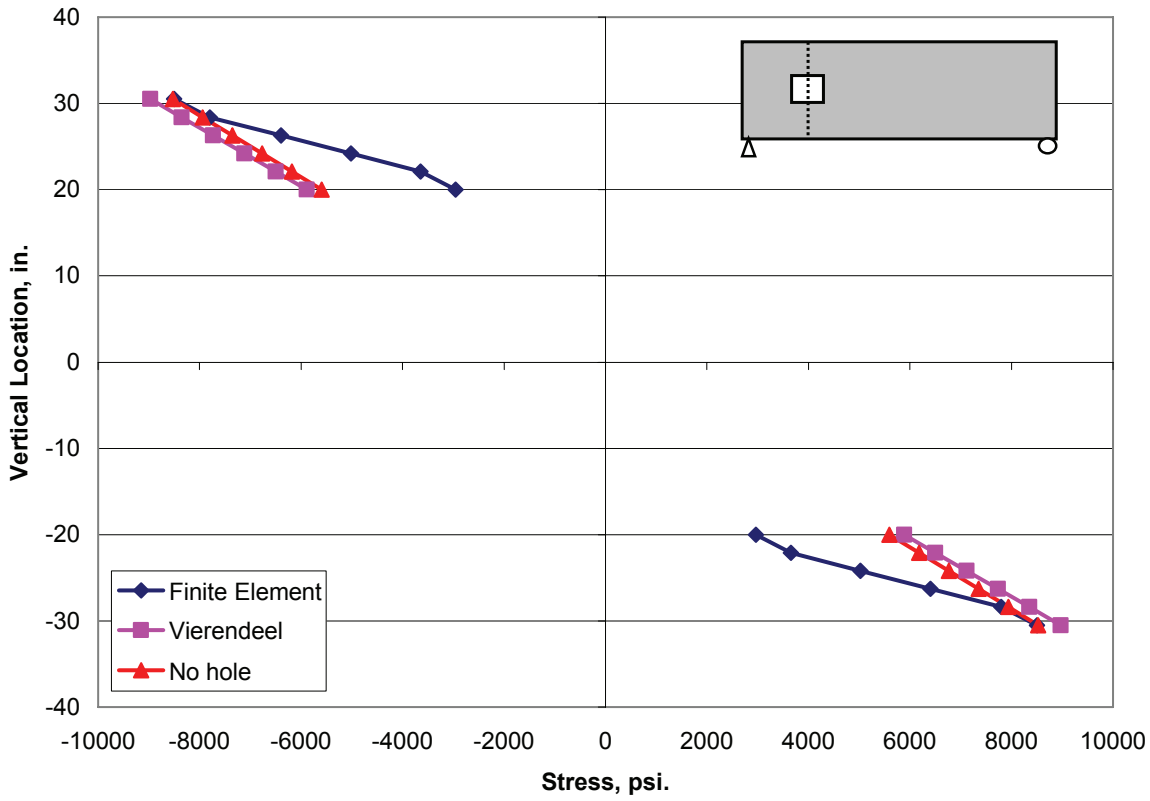

Figure 4.24: Flexural Stress Distribution at Hole Center, 40" x 40"

At the outside hole edge, the Vierendeel method matches finite element results closely near the extreme fibers. However, Figure 4.25 shows that the stresses differ near the hole. Since the Vierendeel stresses near the hole are near 50 ksi, it appears that the section is yielding near the hole. For this beam geometry and loading condition, a hole through 65% of the member depth creates stresses beyond the elastic range. The

Vierendeel method does not have any inherent stress limit; it is up to one performing the calculations to recognize when the method is predicting stresses beyond the yield stess.

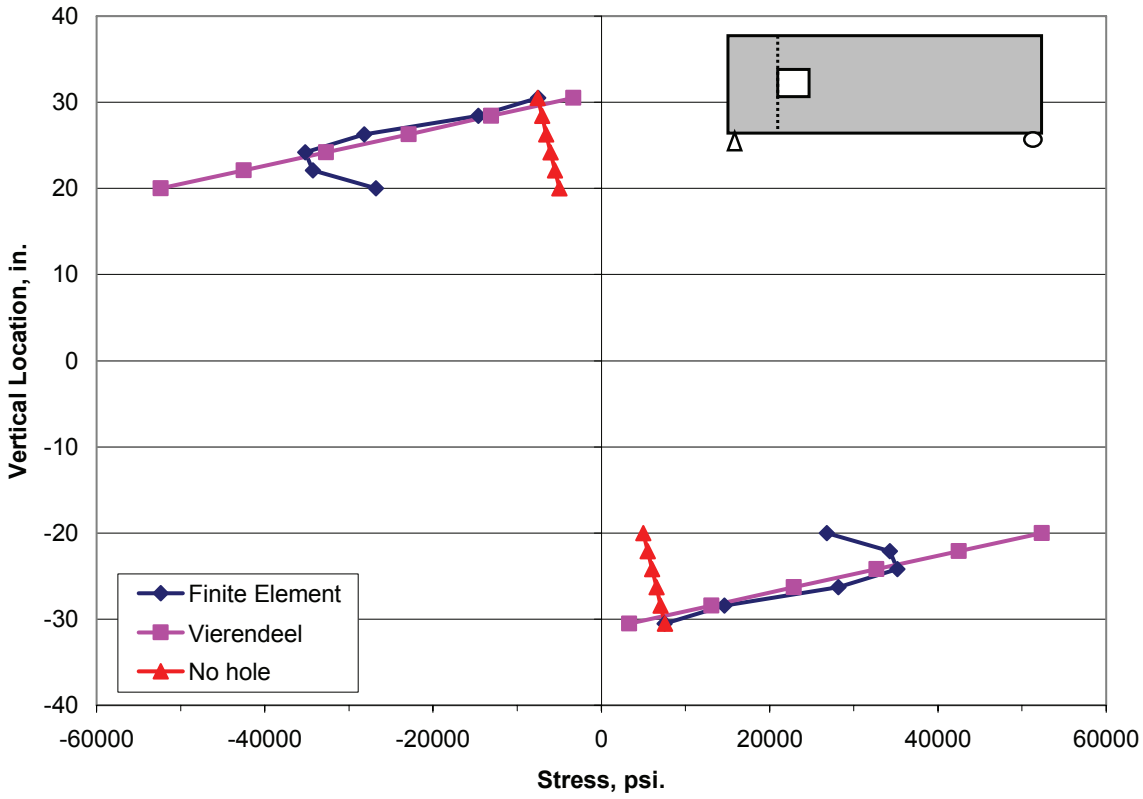

Figure 4.25: Flexural Stress Distribution at Outside Hole Edge, 40" x 40"

Reference material suggested the Vierendeel method was best employed for holes less than half the total member depth, and the final model of Set 2 confirms that. However, Figures 4.23 and 4.25 indicate that for a hole at 65% of member depth, the Vierendeel method will accurately predict the stress distribution until stresses approach the yield point. If stresses were reduced by application of a smaller load, it is likely that the

Vierendeel method would provide accurate results around a hole as deep as 65% of member depth.

Analysis set 2 shows that for small holes, flexural stress distributions are best predicted by beam theory. As holes get larger, the maximum flexural stress will be found next to the hole instead of at the extreme fiber of the beam. At this point, the magnitude and location of the maximum flexural stress appear to be better predicted by the Vierendeel method. This will be dealt with more in sections 4.3.5 and 4.3.6.

4.3.3: Set 3—Four-Point Loading, Hole in No-Shear Region

Sets 1 and 2 focused on simply supported beams with a single concentrated load. Set 3 was another configuration designed to address the possibility of multiple concentrated loads. Figure 4.26 shows such a configuration. The response at A would be analyzed as previously done, however notice point B is an area of no shear. This precludes the use of the Vierendeel method, as shear is the parameter which alters the flexural stress response.

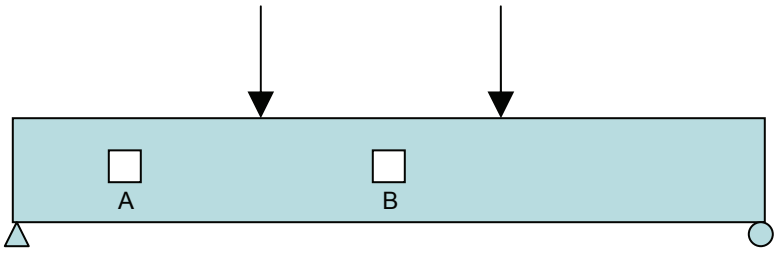

Figure 4.26: Four-Point Loading

Set 3 used the standard 30' W27x94, simply supported with concentrated loads at the third points. A 6" x 6" hole was vertically centered at midspan. Since there is no shear

force present, the Vierendeel procedure would match elementary beam theory for a section with no hole, i.e. $\sigma = My/I$. The stress distribution obtained at the hole edges is provided in Figure 4.27 (the stress distributions at both hole edges are the same because the center of the hole was at midspan and the beam was symmetrically loaded). The finite element distribution in the presence of the hole appears to match almost perfectly with the elementary beam theory distribution with no hole present. This is due to the extremely small change in moment of inertia. A 6" hole vertically centered in a W27x94 will reduce the moment of inertia by about 0.3%.

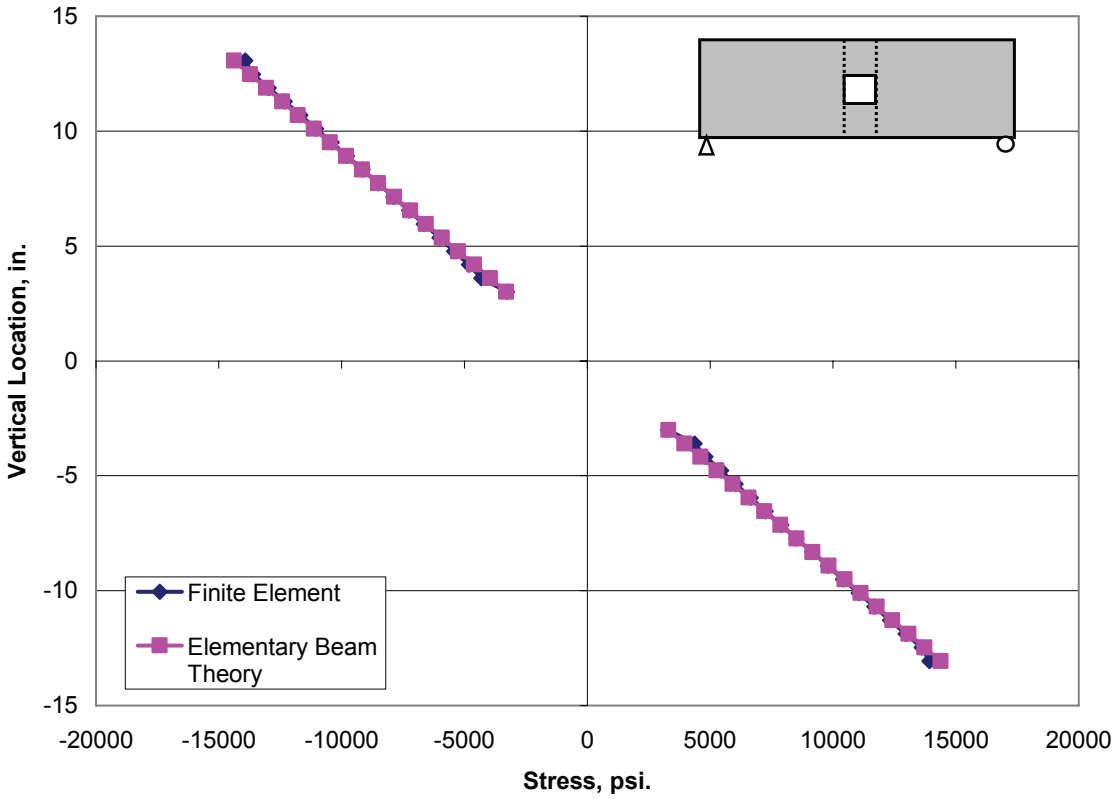

Figure 4.27: Flexural Stress Distribution at Hole Edge, 4 pt. Loading

Figure 4.28 is a plot of the stress distribution through the center of the hole at midspan. Finite element results and elementary beam theory match well, except for a small deviation next to the hole. The Vierendeel stress is about 22% lower than the finite element stress. However, this is at the lowest stress location, so the actual stress difference is not extremely large.

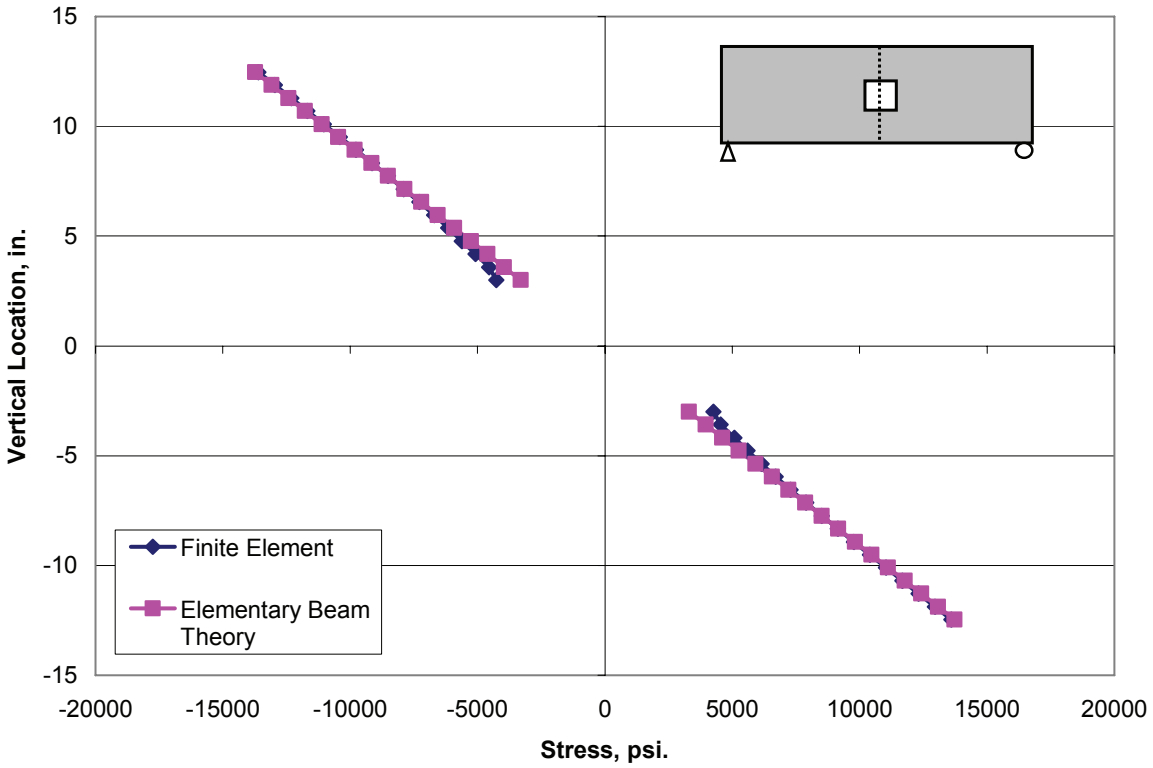

Figure 4.28: Flexural Stress Distribution at Midspan (Hole Center), 4 pt. Loading

Figure 4.29 is a plot of the stress distribution two feet from the hole edge. This location is beyond the hole, but still in the no-shear region.

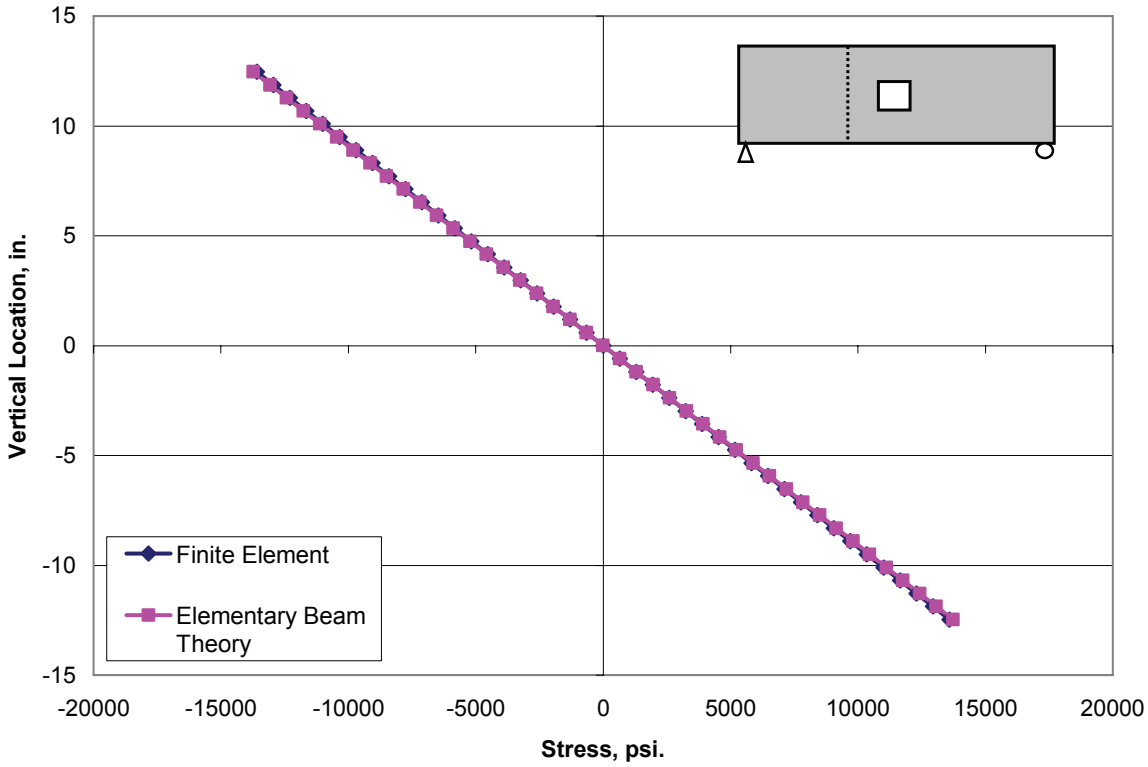

Figure 4.29: Flexural Stress Distribution 2' From Hole Edge, 4 pt. Loading

The stress distributions for Set 3 show that elementary beam theory matches the prediction of the flexural stress distribution given by finite element analysis anywhere in the no-shear region, except for slight deviations next to the hole shown in Figure 4.28. These deviations may still be a result of stress concentrations. Set 3 only modeled a hole at midspan, but the results did not suggest a reason to model a hole at any other location in the no-shear region. Results indicated that elementary beam theory will adequately predict the stress at various locations at and around the hole in the no-shear region. Moving the hole within the region will not create any shear force, so this pattern should continue regardless of hole location within the region.

4.3.4: Set 4— Partial Length Uniformly Distributed Load, Hole at Midspan

The Vierendeel method was derived for a case with constant shear over the length of the hole. Set 4 was run to investigate the accuracy of the Vierendeel method if a distributed load is placed over the hole in the web, thus causing a variable shear over the length of the hole. The test beam was the standard W27x94, 30', simply supported. A uniformly distributed load of 10,000 lb/ft. was applied to the center 7.5' of the beam (1/4 of the total beam length). The flexural stress distribution at the hole edges is shown in Figure 4.30 (again, the beam and hole are symmetrical, so the stress distribution at both sides of the hole is the same).

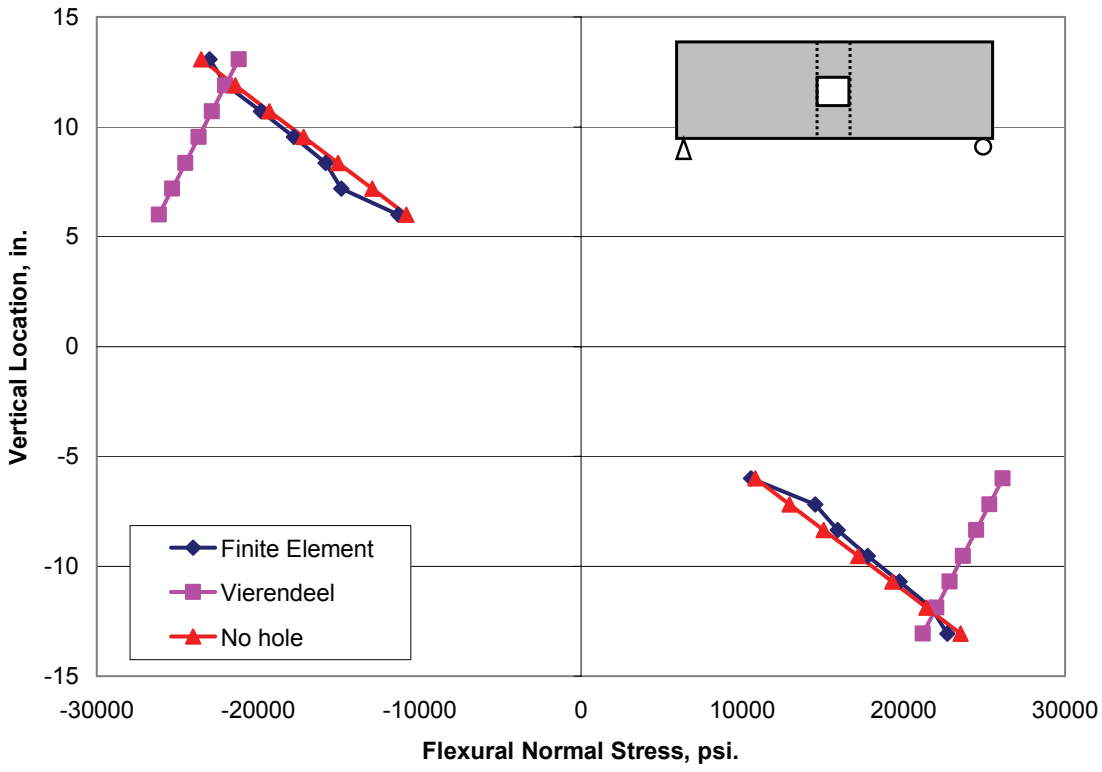

Figure 4.30: Flexural Stress Distribution at Hole Edge, Partial Uniformly Distributed Loading

The Vierendeel method in its original form is not applicable to a distributed load with variable shear across the hole. In an attempt to extend the application of the Vierendeel method, Vierendeel calculations were conducted by replacing the distributed load with an equivalent point load. As Figure 4.30 shows, this results in an extremely inaccurate stress distribution. The "no hole" distribution does provides an accurate prediction of the stress distribution. Closer examination of the scenario reveals that the results make sense. The balanced nature of the distributed load and end reaction leave no shear to act on the remaining tee sections when the beam is cut for analysis. Therefore, the "no-shear" conditions of Set 3 were effectively re-created.

4.3.5: Investigation of Stress Shift

In many practical situations, the magnitude and location of the maximum stress will be more important than predicting the entire stress distribution. Previous analyses for holes of varying sizes indicate that the maximum flexural stress will either occur at the inside hole edge at the extreme fiber (point A in Figure 4.31), or at the outside hole edge at the hole corner (point B in Figure 4.31). The maximum stress will be found at point A for smaller holes, then as the hole size is increased the maximum stress shifts to point B.

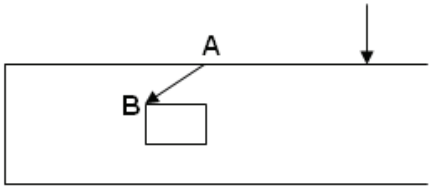

Figure 4.31: Stress Shift

For a simply supported beam with a point load at midspan, elementary beam theory states that the maximum flexural stress will occur at the extreme fiber of the beam at midspan. If a hole is present and beam cross sections at the inside and outside hole edges are considered, elementary beam theory would still predict the maximum stress occurs at the extreme fiber where the moment is highest (point A in Figure 4.31). As the hole size increases, the shear induced moments (see Figure 4.32) become more and more significant, and eventually the location of the maximum normal stress shifts to point B.

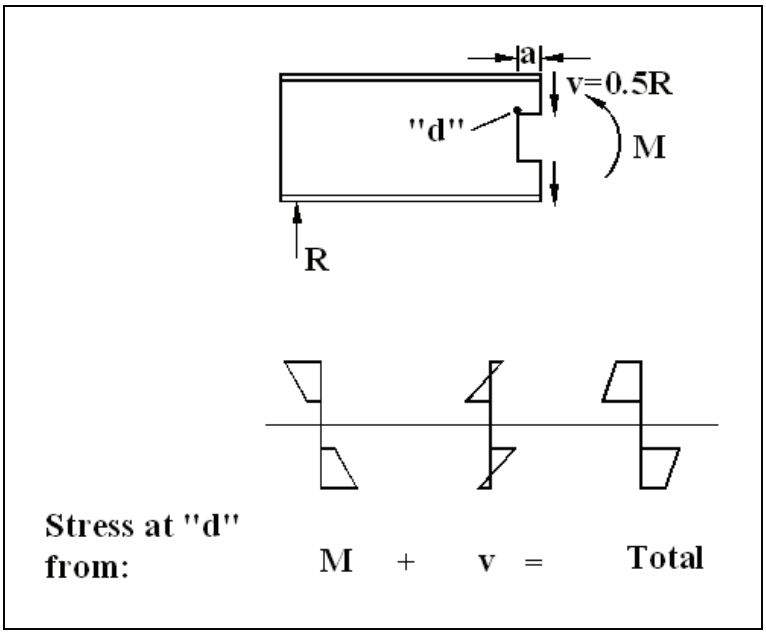

Figure 4. 32: Global and Shear-Induced Moments

The increased significance of the shear induced moments can be more clearly understood if the Vierendeel stress equation and a sample beam are examined. If the statics presented in Figure 4.32 are considered, the stress at both points A and B (Figure 4.31) is given by the expression $\sigma_x = -\frac{Vay}{I_t} - \frac{Mh}{I_n}$. The reason for the shift comes from the "y" term corresponding to the shear-induced moment, as illustrated in Figure 4.33.

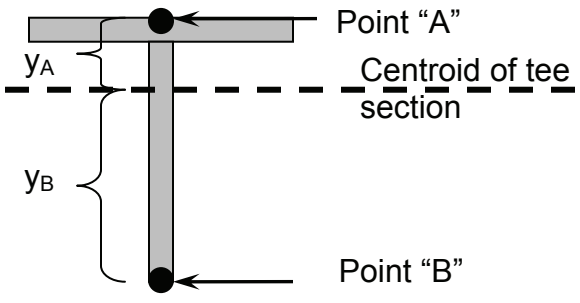

Figure 4.33: "y" Term for Shear-Induced Moment

This term is the distance between the neutral axis of the tee section and the point in question. For the top tee where points A and B are found, the neutral axis will be very near the flange, if not in the flange, depending on beam geometry. Therefore, the "y" term for point B will be larger than that for point A.

For small holes, this is offset by the fact that the global moment at point A is higher. However, as the hole size increases, the value of "y" at point A decreases faster than it does at point B. This is effectively an increase in the value of "y" at point B as hole size increases. For example, see Table 4.2. In this table, "y" values are calculated at points A and B for increasing hole sizes in a beam with 18" x 1" flanges and a 60" x 0.375" web. When the relative size of the "y" values at points A and B are considered, it is apparent that the shear-induced moment is going to play a larger role as hole size increases.

Hole Size	Point A	Point B	Relative Size of "y" (Point B "y"/Point A "y")
10"x10"	4.45	21.05	4.73
20"x20"	3.09	17.41	5.64
40"x40"	0.95	9.55	10.08

Table 4.2: "y" Values for Shear-Induced Moment in Sample Beam

In an effort to determine when stress shift occurs, analysis set 5 modeled several beams with finite element analysis. Preliminary tests which compared a W27x94 to a built-up plate girder suggested that the h/t_w ratio (web depth: web thickness) of a beam might affect the hole size at which stress shift occurs, so analyses focused on the effects of

varying the h/t_w ratio. The first series of beams analyzed is described in Table 4.3 (this beam series is referenced at other times, and will be referred to from this point on as beam Set A). The h/t_w ratios were varied by holding the web thickness constant and changing the web depth.

h/t_w ratio	Flanges	Web	Length	Length/Depth ratio	Load (lb)
76	14" x 1"	0.375" x 28.5"	408"	13.38	75,963
107	14" x 1"	0.375" x 40"	552"	13.14	82,350
144	14" x 1"	0.375" x 54"	744"	13.29	86,853
155	14" x 1"	0.375" x 58"	804"	13.40	87,570
160	14" x 1"	0.375" x 60"	828"	13.35	88,589
165	14" x 1"	0.375" x 62"	852"	13.31	89,592
176	14" x 1"	0.375" x 66"	888"	13.06	92,790
211	14" x 1"	0.375" x 79"	1080"	13.33	95,433
213	14" x 1"	0.375" x 80"	1080"	13.17	96,961

Table 4.3: First Series of Beams Tested for Stress Shift (Set A)

The beam lengths were varied in order to maintain a roughly constant length-to-depth ratio. (Whole foot increments were easiest to use in the Vierendeel spreadsheet, so there is some slight variation in the length-to-depth ratio. However, the largest ratio is only 2.6% larger than the smallest ratio.) This ratio is important because it dictates how much of the flexural stress is caused by shear-induced (Vierendeel) moments and how much is caused by the global moment. For example, one might consider a cross section at quarterspan in a simply supported beam with a point load at midspan. The global moment at that cross section will be given by $M = PL/8$, so if the length of the beam is

doubled but P is held constant, the global moment will double. However, the shear-induced moment is unaffected by beam length (again, see Figures 4.5 and 4.6).

Loads were also varied for the sake of consistency; all of the given loads will yield the same maximum flexural stress in their respective beams when no hole is present. All beams were simply supported with point loads at midspan.

Vertically centered square holes of varying sizes were placed at quarterspan on the beams. The hole size required to cause the stress shift was not determined exactly, but was bracketed in a 2% window. Because of the variation in beam geometry, hole size was dealt with as a percentage of total member depth (a 15" hole in a 30" deep beam is considered the same size as a 20" hole in a 40" deep beam).

Figure 4.34 is a plot of the hole sizes (as a percentage of beam depth) required to cause stress shift as determined by finite element analysis and predicted by the Vierendeel method.

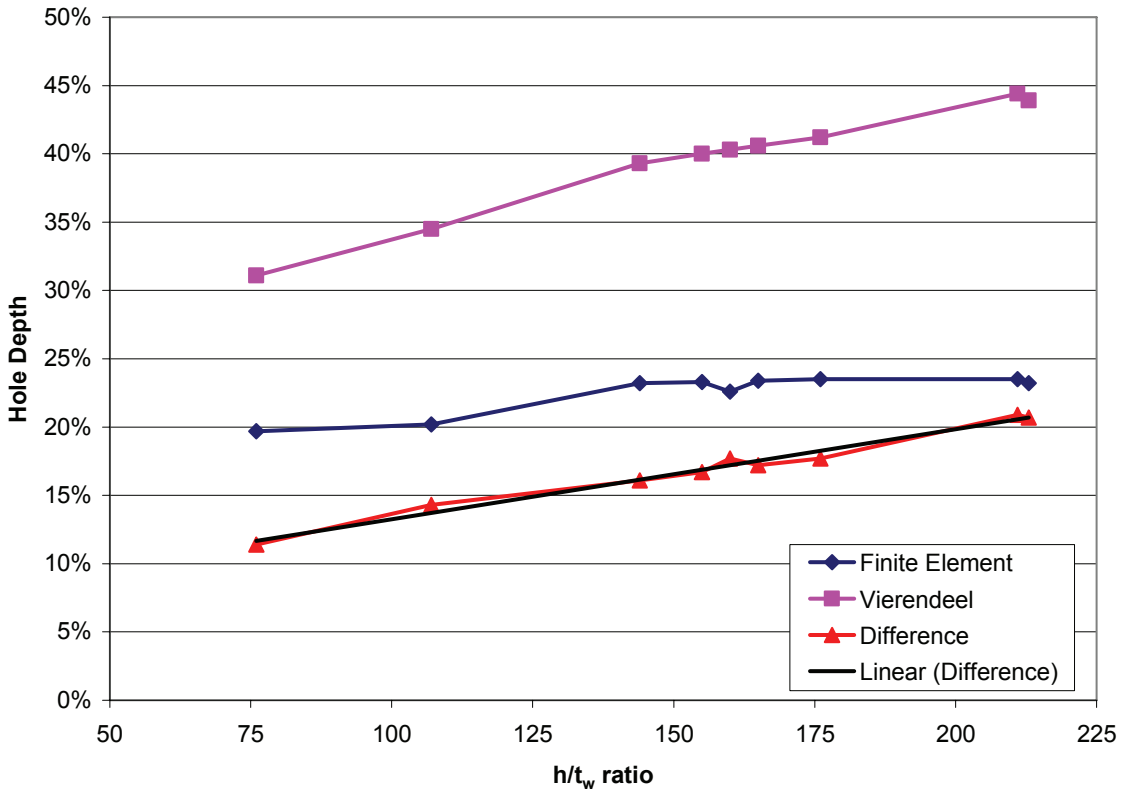

Figure 4.34: Hole Size Required to Cause Stress Shift vs. h/t_w Ratio

Although there is a 10-20% discrepancy between the finite element and Vierendeel results, both trends are approximately linear. The fact that hole sizes weren't determined exactly but were bracketed to within ±2% probably accounts for the deviation from the linear trend line. This bracketing procedure also explains how there can be a deviation between points plotted very close together, such as those for h/t_w ratios of 211 and 213. For example, the beam with an h/t_w ratio of 211 showed stress shift at a hole depth of 36", or 44.4%, according to the Vierendeel method. The previous hole size checked was 35", or 43.2%. Since the difference was less than 2%, the shift was considered to be bracketed and the result was plotted as 44.4%. For the beam with an h/tw ratio of 213, the Vierendeel method showed stress shift at a hole depth of 36", or 43.9%, while the

previous hole checked was 35", or 42.7%. The true stress shift points could lie anywhere in the bracketed windows. The true stress shift for h/t_w=211 could be anywhere between 43.2% and 44.4%, while the true stress shift for h/t_w=213 could be anywhere between 42.7% and 43.9%. This means it is possible for the shift point of h/t_w=213 to be slightly higher than that for h/t_w=211, even though the current plot shows it slightly lower.

To investigate whether the initially observed trends held true for other beam geometries, a second and third series of beams were modeled. In these two series, beams having approximately the same h/t_w ratios as those of the first series were tested. However, the flange geometry and web geometry were altered. The second series of beams, listed in Table 4.4 and referred to from this point on as Set B, still had 0.375" thick webs but had wider flanges. The third series of beams, listed in Table 4.5, had the same 14" x 1" flanges as Set A. It is referred to from here on as Set C. In Set C, the webs were thinned and the overall section depths were reduced.

h/t_w ratio	Flanges	Web	Length	Length/Depth ratio	Load (lb)
76	18" x 1"	0.375" x 28.5"	408"	13.38	95,364
101	18" x 1"	0.375" x 38"	540"	13.50	98,900
128	18" x 1"	0.375" x 48"	672"	13.44	103,447
156	18" x 1"	0.375" x 58"	804"	13.40	107,583
181	18" x 1"	0.375" x 68"	936"	13.37	111,479
208	18" x 1"	0.375" x 78"	1068"	13.35	115,225

Table 4.4: Second Series of Beams Tested for Stress Shift (Set B)

h/t_w ratio	Flanges	Web	Length	Length/Depth ratio	Load (lb)
76	14” x 1”	0.25” x 19”	280”	13.33	69,451
100	14” x 1”	0.25” x 25”	360”	13.33	72,179
128	14” x 1”	0.25” x 32”	454”	13.35	74,628
156	14” x 1”	0.25” x 39”	546”	13.32	77,040
180	14” x 1”	0.25” x 45”	627”	13.34	78,636
208	14” x 1”	0.25” x 52”	720”	13.33	80,547

Table 4.5: Third Series of Beams Tested for Stress Shift (Set C)

As with Set A, hole size was not determined exactly but was bracketed to within ±2%. The finite element results for all three beam sets are plotted in Figure 4.35. Appendix A contains similar to 4.34 for beam sets B and C, comparing Vierendeel and finite element predictions for stress shift.

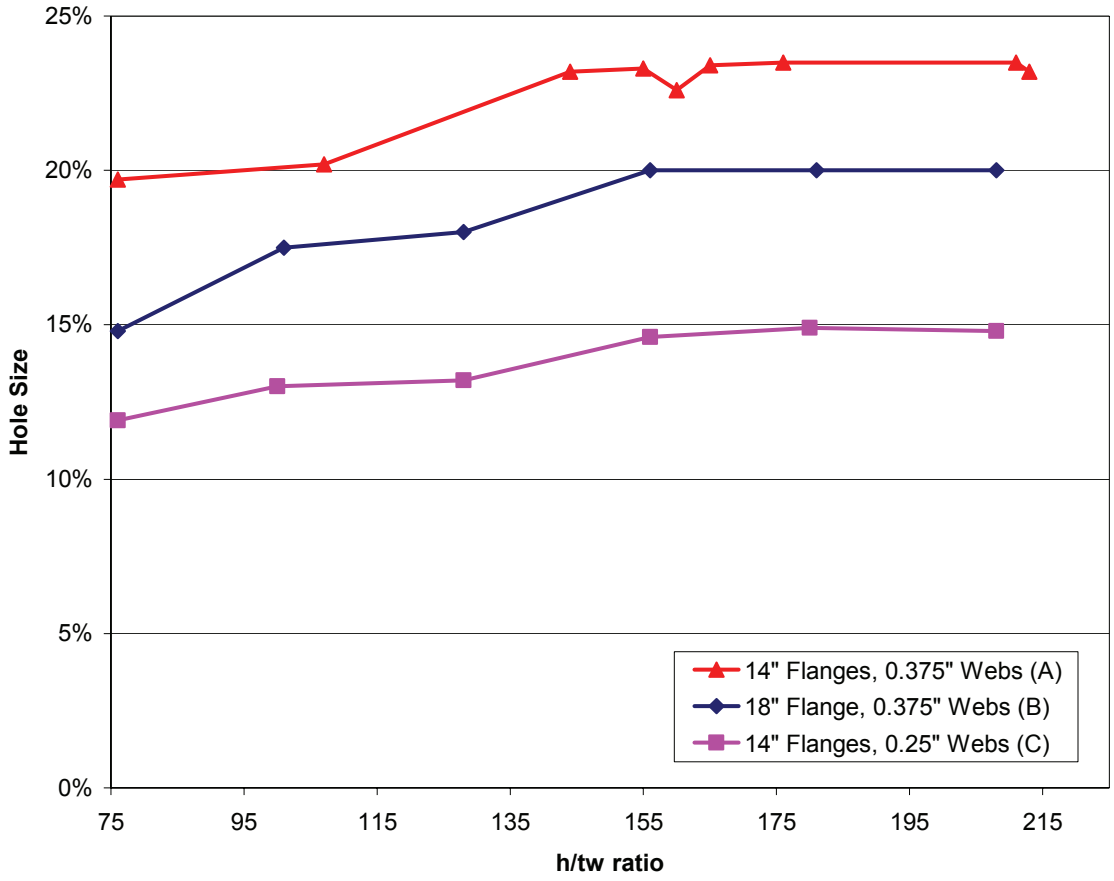

Figure 4.35: Hole Size Required to Cause Stress Shift in Three Sets of Beams

Figure 4.35 shows that altering beam geometry does impact the point of stress shift. The top line plotted in Figure 4.35 corresponds to the beam Set A. The lower two lines show consistently lower points of stress shift for all h/t_w ratios in the modified beam geometries. Also, the plots for all three beam series demonstrate a trend to level out around h/t_w=155. Plots for Vierendeel predictions do not do this; as shown in Figure 4.34 they remain linear throughout the h/t_w range. Since the main thing the Vierendeel cannot account for is stress concentrations, it appears that stress concentrations become especially significant around h/tw=155. After this point, stress concentrations may govern the stress shift (instead of the shear-induced moment).

Figure 4.36 addresses the question of how well Vierendeel predictions for stress shift match finite element results. The differences between Vierendeel and finite element results for all three beam sets are plotted in Figure 4.36.

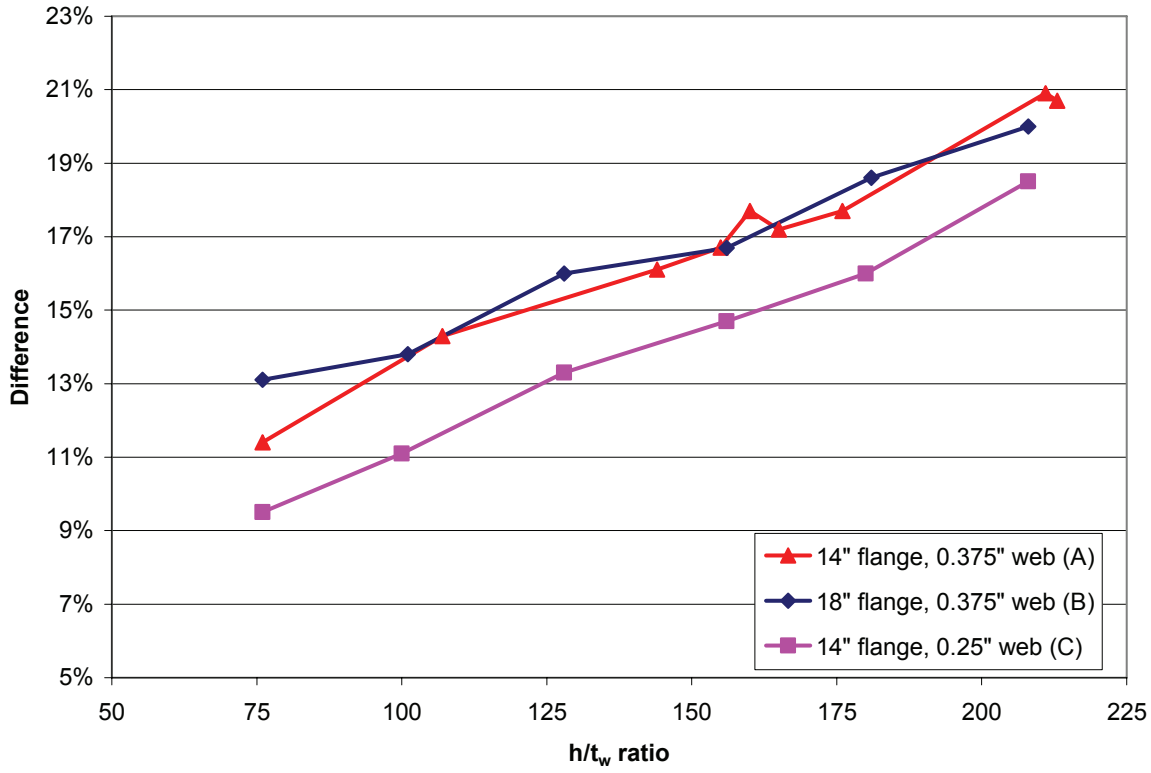

Figure 4.36: Differences Between Finite Element and Vierendeel Hole Sizes to Cause Stress Shift

Note that the percent difference is still expressed in terms of hole size. For example, if Vierendeel predicted stress shift at a hole depth of 30%, and finite element results indicated shift at a hole depth of 12%, then the difference is plotted as 18%. Figure 4.36 demonstrates that altering flange geometry has little to do with how well Vierendeel and finite element results match. However, the section with the thinner web showed consistently less difference between Vierendeel and finite element predictions for stress shift.

Two main trends were illustrated in Section 4.3.5. The first is that the hole size required to cause stress shift tends to increase with h/t_w ratio, until a point at which stress concentrations govern over the shear-induced moment. For the three beam geometries examined, this was around h/t_w=155. The second trend is that the difference between finite element and Vierendeel predictions for stress shift tends to increase linearly over the h/t_w range observed. The differences were similar for all three beam geometries studied, with the thinned flange geometry (Set C) showing slightly less discrepancy between Vierendeel and finite element predictions for stress shift.

The difference between Vierendeel and finite element predictions appears to increase linearly with h/t_w ratio regardless of beam geometry.

It should also be noted that besides the beams modeled in Sets A, B, and C, the W27x94 was also modeled. This section has an h/tw ratio of only 49.5. Finite element analysis predicted stress shift at a hole size of 35%, while Vierendeel predicted stress shift at a hole size of 41%. This 6% difference is in keeping with results shown in Figure 4.36, which demonstrate that there is less discrepancy between finite element and Vierendeel predictions at lower h/tw ratios.

4.3.6: Vierendeel Method Applicability

Section 4.3.2 examined the Vierendeel technique in approximating flexural stress distributions. Results showed that the stress distribution varies with hole size, and for some configurations the stress distribution is still best predicted by beam theory ($\sigma = My/I$). However, since the maximum stress in a cross section (and the location of that

stress) is usually more important, efforts were made to establish ranges for which the Vierendeel method could be used to determine the magnitude and location of the maximum stress around the hole.

Before Stress Shift—As discussed in section 4.3.5, the maximum flexural stress will be found at the extreme fiber of the inside hole edge until the hole is large enough to induce stress shift (see point A, Figure 4.37). This is because the global beam moment dominates the shear-induced moments for small holes.

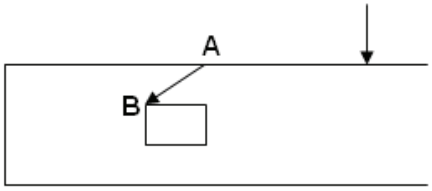

Figure 4.37: Maximum Stress Locations Before and After Stress Shift

Figure 4.38 examines the difference between maximum stresses predicted by the Vierendeel method and finite element analysis. The hole sizes plotted were too small to have induced stress shift, so the maximum stresses are all at the inside hole edge. Beam Set A (14”x1” flanges, 0.375” webs) was used to generate Figure 4.38.

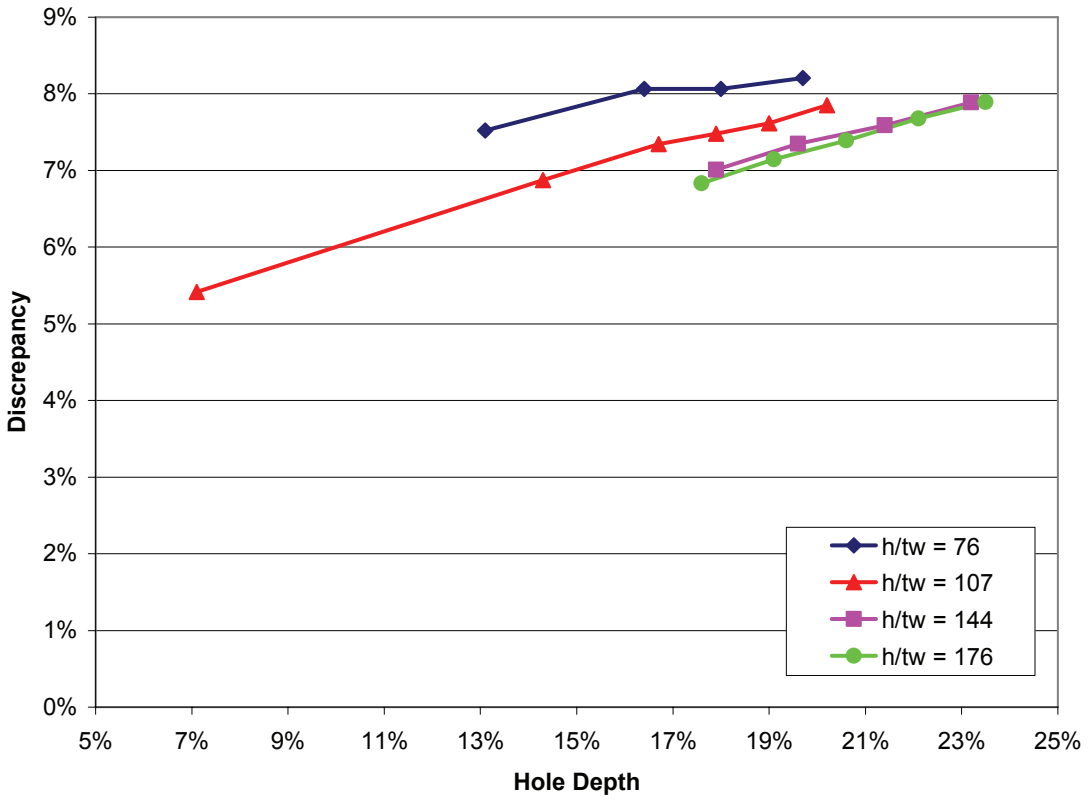

Figure 4.38: Discrepancy Between Finite Element and Vierendeel Max Stresses (Before Stress Shift)

In Figure 4.38, few data points are plotted for each beam because data were obtained while attempting to determine hole size required for stress shift. Analysis was begun with hole sizes estimated to be near the stress shift size. The last hole size plotted is the size at which stress shift occurred. Figure 4.38 demonstrates that as hole sizes increase, the discrepancy between Vierendeel and finite element maximum stresses increases. However, the maximum discrepancy for all beam geometries plotted remained around 8% and the Vierendeel stresses were always conservative when compared to finite element stresses. Similar plots for the beam Sets B and C are included in Appendix B, with similar results.

Figure 4.39 plots the difference between maximum stresses predicted by beam theory and the finite element method at the inside hole edge (before stress shift) for the beams of Set A. The largest hole size plotted for each beam was the largest hole modeled before finite element analysis predicted stress shift to occur. Errors for hole sizes between 5% and 30% of member depth are less than 4%. When compared with Figure 4.38, which often shows discrepancies in the 8-9% range, it is apparent that before stress shift occurs beam theory does an adequate job of predicting the maximum flexural stress.

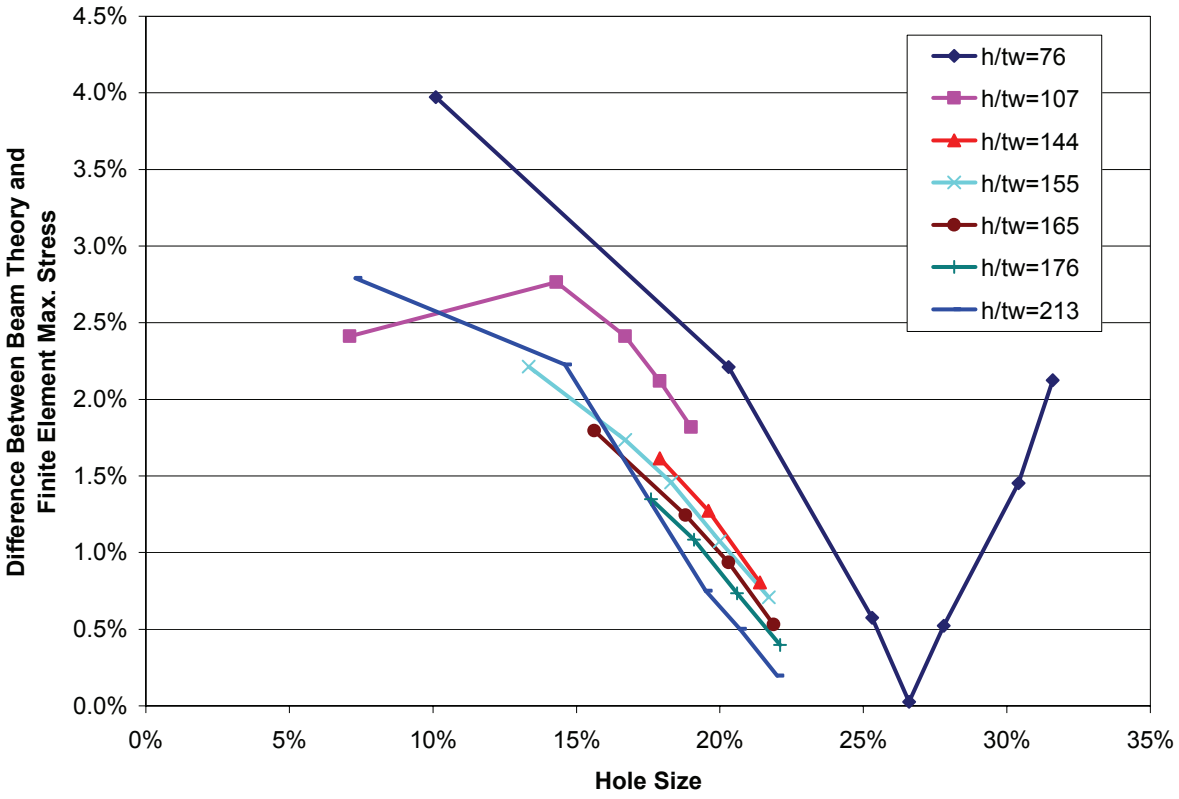

Figure 4.39: Difference Between Beam Theory and Finite Element Maximum Stresses Before Stress Shift

After Stress Shift—For holes large enough to have caused stress shift, the maximum flexural stress will be located next to the hole at the outside hole edge (point B in Figure 4.37). In this case, beam theory will never predict the correct location for the maximum stress, because it always yields highest stresses at the extreme fibers. The Vierendeel method is better able to predict the correct location of maximum stress after stress shift has occurred. Figure 4.40 plots the discrepancy between maximum stresses predicted by the Vierendeel method and finite element analysis after stress shift has occurred. The beams modeled were those from Set A.

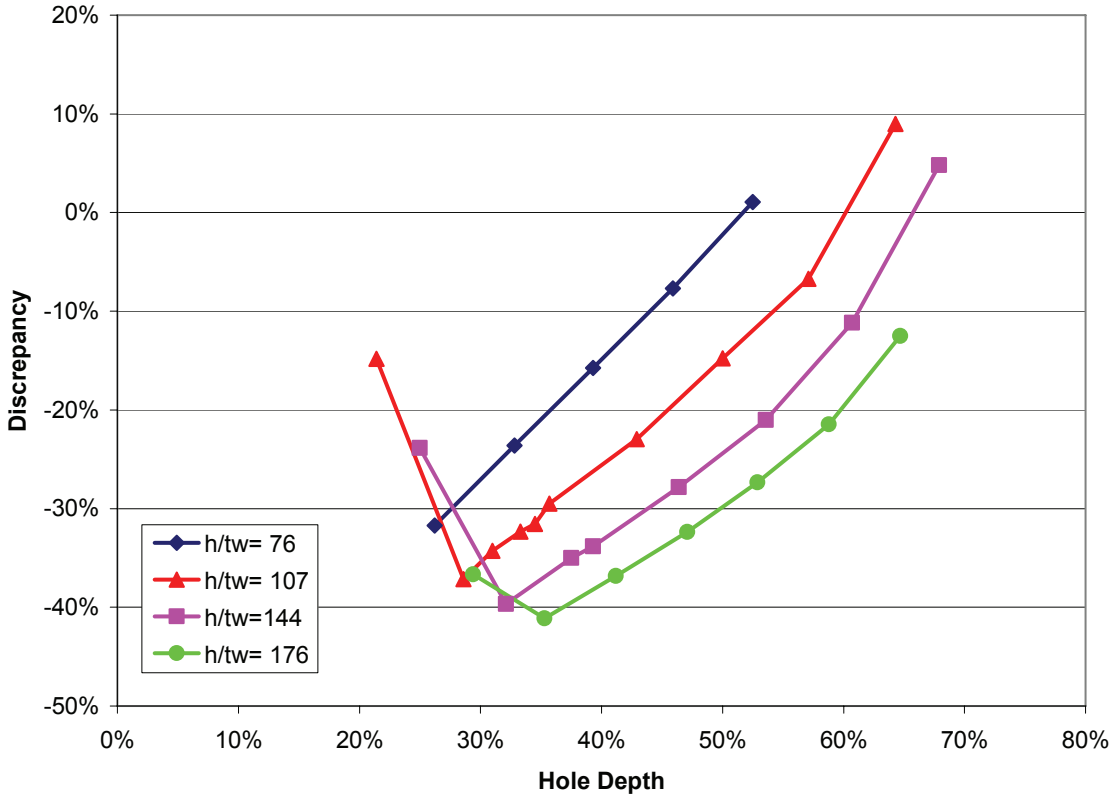

Figure 4.40: Discrepancy Between Finite Element and Vierendeel Max Stress (After Stress Shift)

The discrepancy between Vierendeel and finite element maximum stresses tends to decrease as hole size increases. In some cases, the discrepancy is positive, meaning the Vierendeel stress is conservative.

Figure 4.41 brackets the ranges of Vierendeel applicability for beam sets A, B, and C (three series of beams are included to illustrate the effects of varying beam geometry). Applicability was defined as predicting a stress which was no more than 5% less than the finite element stress.

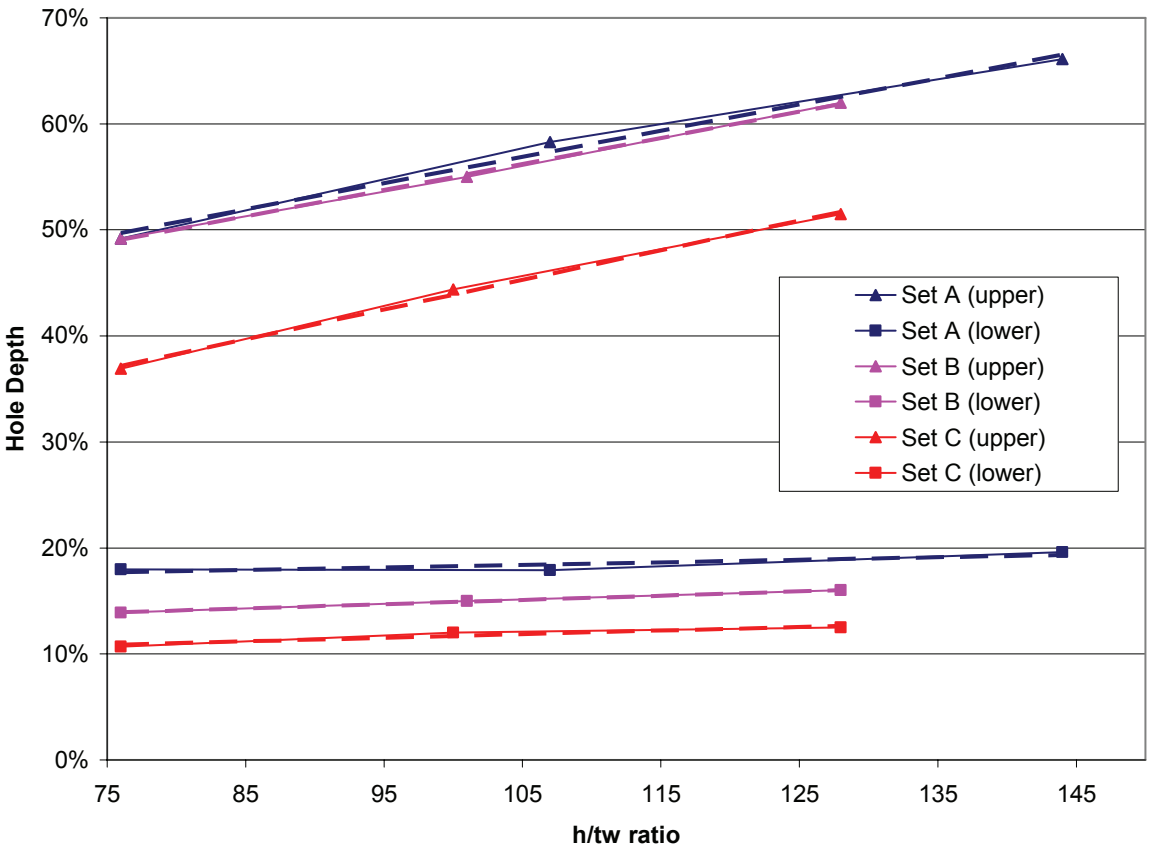

Figure 4.41: Upper and Lower Bounds on Vierendeel Applicability

Two lines are plotted for each beam geometry. The uppermost line is the upper bound of applicability; for hole sizes above this line the Vierendeel procedure should yield maximum flexural stresses within 5% of finite element maximums. For example, a beam might fit the geometry of the Set C (0.25" thick web) and have an h/t_w ratio of 105 and a square hole depth of 50%. This point would fall above the upper bound line for that beam geometry (the upper red line), so the Vierendeel method and finite element analysis should agree within 5% on the maximum flexural stress. Likewise, the lower line is the lower bound of applicability; for hole sizes below this line the Vierendeel procedure should yield maximum flexural stresses within 5% of finite element maximums. The lower bounds are not particularly useful, because they are typically below the hole size required for stress shift, and maximum stresses can be adequately predicted by beam theory. The heavy dashed lines in Figure 4.41 are the linear trend lines for each bound. Changing the flange geometry had little affect on the upper bound, but thinning the web significantly lowered the upper bound line (meaning the Vierendeel method has a wider range of application for beams with thinner webs).

Although all three beam sets included members with h/t_w ratios into the lower 200's, Figure 4.41 only includes a few data points. This is because the hole size is becoming quite large for the upper bounds of the last h/t_w points plotted. As hole size continues to increase, yielding is occurring next to the hole edge. If the error is not less than 5% when yielding begins to occur, it will never be less than 5%—finite element stress will remain at yield stress, while Vierendeel stresses will continue to increase. For the higher h/t_w ratios, Vierendeel stresses were never applicable (within 5% of finite element values).

4.3.7: Stress Increase at Hole Corner, Inside Hole Edge

As discussed in previous sections, the maximum stress around a hole will be at the extreme fiber of the inside hole edge before stress shift occurs. After the shift occurs, the maximum stress is located next to the hole on the outside hole edge. At no point is the maximum stress located at the inside hole edge next to the hole. However, that does not necessarily mean that there are not significant stress increases at that location (marked as point "x" in Figure 4.42).

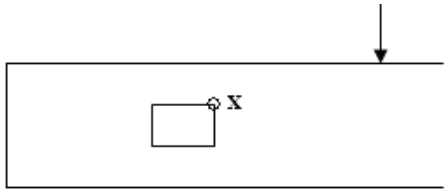

Figure 4.42: Inside Hole Edge, Next to Hole

Although yielding will not be a concern, elevated stress levels could be high enough to exceed threshold levels for fatigue. Figure 4.43 plots the results of analysis set 6, which utilized the beams from Set A to investigate the difference between stresses yielded by finite element analysis and those predicted by beam theory.

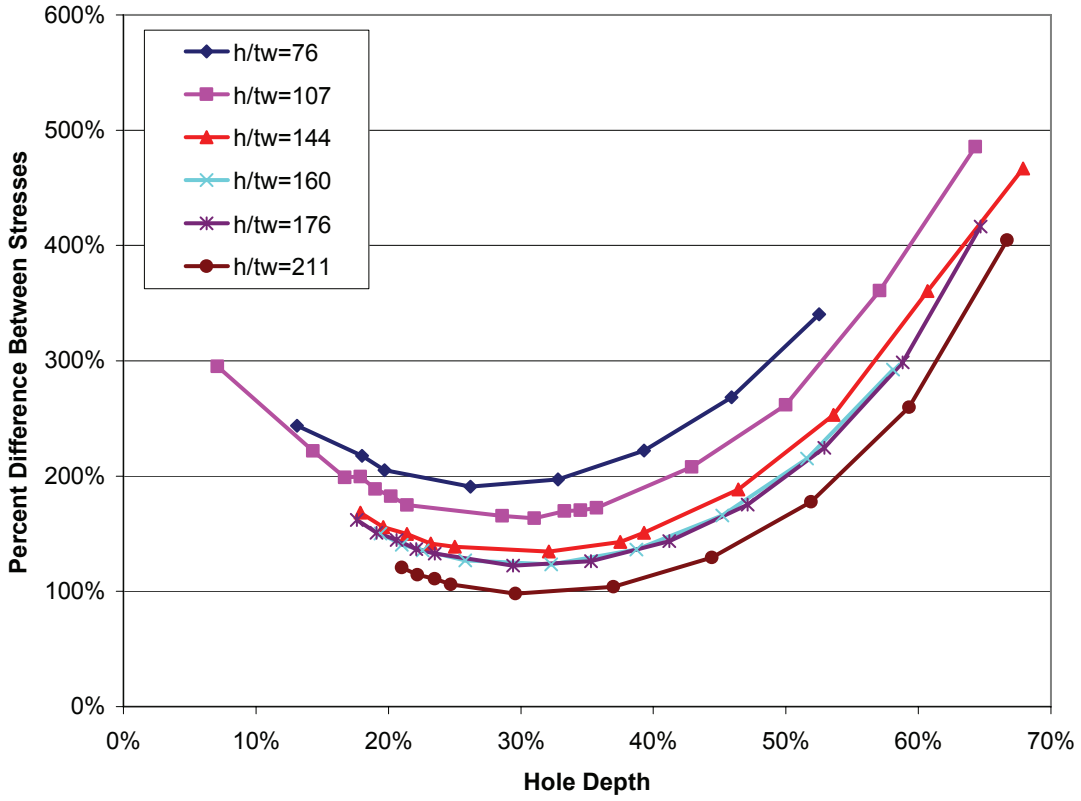

Figure 4.43: Difference Between Beam Theory and Finite Element Stresses, Inside Edge Next to Hole

It is important to note that the finite element stress was higher than the beam theory stress in all cases. The minimum discrepancy between beam theory and finite element stresses typically occurred at hole sizes around 30% of member depth. For small holes, the location in question (shown in Figure 4.42) is near the neutral axis. Because of the low flexural stresses near the neutral axis, the large discrepancies encountered for hole sizes below 30% of member depth may or may not be significant. However, the increased stresses for holes larger than 30% are likely more significant since the hole edge is further from the neutral axis. Similar plots were created for beam sets B and C to confirm similar trends in members with varied geometries. These plots are attached as Appendix C. Although the maximum flexural stress is not at the inside edge next to the

hole, stresses at that location may elevate significantly, necessitating inspection for small cracks/tears in the web that could initiate a fatigue failure.

4.3.8: Vertically Shifted Holes

Previous sections have all focused on holes which are vertically centered on the web. This was a simple place to begin analysis, but it is possible that holes encountered in the field would not be vertically centered in the web. The trends developed for vertically centered webs required several dozen tests to be run with finite element analysis, and time constraints did not allow as many tests to be run again for members with vertically shifted holes. Analysis set 7 employed finite element analysis to make some basic comparisons between maximum stresses in vertically centered and vertically eccentric holes. Beam set A was employed.

Before Stress Shift: It has been established that while holes are smaller than a certain size, the maximum flexural stress around the hole is still found at the extreme fiber of the cross section on the inside hole edge. Figure 4.44 demonstrates the trend in the maximum flexural stress at the inside hole edge as vertical eccentricity increases.

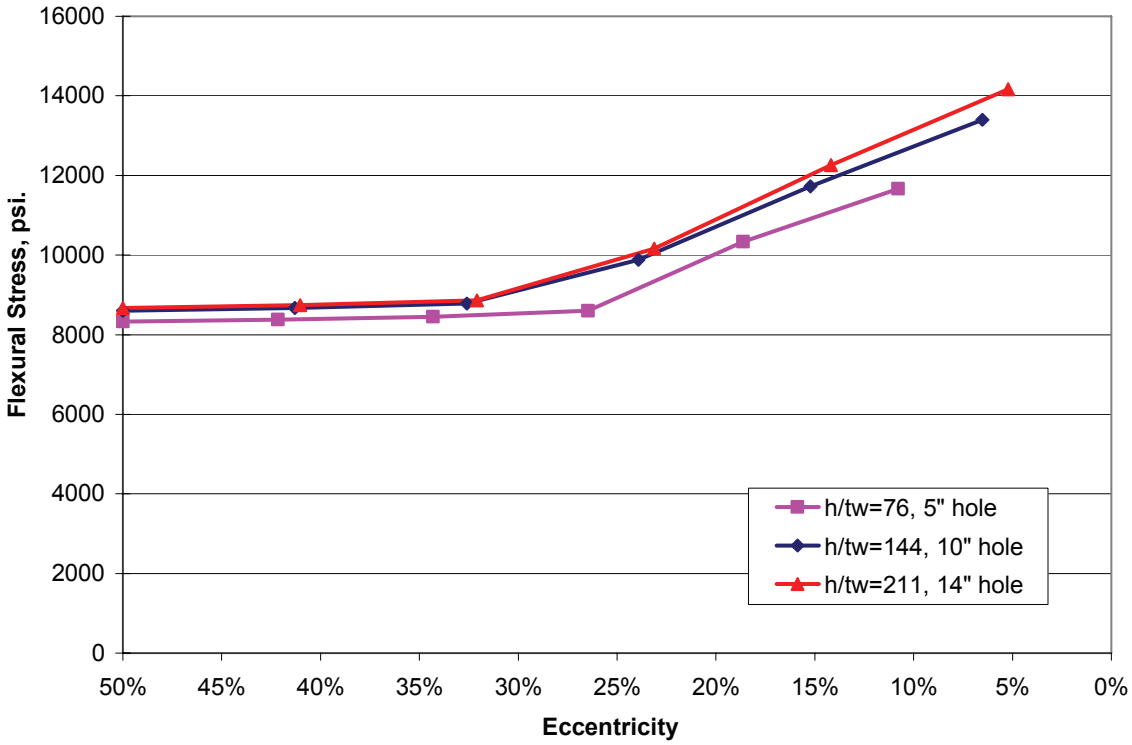

Figure 4.44: Maximum Stress at Inside Hole Edge with Increasing Vertical Eccentricity

Three widely varied h/t_w ratios were used, and each case employed a hole depth about 17% of total member depth (this hole was smaller than the stress shift size in each case). Vertical eccentricity is increasing from left to right across the x-axis; eccentricity is defined here as a ratio of the web area below the hole divided by the total remaining web area, a/(a+b). See Figure 4.45 for "a" and "b." Note that 50% will be vertically centered, and decreasing percentages correspond to downward shifting of the hole.

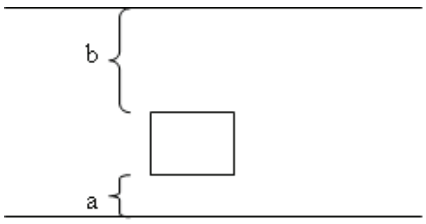

Figure 4.45: "a" and "b" in Eccentricity Definition

Figure 4.44 demonstrates that depending on h/t_w ratio, the hole can be shifted down until only 1/3 to 1/4 of the remaining web area is below the hole without causing significantly higher stresses than those caused by vertically centered holes. For greater amounts of eccentricity, the maximum stresses begin to increase at roughly 2% for each additional 1% eccentricity.

After Stress Shift: After stress shift has occurred, the maximum flexural stress will occur next to the hole at the cross section on the outside hole edge. Figure 4.46 is similar to Figure 4.44; it utilizes the same three beams and displays the maximum stresses at the outside hole edge as vertical eccentricity increases.

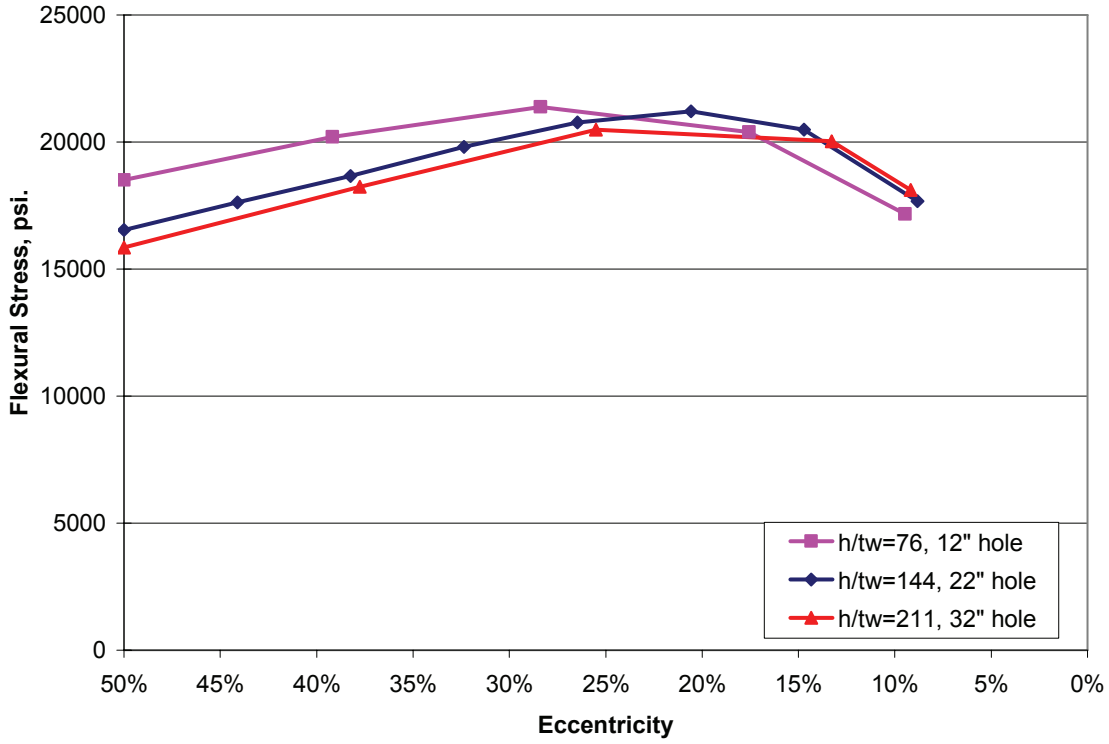

Figure 4.46: Maximum Flexural Stress at Outside Hole Edge with Increasing Vertical Eccentricity

The holes used in Figure 4.46 are all about 39% of total member depth, and were large enough that stress shift has already occurred. At the outside hole edge after stress shift, eccentricity immediately causes an increase in maximum flexural stress. The stress increases at a rate of approximately 1% for each 1% of vertical eccentricity (0.84%/1% for h/t_w=76, 1.08%/1% for h/t_w=144, and 1.23%/1% for h/t_w=211). This may continue until 1/3 to 1/5 of the remaining web area is below the hole (depending on h/t_w ratio), at which point the maximum stresses begin to decrease again.

Chapter 4 dealt with several issues regarding flexural stress distributions around web holes. Analysis set 2 showed that for small holes, flexural stress distributions are best predicted by beam theory. As holes get larger, the maximum flexural stress will be found

next to the hole instead of at the extreme fiber of the beam. At this point, the magnitude and location of the maximum flexural stress appear to be better predicted by the Vierendeel method. Analysis set 5 demonstrated that the hole size required to cause stress shift tends to increase with h/t_w ratio, until a point at which stress concentrations govern over the shear-induced moment. Also, the difference between finite element and Vierendeel predictions for stress shift tends to increase linearly over the h/t_w range observed. Analysis sets 3 and 4 showed that for holes in no-shear regions of beams, beam theory adequately predicts the location and magnitude of the maximum flexural stress. Analysis set 6 revealed that even at hole corners where flexural stress is not at a maximum level, stresses can be significantly elevated from beam theory predictions. This stress elevation is pertinent because it could lead to fatigue failures. Finally, analysis set 7 dealt with maximum flexural stresses around vertically eccentric holes. Before stress shift, holes can be shifted so that only 1/3 to 1/4 of the remaining cross section is below the hole before maximum stress is significantly higher than for a vertically centered hole. After stress shift, maximum stress begins to elevate immediately with vertical eccentricity. For the three geometries studied, stress increases at a rate of approximately 1% for each 1% of eccentricity, until a maximum stress is reached and maximum stresses begin to decline again.

CHAPTER 5: PLASTIC MOMENT CAPACITY

Bridge design often utilizes the plastic capacity of members as a limit state. The plastic capacity (or the plastic moment) is defined as the moment which causes (theoretically) every fiber in the member to yield. This requires a member with elements compact enough to fully yield before buckling. Chapter 2 demonstrated that for many members with thinned flanges or holes in the web, the loss in lateral torsional buckling capacity was overshadowed by the loss in plastic moment capacity. Chapter 3 focused largely on the location of maximum flexural stresses, which can be a concern for first yielding and fatigue. Chapter 5 considers the plastic moment capacity of sections with web holes in greater depth. For a beam with a hole in the web, the plastic moment (Mp) can easily be calculated without the help of the finite element method. A spreadsheet was used to calculate Mp by simply performing a force balance to determine the location of the plastic neutral axis (PNA), then summing moments about the PNA to determine capacity.

5.1 Vertically Centered Holes

Figure 5.1 demonstrates the loss in plastic moment capacity versus hole size for beam Set A (14”x1” flanges, 0.375” thick variable height webs). In addition to the beams from Set A, a W27x94 is plotted. Holes are vertically centered. For all beams, the loss in plastic capacity increased non-linearly with increasing hole size. This is to be expected; if the moment capacity were simply affected by the loss of area, a linear increase would occur. However, for increasing hole sizes, more area is being removed further and further away

from the neutral axis. Since a moment is the product of a stress over an area times the distance to the neutral axis, the location of the area removed affects the plastic moment as well as the amount of area removed. Thus, the two factors affecting Mp yield second degree curves.

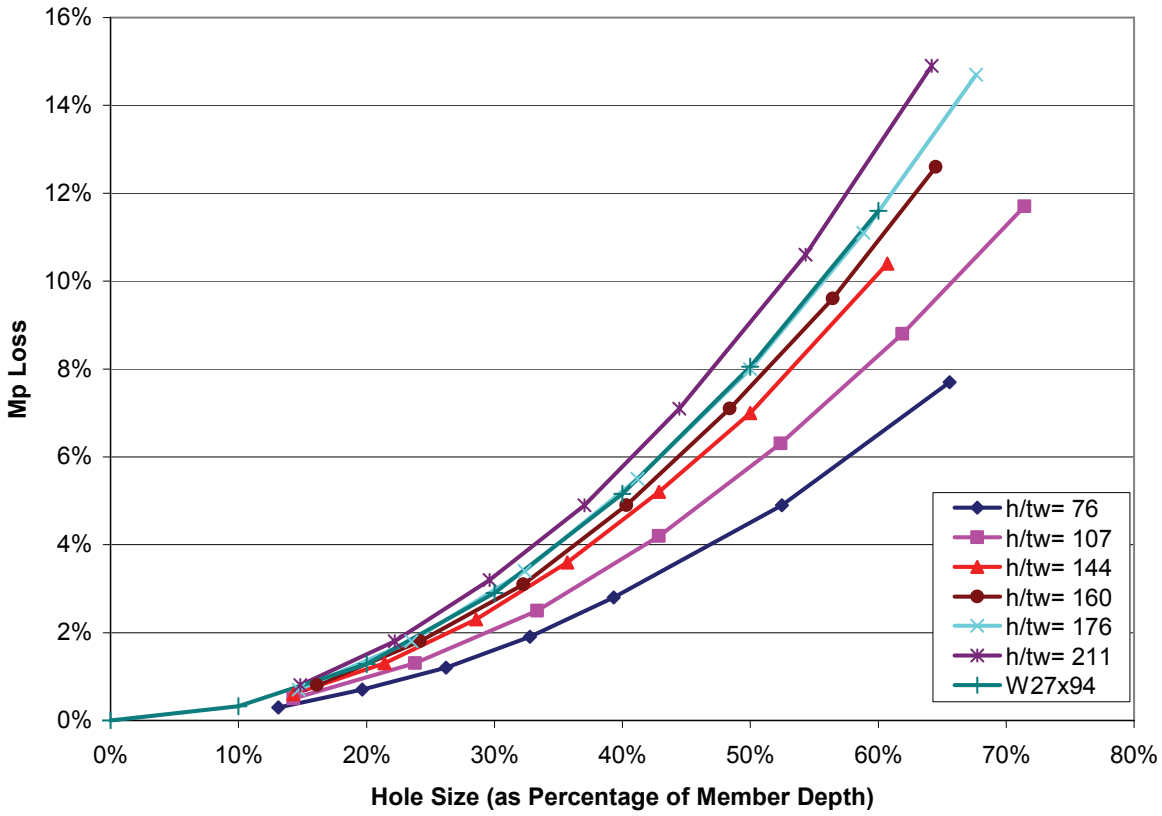

Figure 5.1: Mp Loss vs. Hole Size

Figure 5.1 also first appears to demonstrate that the loss in plastic moment capacity occurs more rapidly for beams with higher h/t_w ratios. However, the W27x94 has an h/t_w ratio of only 49.5, and it lies on almost the same curve as the Set A beam with an h/tw of 176. This indicates that sensitivity to hole size is actually dictated by how much of a beam's cross-sectional area is found in the web. The Set A beam with h/tw=176 has 46.9% of its cross sectional area in the web, while a W27x94 has about 45.3% of its area

in the web. The plot immediately above these, which is even more sensitive to web hole size, corresponds to the Set A beam with h/t_w=211. The plot below, which is less sensitive to web hole size, corresponds to Set A beam with h/t_w=160. These beams have 51.4% and 44.6% of their areas in their webs, respectively. This confirms that sensitivity to web holes is directly linked to the percentage of a beam's total area found in the web.

Similar plots were generated for beam Set B (18"x1" flanges, 0.375" variable height webs) and beam Set C (14"x1" flanges, 0.25" variable height webs), and are included in Appendix D. These plots confirm that for the other two geometries, the trend is the same. Differences in the individual plots are the result of a difference in web areas. Again, the more of a beam's area is contained in the web, the more sensitive it will be to the loss of web area.

Figure 5.1 demonstrates that vertically centered web holes need to be relatively large to affect most beams. For a beam with an h/t_w ratio of 76 (27.6% of area in the web), a hole of approximately 65% of total member depth only reduces plastic moment capacity about 8%. For a beam with an h/t_w ratio of 211 (51.4% of area in web), a hole of approximately 65% of total member depth reduces plastic capacity about 15%.

5.2 Vertically Eccentric Holes

As shown previously, vertical hole eccentricity affected maximum flexural stress. In a similar fashion, shifting the hole vertically will also affect the extent of Mp loss. To examine the effects of vertical eccentricity, beam Set A was again studied. Three beams were picked out of the set, and similar sized holes were placed in all three beams (all

holes sizes were approximately 17% of member depth). Figure 5.2 demonstrates the results. Note that eccentricity is denoted by the percent of the remaining cross section located in the bottom tee, as it was in section 4.3.8. Fifty percent on the x-axis corresponds to a vertically centered hole. As can be seen, plastic capacity decreases linearly with increasing eccentricity. Shifting the hole away from the neutral axis means more area remains near the neutral axis and less area remains at the extreme regions of the web. However, merely shifting the hole does not decrease the total amount of steel present. Thus, there is one parameter affecting plastic capacity loss, yielding a first degree curve. As with vertically centered holes, the beams with higher h/t_w ratios show steeper slopes when plastic capacity loss is plotted. This is again explained by the fact that for the beams with higher h/t_w ratios, more of the cross-sectional area is in the web.

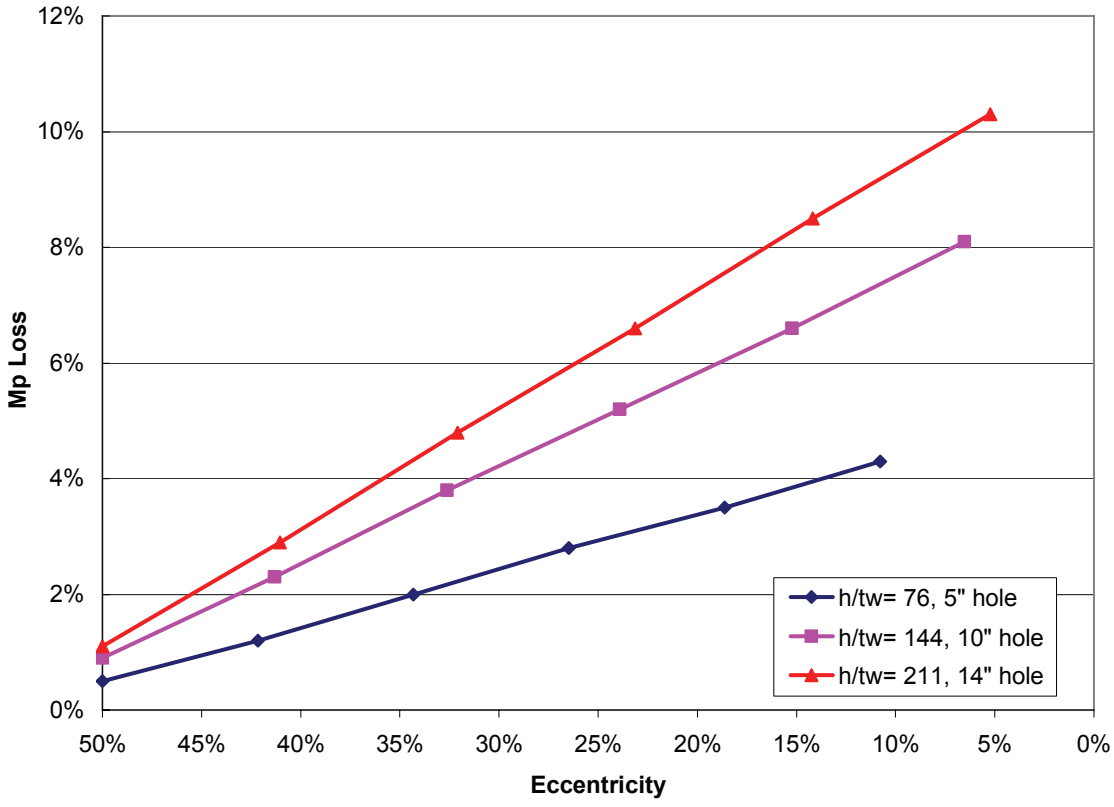

Figure 5.2: Mp Loss vs. Hole Eccentricity

Figure 5.3 provides an upper bound for the problem; for the three different beam geometries which have been used, the webs were removed entirely and the loss in capacity plotted against varying h/t_w ratios. As can be seen, the rate of Mp loss gradually slows as h/t_w ratio increases. For these beams, increasing h/tw ratios were achieved by increasing web depth. The increase in lost web area is more than offset by the increasing distance between the flanges and the plastic neutral axis. Clearly, beams with more cross-sectional area in the web are more sensitive to the loss of the web, so compact sections such as the W27x94 previously mentioned will suffer even greater loss. The plastic moment capacity of the W27x94 is reduced by 28.7% when the entire web is removed. Note that this is a hypothetical situation. Full web removal would likely lead to other failure modes, such as shear failure or vertical compression flange buckling.

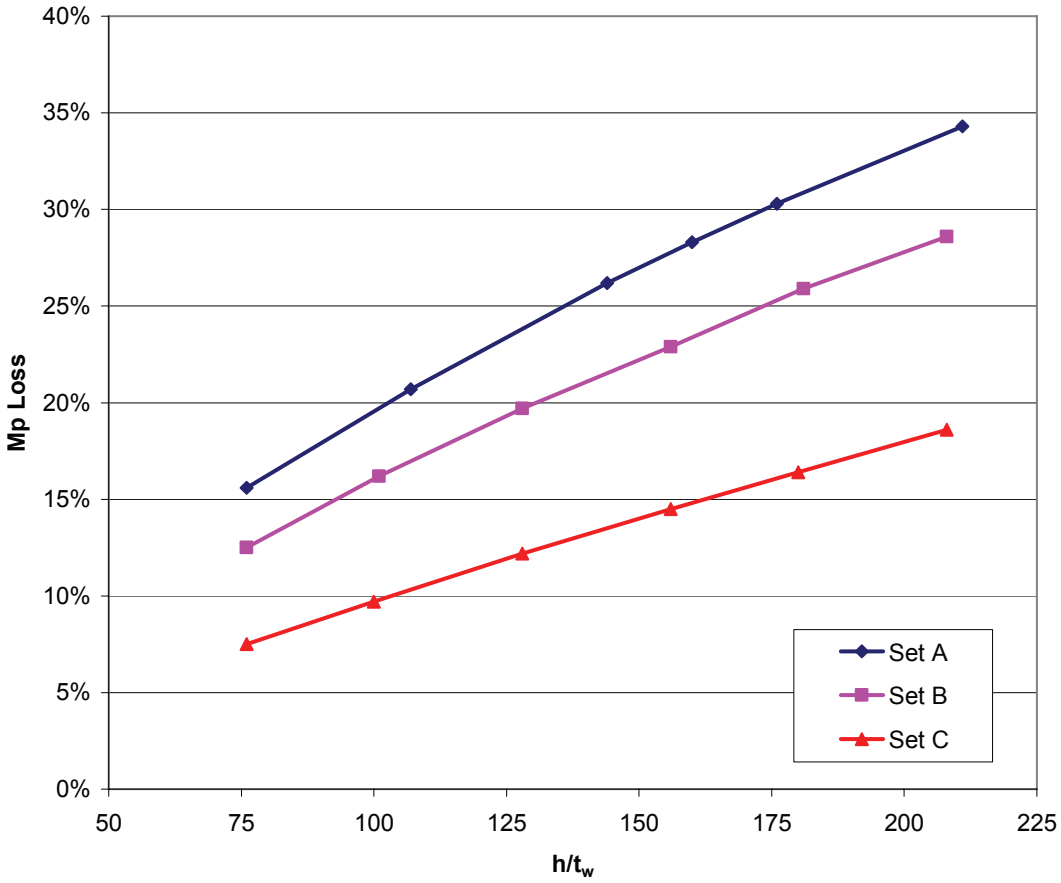

Figure 5.3: Mp Loss with Entire Web Removed

Because decreased plastic capacity is directly affected by variations in beam geometry, it is difficult to make specific statements about plastic moment capacity. In general, calculating plastic capacity for the specific situation at hand is probably the most effective means of determining capacity loss. However, Table 5.1 provides a snapshot of capacity loss for beams with a 4" hole at the bottom of the web. (Four inches was chosen arbitrarily; and it is assumed that corrosion may frequently cause holes at the bottom of the web. This is a very damaging location for the hole as well, since the missing area is far from the neutral axis.) The bottom edge of the hole is assumed to rest on the top surface of the bottom flange. The beams used are rolled sections provided in the

Oklahoma Department of Transportation Bridge Standards for spans from 30' to 50'. A 4" hole is large for these beams, even for the deepest section it is 12% of the member depth. For the smallest section, the hole is 15% of the member depth. However, Table 5.1 shows that plastic capacity losses range between 7% and 9%. It is not likely that a 4" hole would be allowed to go unrepaired, and for commonly used beam sizes this hole would still result in plastic capacity losses less than 10%. In general, beams with large percentages of their total cross sectional area in the web will be more susceptible to plastic capacity loss in the presence of web holes. However, it takes large holes to cause significant capacity loss.

Beam	Mp Loss
W27x84	9.0%
W30x90	8.9%
W30x99	8.9%
W30x116	8.0%
W33x130	7.4%

Table 5.1: Mp Loss For Common Rolled Sections, 4" Hole Bottom of Web

CHAPTER 6: IMPACT DAMAGE

The objectives discussed in section 1.3 included an examination of vehicular impact damage. An extensive study of impacted members was not performed, but several basic tests were run to demonstrate some general trends present in impacted members.

Tests utilized the standard test section (W27x94). The beam consisted of two continuous 30' spans, with a total length of 60'. The beam was simply supported, but the entire top flange was restricted from lateral translation and rotation about the longitudinal axis. These conditions were implemented to model full composite action with a concrete deck. A rigid cube 6' wide (to simulate the width of a truck) impacted the bottom of the beam at three different velocities. Figure 6.1 shows an ABAQUS screen shot of the cube and beam before impact.

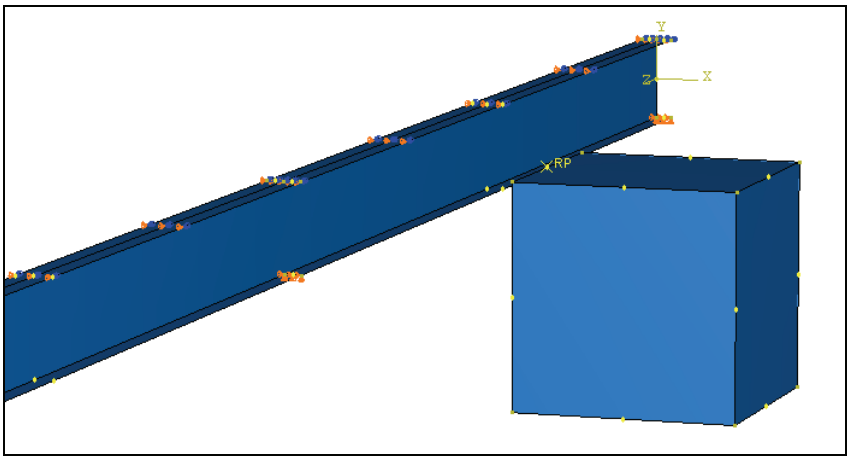

Figure 6.1: Block and Beam Before Impact

The top edge of the block extended just above the bottom flange, reaching approximately 5/8" into the web. The center of the block impacted the beam 11.25' from one end (3/8 of one span), which coincides with the point of maximum positive moment under a uniformly distributed load. The three different impact velocities were 100 in/s, 200 in/s, and 400 in/s. These convert to 5.7 mph, 11.4 mph, and 22.7 mph, respectively. These velocities were somewhat arbitrarily chosen to provide different degrees of damage. Although these are not typical highway speeds, note that the impacting block is modeled as a perfectly rigid body. Actual impacts will likely be at higher speeds, but the impacting bodies will never be perfectly rigid. The purpose of the impacts was not necessarily to match the mechanics of an accident, but rather to generate reasonable initially deformed shapes. (Initial attempts utilized an impact speed of 1,232 in/s, or 70 mph, but the finite element simulation aborted and no damaged shape was generated. Since generating a damaged shape was more important than using a specific speed, lower speeds were adopted.) Figures 6.2, 6.3, and 6.4 demonstrate the web and flange distortion caused by the three different impact velocities.

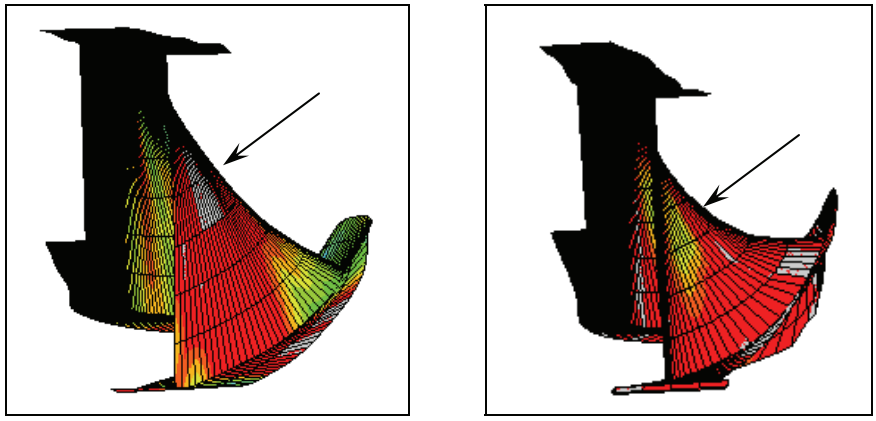

Figure 6.2: Impact Damage at 100 in/s
Figure 6.3: Impact Damage at 200 in/s

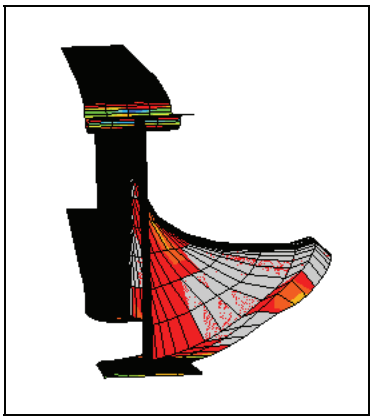

Figure 6.4: Impact Damage 400 in/s

At first glance, the damaged shape for 200 in/s does not appear to be much more distorted than the shape for 100 in/s. However, the difference is apparent if the web curvature at the center of the damage is examined (see arrows in figures). Figure 6.3 (on the right) shows that the 200 in/s impact has left the web more curved, while the 100 in/s impact pushed the web out in more of a straight line. The 400 in/s impact has clearly created a severe distortion.

To examine the effect of impact damage on beam behavior, a uniformly distributed load was applied to the top flange of the damaged beams. As the load was applied, the vertical displacement at midspan (of the damaged span) was recorded. Midspan was actually 3.75 feet from the center of impact. This location was chosen because it is still near the maximum moment location, but not directly over the impact site. Displacements at this location should be more indicative of global beam behavior, instead of simply reflecting local behavior at the damage site. Load vs. displacement plots for an undamaged beam and for all three impact velocities are shown in Figure 6.5.

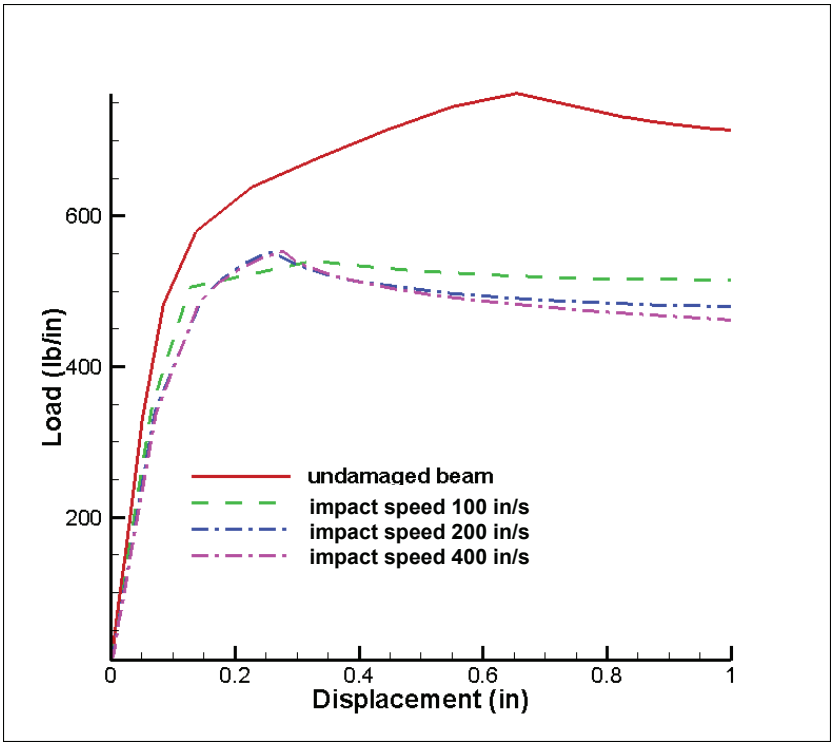

Figure 6.5: Load vs. Displacement Plots for Impact Damaged Beams

The undamaged section does not show a well-defined upper limit. For purposes of comparison, the load values at a displacement of approximately 0.26" are examined (at 0.26", the 200 in/s and 400 in/s impacted beams have a more clearly defined upper limit. The load values at 1" of vertical deflection are compared to examine post-buckling strength. Results are shown in Table 6.1.

Impact Velocity (in/s)	Load (k/ft) at 0.26 in. Vertical Deflection	Load (k/ft) at 1.0 in. Vertical Deflection
0	7.80	8.58
100	6.36	6.24
200	6.50	5.70
400	6.50	5.52

Table 6.1: Load and Displacement Values for Impacted Beams

At 0.26" deflection, the load capacity of the undamaged section is 18.2% higher than that of the 200 and 400 in/s damaged beams (22.6% higher than the 100 in/s beam). At 1.00" deflection, the capacity losses are 27.3%, 33.6%, and 35.7% for the 100 in/s, 200 in/s, and 400 in/s damaged beams, respectively. These numbers indicate that there is a significant decrease in yield capacity (up to approximately 35%). Post-buckling capacity losses are even more significant, as indicated by Figure 6.6. Figure 6.6 also demonstrates the fact that the loss in post-buckling strength is not linear; doubling the impact velocity does not double the loss in post-buckling strength.

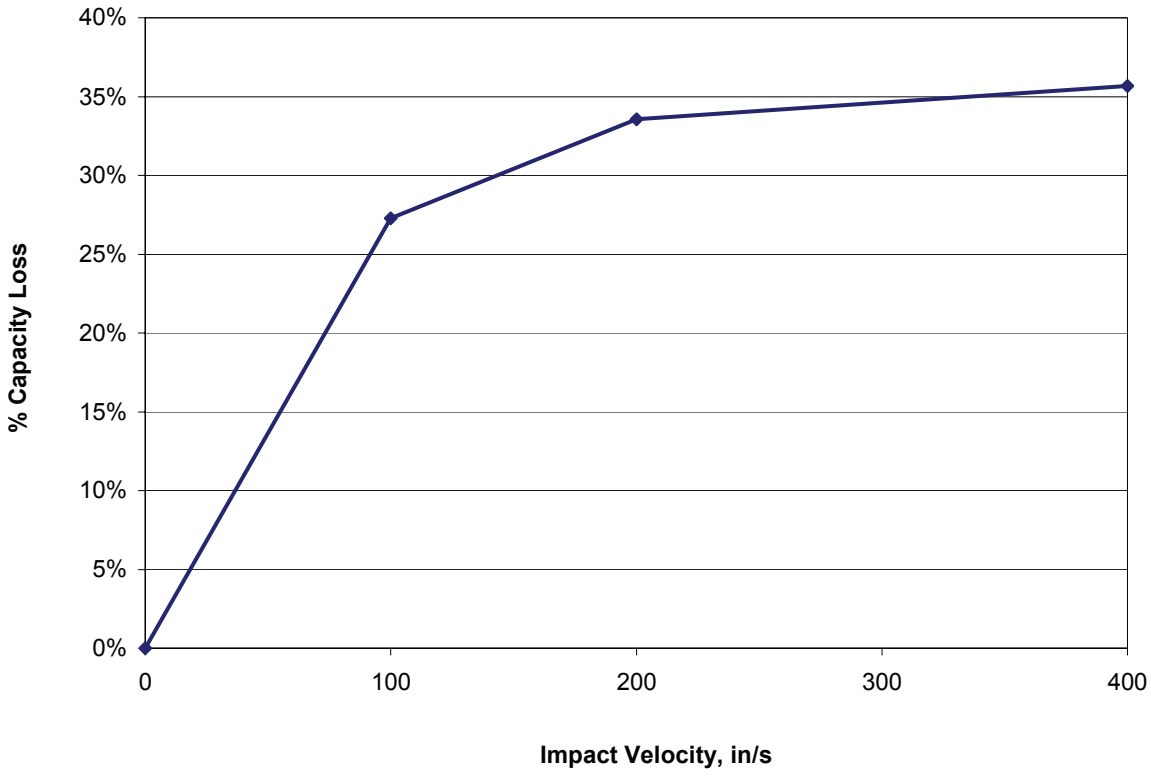

Figure 6.6: Post-Buckling Capacity Loss for Different Impact Velocities

CHAPTER 7: STRESS ANALYSIS WITH MISSING BEAM

Previous analyses have examined the effects of damage on a single member. However, beams in bridges are part of a structural system consisting of multiple beams and a deck. If a single beam sustained severe enough damage, engineers may decide it has little to no effective capacity remaining. In this case, it may be of interest to examine the remaining structural capacity of the system, i.e. the entire bridge. The question is if enough capacity remains for the bridge to carry limited traffic (closing the lane over the damaged member, restricting the traffic to emergency vehicles only, etc.) To examine this, a very preliminary analysis with a simple four-beam bridge was studied to determine how stresses were redistributed if one beam were completely removed.

7.1 Bridge Model

After discussion with the Oklahoma Turnpike Authority, a basic bridge model was developed. Figure 7.1 shows a sketch of the bridge cross section.

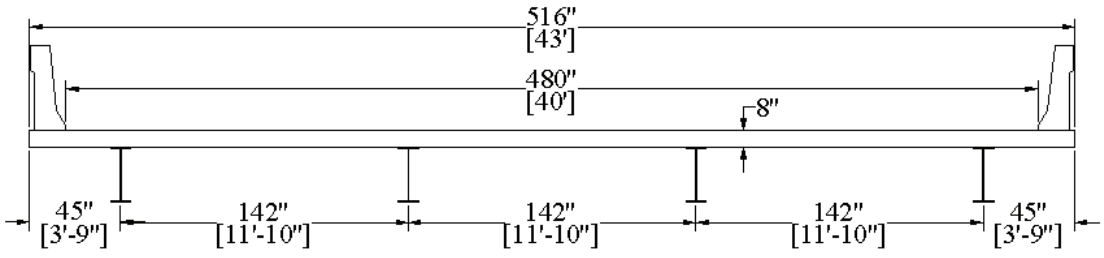

Figure 7.1: Cross Section of Bridge Model

The cross section was derived from Oklahoma Department of Transportation standards B-263 and B-346. An F-shaped parapet was also added, (standard B-004) which affected the overhang widths. However, this parapet was later removed from the finite element model, but the deck dimensions were left the same. (Including an integral parapet created an extremely stiff deck. The parapet was excluded to ensure conservatism of the model.) Beams are W27x84, 50 ksi steel. The deck is 8" thick, 4000 psi concrete, and is assumed to be fully composite with the beams. For simplicity, the bridge is one 30' simple span, with no additional lateral support.

7.2 Loading Conditions

The bridge was loaded as shown in Figure 7.2. The black rectangles labeled 1-6 are 10" x 20" tire contact areas. Areas 1 and 2 carry a total weight of 4000 lbs. each, while areas 3-6 each carry 16000 lbs. These weights correspond to those of the standard HS20 truck. The second axle (areas 3 and 4) is centered directly over midspan of the bridge.

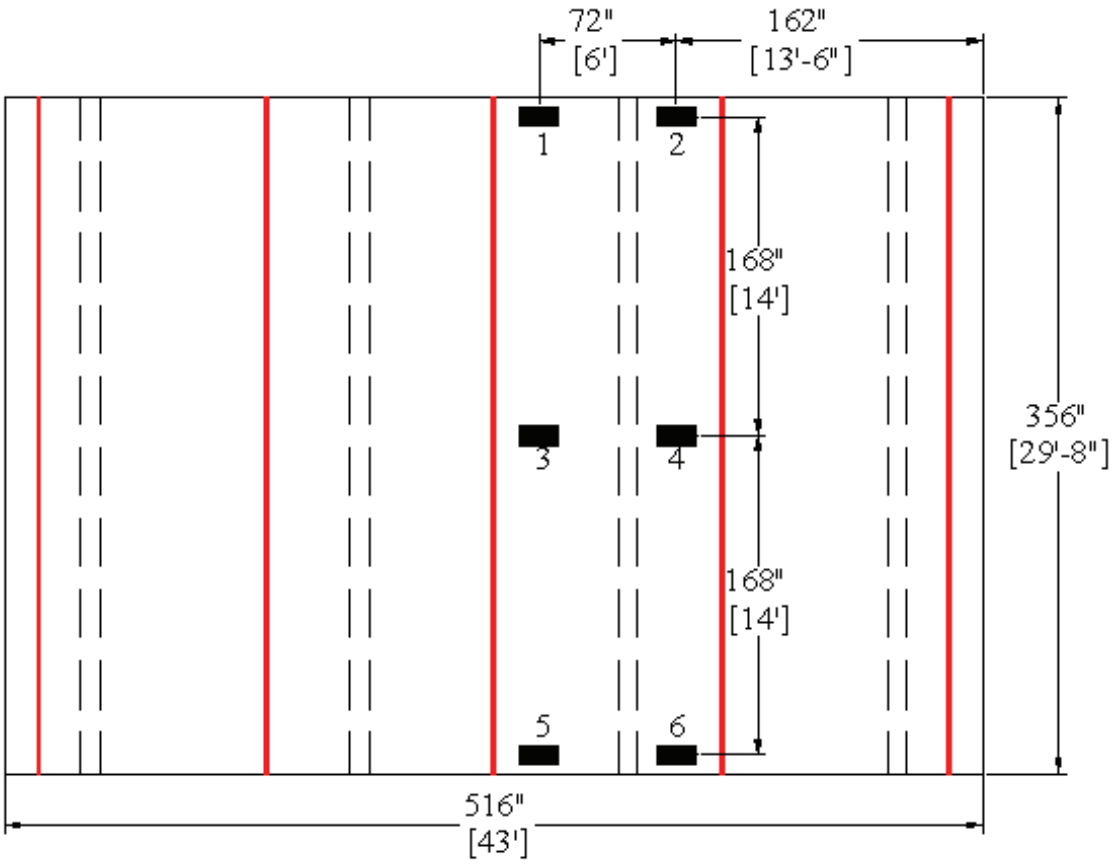

Figure 7.2: Load Positioning on Bridge

The dashed lines in Figure 7.2 indicate the position of the beams beneath the bridge deck. Beams are numbered 1-4 from left to right. The truck is not centered directly over a beam because the clear span of the deck was originally divided into four lanes of 10' width (indicated by the red lines in Figure 7.2). The truck has been centered in the 10' lane, not over the beam. As this was only a preliminary examination, tests were only run with the truck in the lane indicated in Figure 7.2.

7.3 Flexural Stresses in Beams

After loads were applied as shown in Figure 7.2, finite element analysis was used to analyze the flexural stress distributions through midspan of the beams. Stress

distributions were first obtained for the undamaged condition when all beams were present. Two more conditions were also analyzed, one for each outside beam being completely removed. These two conditions were chosen because the outside beams are most exposed to vehicular impact; thus it is most likely that these beams would be taken out of service.

7.3.1: All Beams Present

Stress analysis was first performed with all beams present. A snapshot of the finite element model used is shown in Figure 7.3.

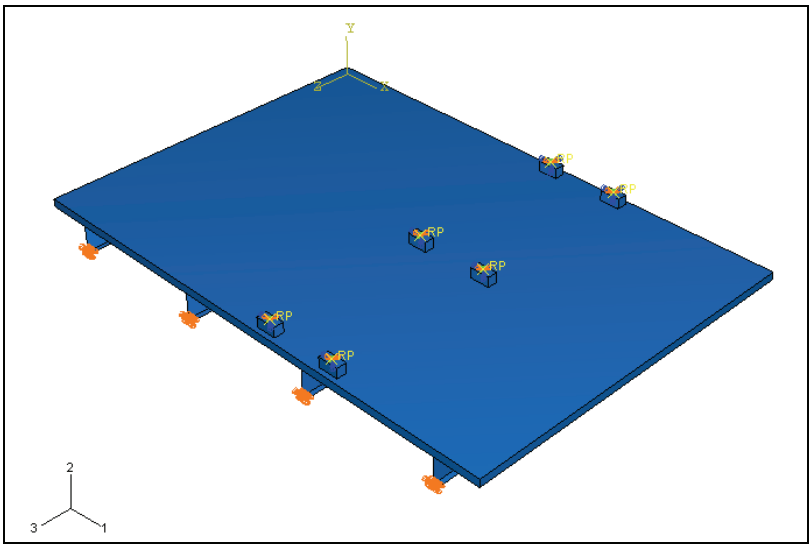

Figure 7.3: Finite Element Model, All Beams Present

Note that the parapets have been removed, and the loads are applied by point loads acting through rigid blocks. Results from the stress analysis with all beams present are plotted below in Figure 7.4. The top of the beam has been used as the reference point for vertical positioning, giving all points in the beam cross section negative location values.

As shown, the highest stress occurs in the beam beneath the truck and the lowest stress is in the beam farthest from the truck. The beams adjacent to the truck (beams 2 and 4) have nearly equal maximum stresses, but the stress in beam 2 is slightly higher. This is due to the fact that the truck is not centered over beam 3 but is shifted toward beam 2. Note the beams are entirely in tension due to the composite nature of the system.

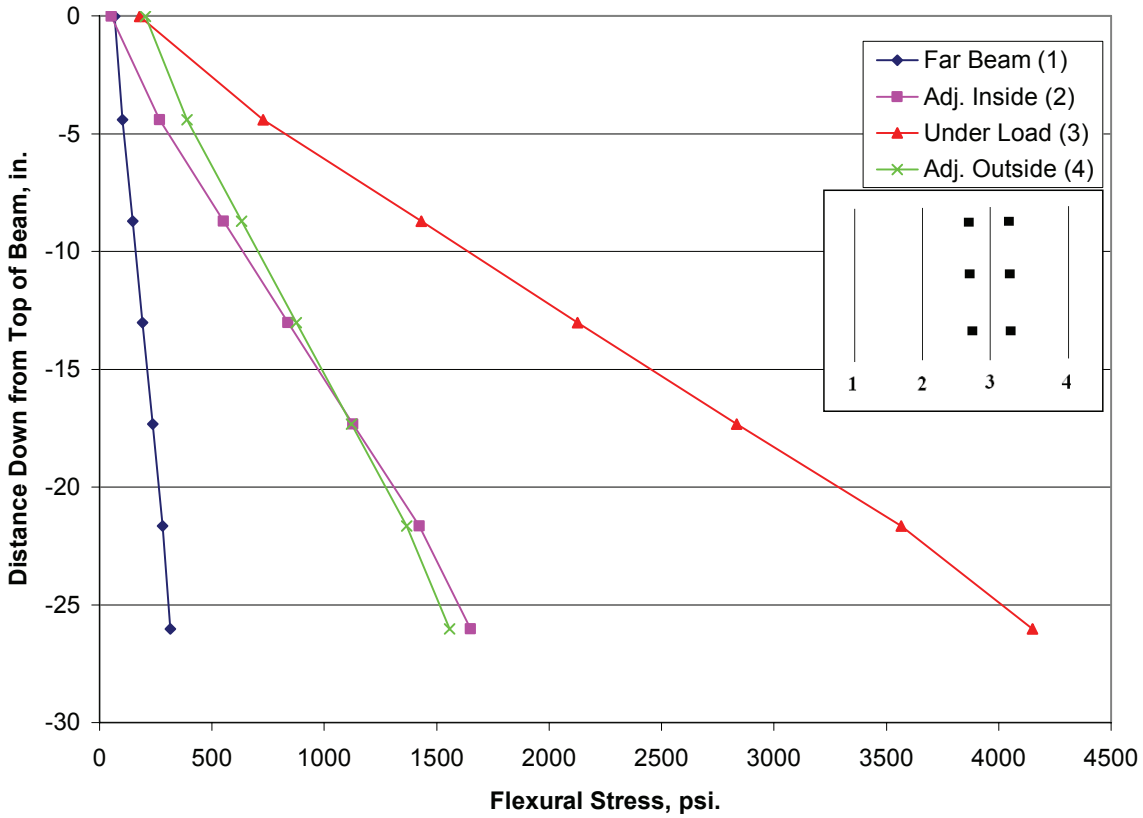

Figure 7.4: Flexural Stress Distributions, All Beams Present

7.3.2: Beam 1 Removed

The next test was run with Beam 1 (farthest from the truck) removed. The results are plotted in Figure 7.5. The dashed lines are present for comparison; they represent the stress distributions obtained when all beams were present. Figure 7.4 demonstrated that Beam 1 was carrying a small portion of the load, so its removal did not have a large

effect on the remaining beams. The maximum flexural stress in Beam 2 increased by 7.4%, while the maximum flexural stress in Beam 3 increased by 5.7%. The maximum flexural stress in Beam 4 actually decreased by 9.3%. It is suspected that this is a result of the unsupported deck area where Beam 1 used to be. The weight of the deck is now unbalanced and tries to pivot about Beams 2 and 3, causing an upward force on Beam 4 which counteracts part of the truck loading.

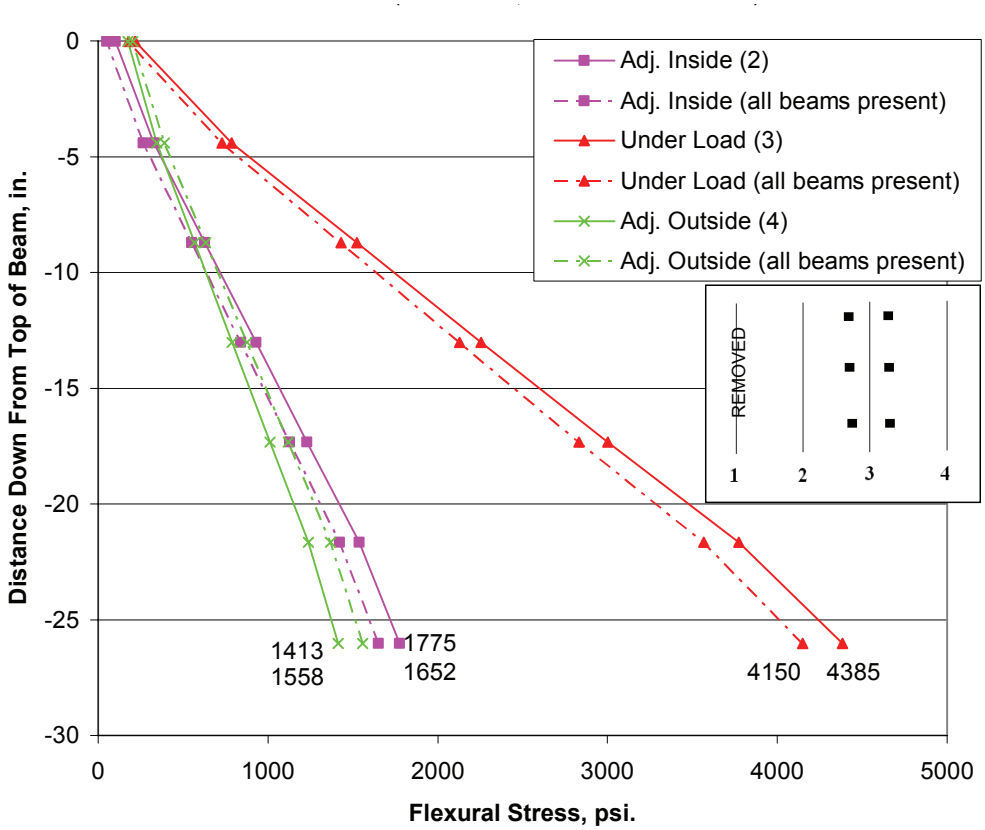

Figure 7.5: Flexural Stress Distributions, Beam 1 Removed

7.3.3: Beam 4 Removed

The next test was run with Beam 4 removed. Results are plotted in Figure 7.6. Because Beam 4 was next to the load, its removal had a larger impact than the removal of Beam 1.

The maximum flexural stress in Beam 2 increased 21.4%, and the maximum flexural stress in Beam 3 increased 37.6%. The maximum flexural stress in Beam 1 went from 0.315 ksi (tensile) to -0.222 ksi (compressive). It is again theorized that this is a result of uplift from the slab due to the unbalanced deck support.

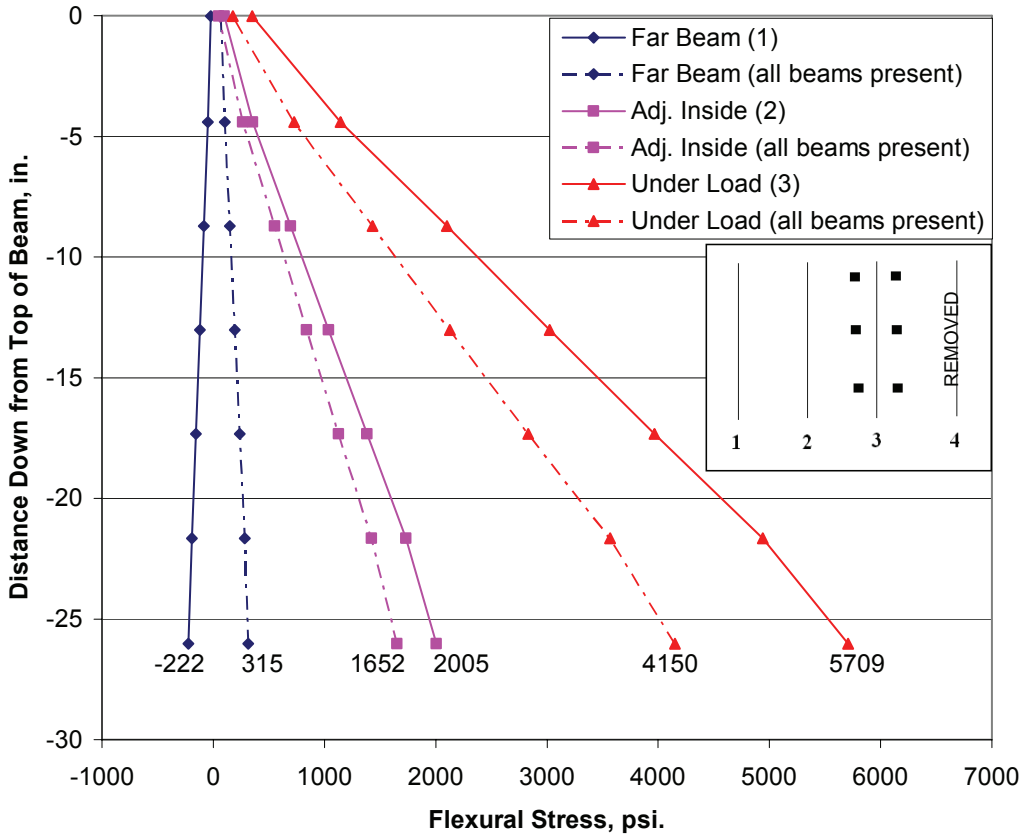

Figure 7.6: Flexural Stress Distributions, Beam 4 Removed

The three test cases examined do not provide comprehensive results as they do not address all load cases and conditions, nor do they look at all failure modes in the bridge. However, they do seem to indicate that if an outside beam of a standard four-beam bridge is removed, it may be possible for some traffic to be allowed without causing unsafe flexural stresses in the remaining beams. In a case such as Section 7.3.2 (Beam 1 removed, trucks passing over Beam 3), truck traffic will cause less than a 10% increase in

flexural stress. Hence, in examining flexural stress in the beams, removing an outside beam may still allow at least one lane of traffic to pass safely. Further testing would be necessary to determine whether two narrow lanes of traffic could be safely permitted in the absence of an outside beam, and the best position for a single lane.

CHAPTER 8: CONCLUSIONS

8.1 Introduction

The affects of three main damage types on bridge girders have been considered: flange thinning, square or rectangular web holes, and vehicular impact. Non-linear finite element analysis was used to model beams with flanges which had been thinned to varying extents, and the buckling capacity was analyzed. In some cases the bottom flange had been thinned for the full length of the beam and only part of the flange width, and in other cases the full width of the flange was thinned for only part of the beam length. Beams were also modeled with holes of various sizes and locations in the web, and the buckling capacity examined.

Flexural stress distributions at the edges of vertically centered web holes were also examined with finite element analysis, and were compared to flexural stress distributions predicted by a technique known as the Vierendeel method. Holes of widely varying sizes were examined with both the Vierendeel method and finite element analysis, and finite element analysis was also used to briefly examine the effect of vertical eccentricity on the stress distributions around web holes. Also, calculations were performed in spreadsheets to examine the effects of web holes on plastic moment capacity. Finite element analysis was used in a preliminary study of the ultimate and buckling capacity of a beam

subjected to impact damage, as well as a preliminary study of the effects of removing a beam from a four-beam bridge system.

8.2: Flange Thinning

If a portion of the bottom flange width is thinned for the entire length of the beam, buckling capacity decreases linearly with the increase in damage width. If the full width of the flange is thinned for part of the beam length, there is a non-linear decrease in buckling capacity. However, as with web holes, the buckling capacity loss is overshadowed by the loss in ultimate moment capacity. Thinned flanges will affect the flexural stress distribution because they will change the location of the neutral axis. With a new neutral axis calculated, the flexural stress distribution can still be determined using simple beam theory, $\sigma = My/I$.

8.3: Web Holes

8.3.1: Buckling Capacity

Web holes have relatively small impact on the buckling capacity of beams, typically causing less than 1% capacity loss. If web holes become large enough, they may cause a buckling capacity loss of a few percent. For example, a 30' long W27x94 with a vertically and horizontally centered web hole of dimensions 120" x 12" (33% of member length and 45% of member depth) caused approximately 2% loss in lateral torsional buckling capacity. Extensive parameter testing was not done on web holes and buckling capacity, because it became apparent that by the time web holes were large enough to cause significant buckling capacity losses, other failure modes would govern.

8.3.2: Web Holes and Flexural Stress Distribution

The presence of a web hole affects the magnitude and location of the maximum flexural stress. For small holes, the maximum flexural stress is still found at the extreme fiber of the beam, and the magnitude can still be reasonably (within 5%) predicted with the elementary beam formula, $\sigma = My/I$. As the hole becomes larger, the maximum stress will be shifted away from the extreme fiber. However, the hole size required to initiate this shift is dependent on beam geometry. Three sets of beams were modeled, with varying h/t_w ratios, flange widths, and web thicknesses. For these beam sets, the finite element method indicated stress shift would occur at hole sizes ranging from about 12% to 24% of member depth (for the W27x94, finite element predicted shift at 35%). A simple hand method, (the Vierendeel procedure discussed in section 4.2) predicts the shift in location of maximum stress. However, the Vierendeel method consistently predicts a larger hole is required to induce stress shift than the finite element method predicts (Vierendeel predictions for hole size tended to range from 20% to 45% of member depth). This is due to the fact that the Vierendeel method does not account for stress concentrations at the hole corners. The difference between the hole size predicted by the finite element method and the Vierendeel method to cause stress shift will increase linearly with an increasing h/t_w ratio for a given beam geometry. For a W27x94, which has a relatively low h/t_w ratio and is similar to commonly used rolled shapes, finite element predicts a hole 6% smaller than that predicted by the Vierendeel method. After the maximum stress location has shifted, the Vierendeel procedure will predict the magnitude of the stress better than simple beam theory, but underestimates the stress as compared to finite element analysis by as much as 40%. After hole sizes become quite

large (square hole dimensions approximately 50-65% of member depth), Vierendeel predictions of maximum stress are again within 5% of those predicted by finite element analysis.

8.3.3: Web Holes and Plastic Moment Capacity (Mp)

The presence of a web hole will reduce the ultimate moment capacity of the beam. How sensitive capacity loss is to web loss is reflected by how much of the beam's cross sectional area is located in the web versus how much area is in the flanges; the higher the percentage of total area located in the web, the greater the impact of web area loss. Beam Set A utilized throughout chapter 4 showed Mp loss varying from about 5-11% with a vertically centered square hole, side dimensions equal to about 55% of member depth. Hole eccentricity (vertical shift) also increases the impact of a web hole. For a given hole size, the loss in Mp increases linearly as eccentricity increases. Again, the sensitivity to eccentricity is affected by the web area ratio. For example, holes sized at about 17% of member depth were placed in the beams of Set A. As the holes are shifted down until only about 5% of the remaining web area is below the hole, capacity loss goes from about 1% to between 4% and 10%.

8.4: Impact Damage

Although the analysis was not extensive, it appears that impact to the lower flange/web area can reduce yield capacity of a beam in a composite bridge by about 20%. However, post buckling strength may decrease even more; basic tests showed severe web distortion decreasing post-buckling capacity as much as 36%.

8.5: Bridge Deck Capacity Loss Due to an Incapacitated Member

On the basis of increased flexural stress, it appears that an entire outside beam from a four-beam bridge deck may be removed from service and still allow some traffic on the bridge. This is a preliminary result, and specific bridge configurations would require further testing. However, for a 30' simple span with an outside beam removed, an HS20 truck placed over an interior beam will result in approximately an 8% increase in the maximum flexural stress beneath the loaded beam. This indicates that at least one lane could remain open for emergency traffic. Further testing would be required to determine whether two traffic lanes could be allowed, or if other failure modes would govern (prohibiting even one lane of traffic).

8.6 Future Research

The research conducted by the investigators was of limited scope due to the time constraints of the project. Various items could be addressed in the future to expand upon the previous research.

1. Stress Concentrations: One of the main reasons that Vierendeel stress predictions did not match finite element stress predictions was the apparent presence of stress concentrations at the hole edges. Current literature does not appear to address stress concentrations around square holes in flexural members. However, there is information available for round and elliptical holes (Pilkey 1997). The formulae for round and elliptical holes could be adapted to provide accurate approximations of the stress concentration factors for square holes. These could then be used in conjunction with the

Vierendeel method to provide an accurate prediction of the full flexural stress distribution, regardless of hole size, using simple hand calculation procedures.

2. Beam Geometry: Geometric parameters could be increased to encompass a greater number of sections. Current research primarily used the three girder series presented in section 4.3.5. An original series was modeled, then one series modified flange width while the other modified web thickness. These three basic beam geometries were enough to point out various trends, such as the fact that thinning the web results in less error between finite element and Vierendeel predictions for stress shift. However, if more beam geometries were studied, it might be possible to develop comprehensive design charts in which the trends illustrated here were quantified.

3. Loading Configurations: Loading configurations could also be further explored. The theory behind the Vierendeel procedure basically requires that the shear over a hole be constant, which means it applies to point loaded beams. However, if a hole were present in a uniformly loaded beam, the shear would not be constant over the length of the hole and the statics as originally presented in Chapter 4 would have to be slightly modified. This scenario could be investigated to see if the Vierendeel formula, or a modified version, could still provide useful information on the flexural stress distribution.

4. Impact Damage and Full Beam Removal: Two other areas to further investigate include impact damage and removal of one beam. Both of these areas were examined briefly for very specific circumstances. Impact could be examined with different beam geometries, support conditions, impact location, impact speed, and impacting object.

Similarly, bridge serviceability after removal of one beam could be examined with differing span lengths, loading conditions, and failure modes in order to obtain more broadly applicable data. Further literature review on this topic would be warranted, since the original literature review focused on local impact and corrosion damage.

BIBLIOGRAPHY

(2000). "National Bridge Inventory." Retrieved March 12, 2005, from http://www.nationalbridgeinventory.com/.

(2006). ABAQUS Analysis User's Manual, ABAQUS, Inc.

(2006). "International Straightening, Inc." Retrieved January 28, 2006, from http://www.steelstraightening.com/index.htm.

AISC (2001). Manual of Steel Construction: Load and Resistance Factor Design, American Institute of Steel Construction.

Allen, G. (2004). A. Finley. Stillwater, Oklahoma**:** personal electronic mail from Assistant Bridge Engineer--Design, Oklahoma Department of Transportation.

Bower, J. E. (1966). "Experimental Stresses in Wide-Flange Beams with Holes." Journal of the Structural Division, American Society of Civil Engineers **92**(ST5): 167-186.

Bower, J. E. (1966). "Experimental Stresses in Wide-Flange Beams with Holes." J. Structural Division, American Society of Civil Engineers **92**(ST5): 167-186.

Darwin, D. (1990). "Steel and Composite Beams with Web Openings." Steel Design Guide Series **2**.

Dinno, D. K. and P. C. Birkemoe (1997). Loss of Strength Associated with Corrosion of Plate Girder Webs. Annual Conference of the Canadian Society for Civil Engineering, Sherbrooke, Quebec.

Frangopol, D. M. and R. Nakib (1991). "Redundancy in Highway Bridges." Engineering Journal, American Institute of Steel Construction.

Galambos, T. V. (1998). Guide to Stability Design Criteria for Metal Structures. New York, John Wiley & Sons, Inc.

Kayser, J. R. and A. S. Nowak (1989). "Capacity Loss Due to Corrosion in Steel-Girder Bridges." Journal of Structural Engineering **115**: 1525-1537.

Kulicki, J. M., Z. Prucz, et al. (1990). "Guidelines for Evaluating Corrosion Effects in Existing Steel Bridges." National Cooperateve Highway Research Program Report **333**.

Lindt, J. W. v. d. and T. M. Ahlborn (2004). Development of Steel Beam End Deterioration Guidelines. Houghton, MI, Michigan Technological University**:** 62.

Olsson, A. M. J., G. E. Sandberg, et al. (1999). "Load-Carrying Capacity of Damaged Steel Columns with Channel Sections." Journal of Structural Engineering: 338-343.

Pilkey, W. D. (1997). Peterson's Stress Concentration Factors, John Wiley & Sons, Inc.

Salmon, C. G. and J. E. Johnson (1996). Steel Structures: Design and Behavior. Upper Saddle River, New Jersey, Prentice-Hall.

Shanafelt, G. O. and W. B. Horn (1984). "Guidelines for Evaluation and Repair of Damaged Steel Bridge Members." National Cooperateve Highway Research Program Report **271**.

Timoshenko, S. P. and J. M. Gere (1961). Theory of Elastic Stability. New York, McGraw-Hill Book Company.

APPENDIX A: FINITE ELEMENT VS. VIERENDEEL PREDICTIONS FOR STRESS SHIFT, BEAM SETS B AND C (SECTION 4.3.5)

Figure A1: Beam Set B

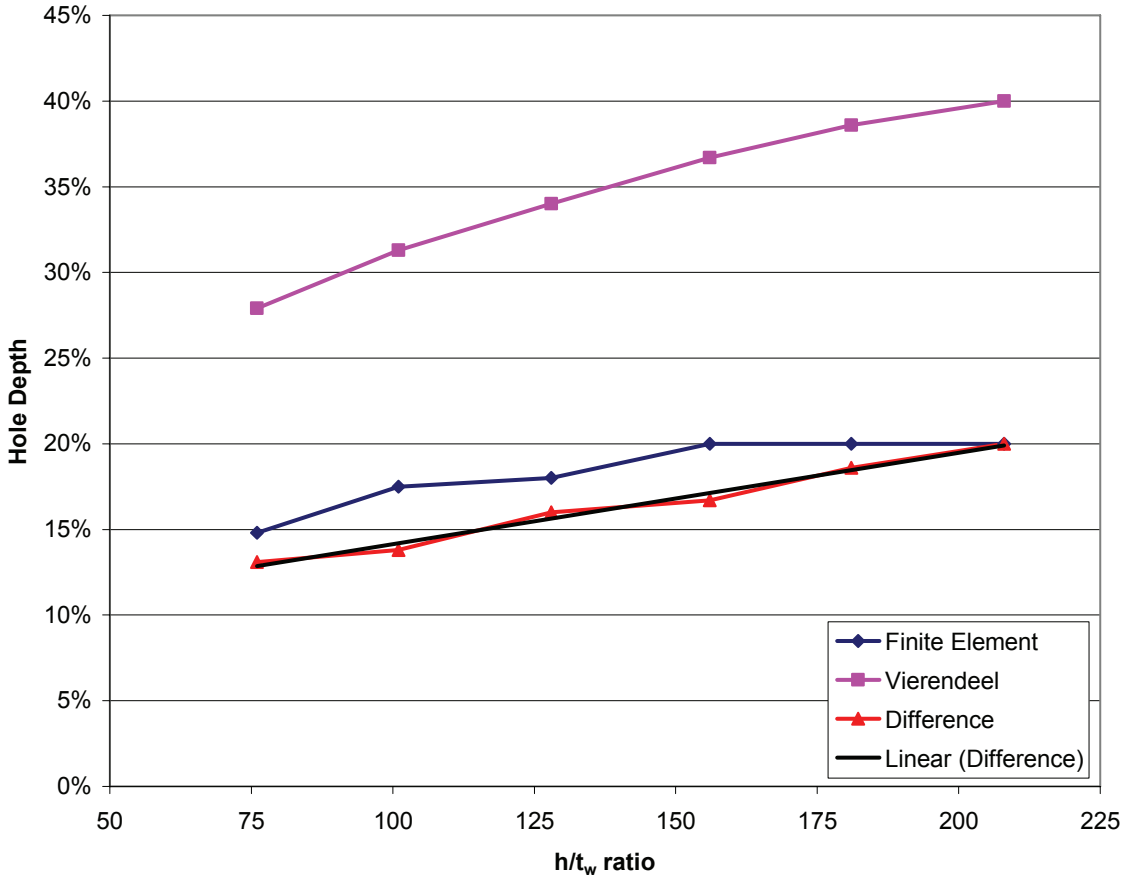

Figure A2: Beam Set C

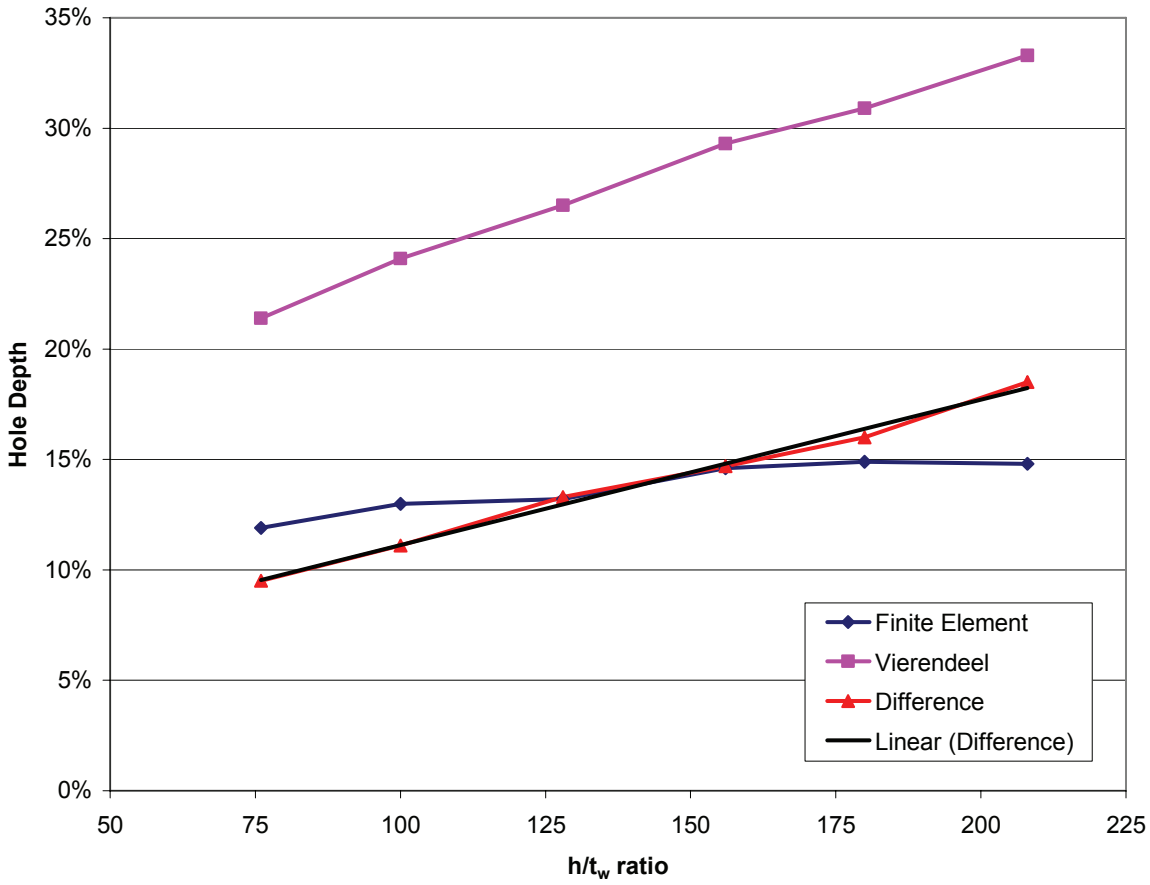

APPENDIX B: DIFFERENCE BETWEEN VIERENDEEL AND FINITE ELEMENT, BEAM THEORY AND FINITE ELEMENT MAXIMUM STRESSES AT INSIDE HOLE EDGE (SECTION 3.3.6)

Figure B1: Discrepancy Between Max Stress Predicted by Vierendeel and Finite Element, Inside Hole Edge, Second Girder Series (18"x1" flanges, 0.375" web)

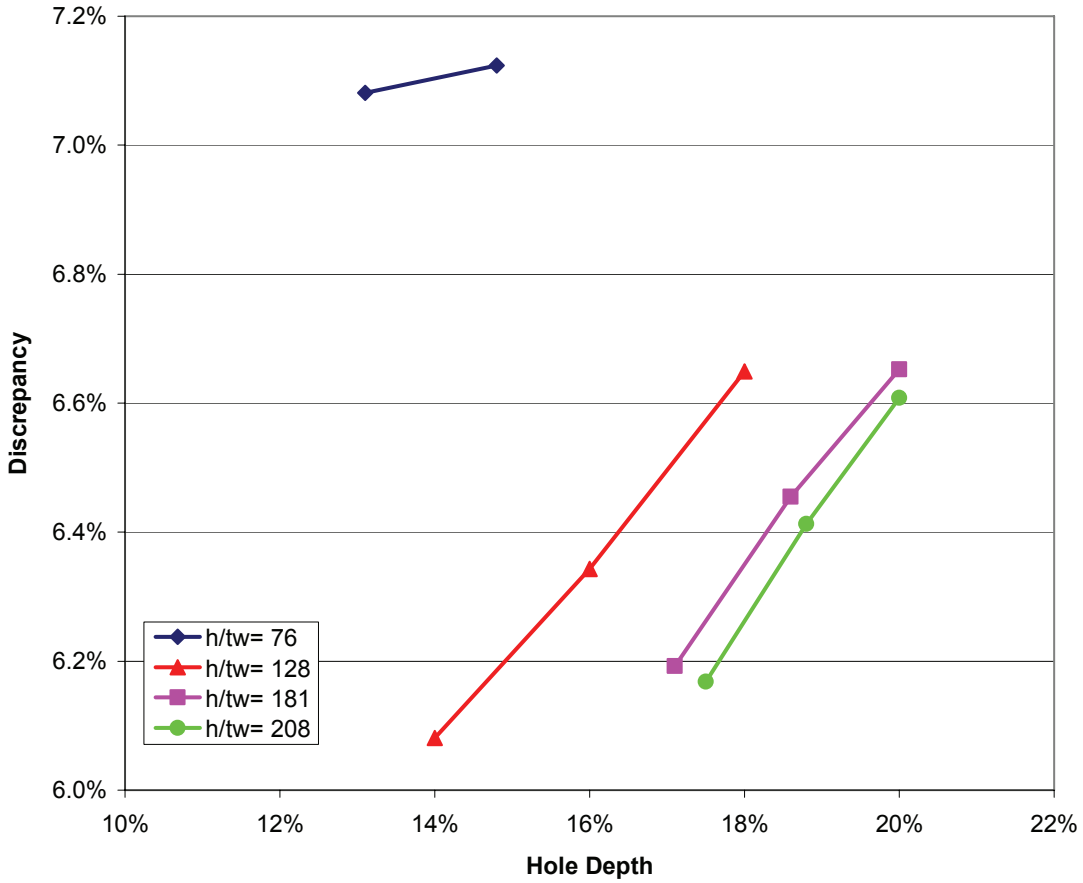

Figure B2: Discrepancy Between Max Stress Predicted by Beam Theory and Finite Element, Inside Hole Edge, Second Girder Series (18"x1" flanges, 0.375" web)

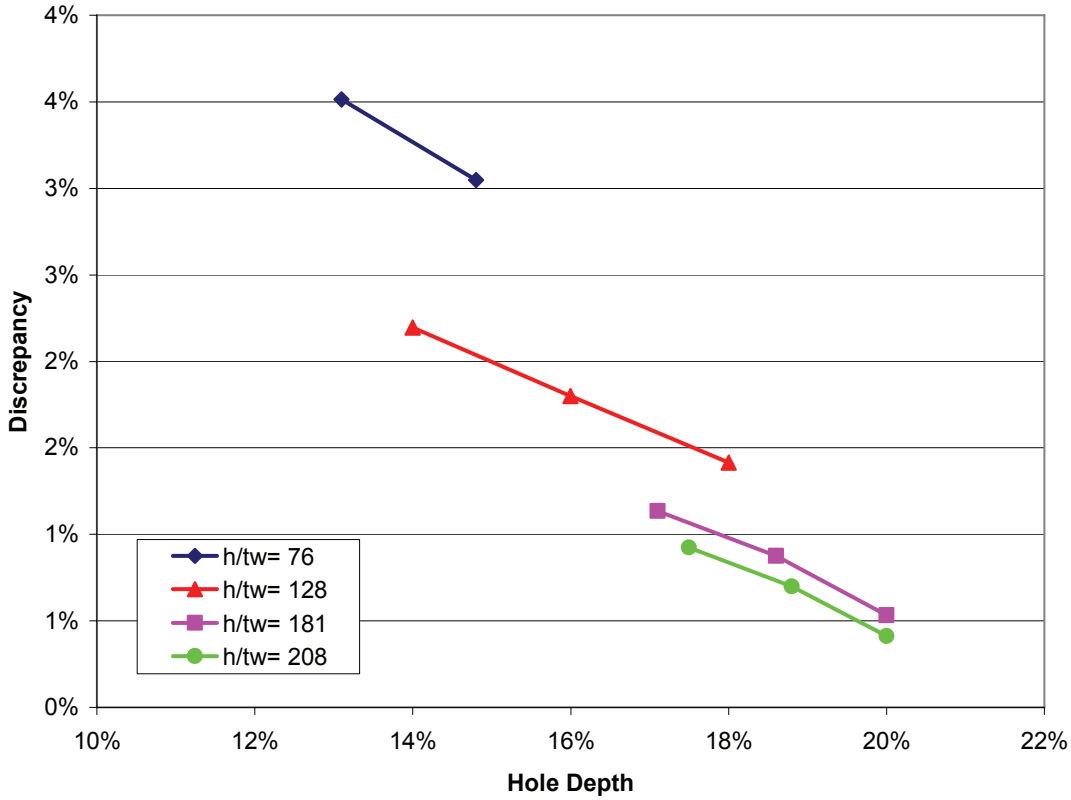

Figure B3: Discrepancy Between Max Stress Predicted by Vierendeel and Finite Element, Inside Hole Edge, Third Girder Series (14”x1” flanges, 0.25” web)

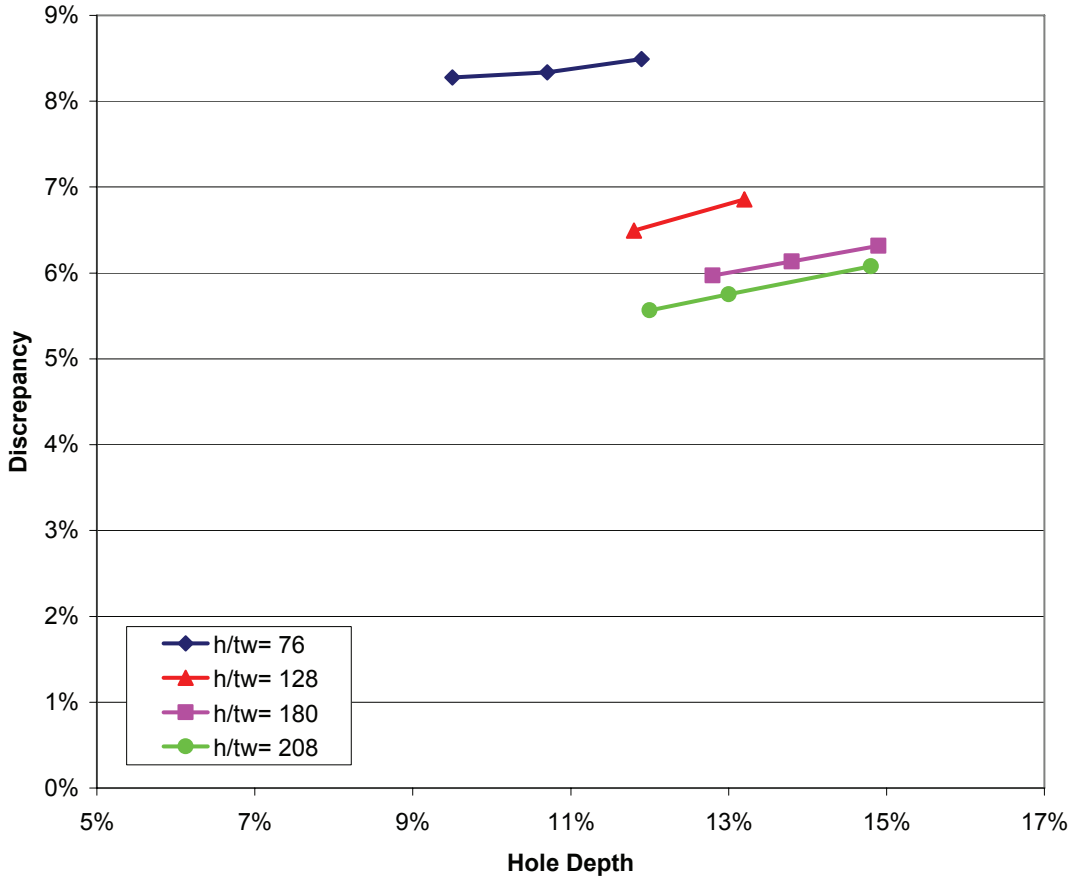

Figure B4: Discrepancy Between Max Stress Predicted by Beam Theory and Finite Element, Inside Hole Edge, Third Girder Series (14"x1" flanges, 0.25" web)

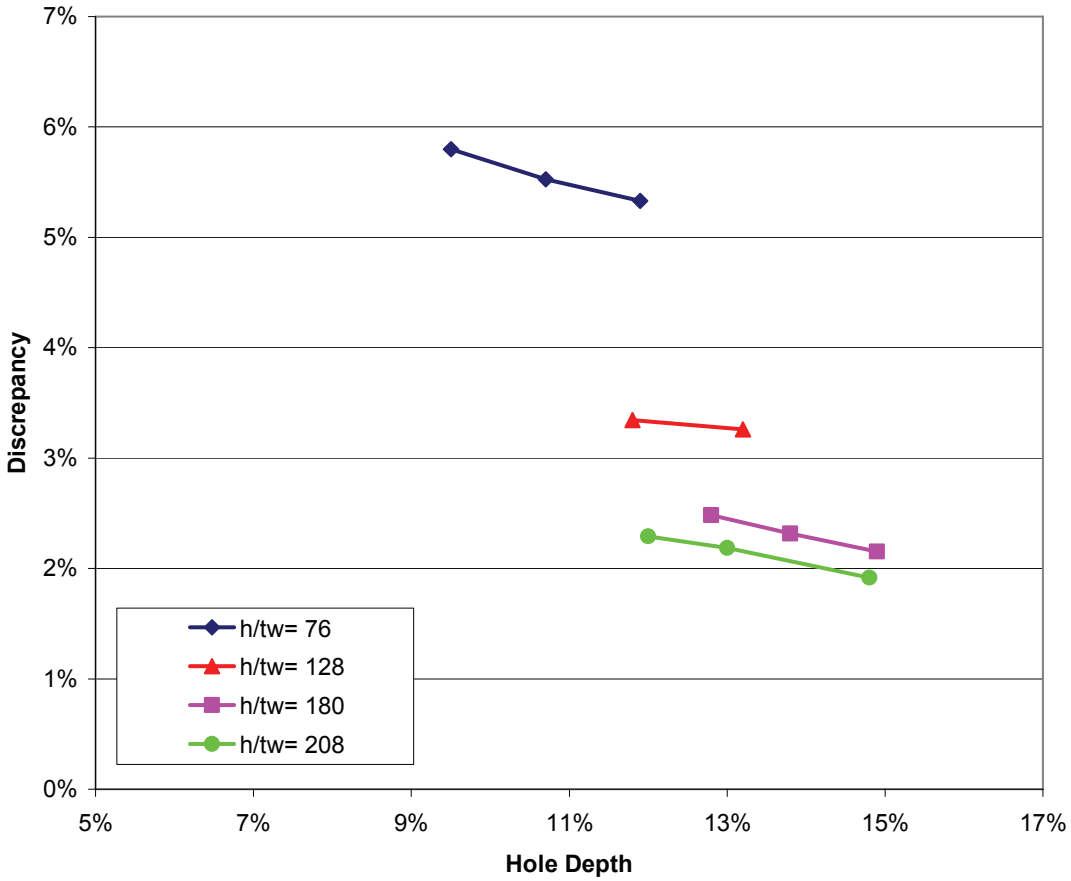

APPENDIX C: DIFFERENCE BETWEEN ABAQUS AND BEAM THEORY FLEXURAL STRESS PREDICTIONS AT INSIDE HOLE EDGE, NEXT TO HOLE

Figure C1: Difference Between Beam Theory and Finite Element Stresses, Second Girder Series (18"x1" Flanges, 0.375" Webs)

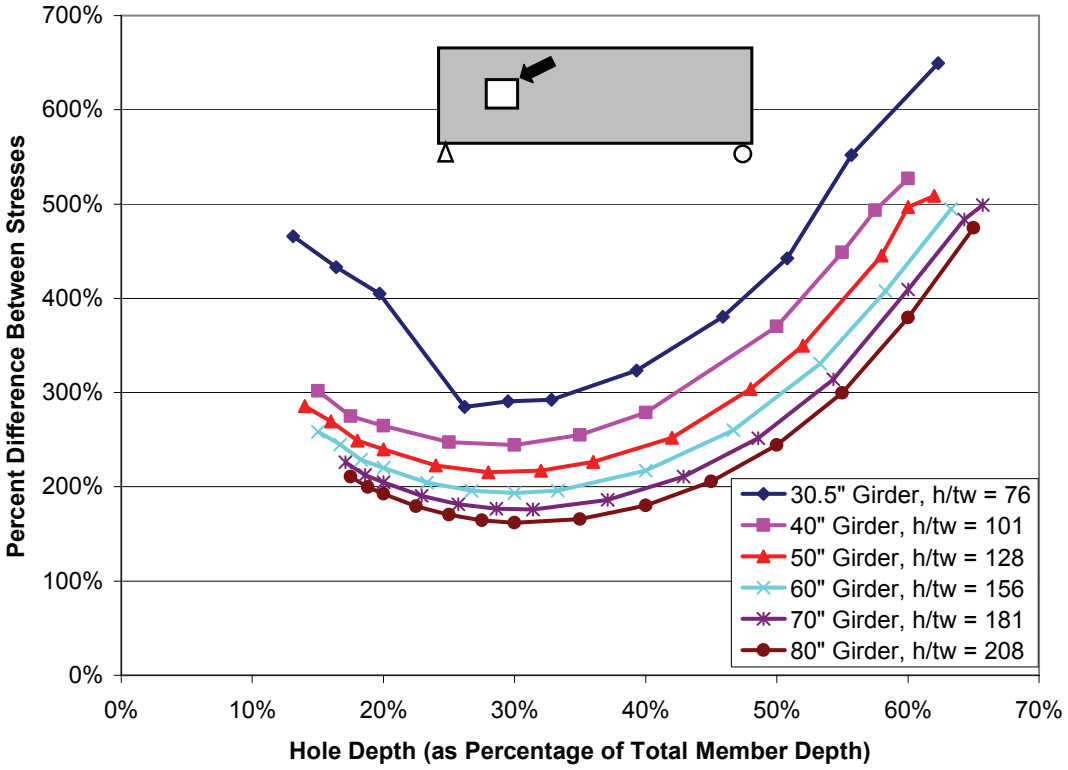

Figure C2: Difference Between Beam Theory and Finite Element Stresses, Third Girder Series (14”x1” Flanges, 0.25” Webs)

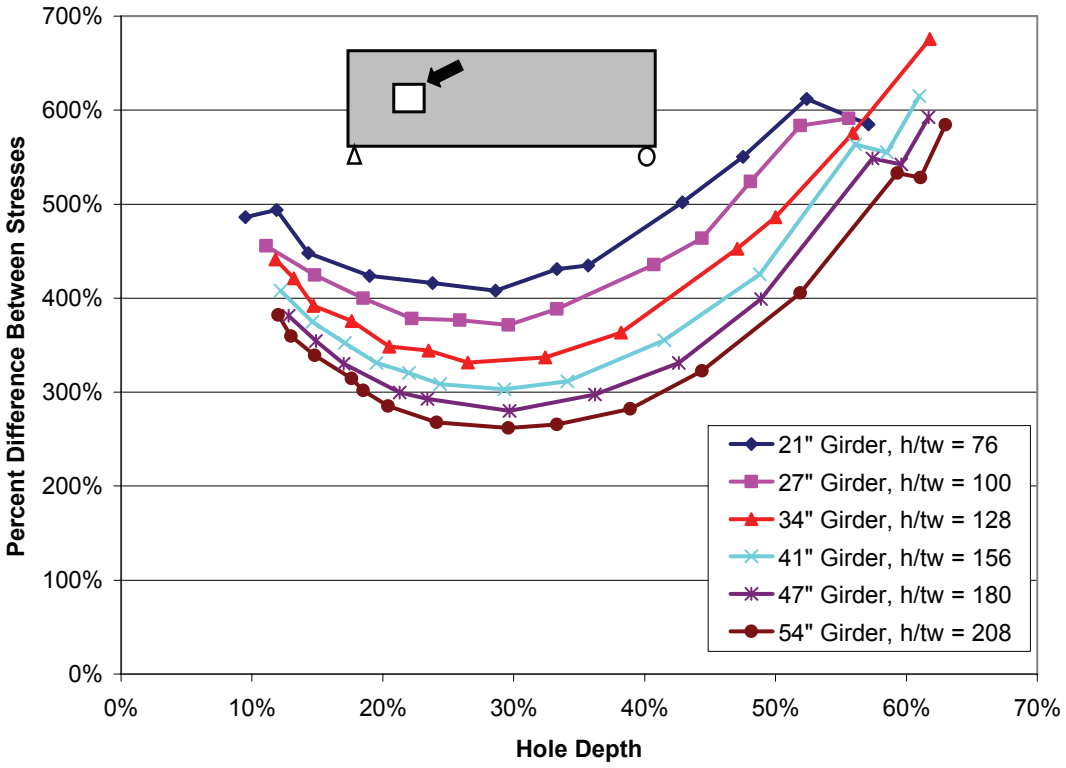

APPENDIX D: M_P LOSS VS. HOLE SIZE, BEAM SETS B AND C

Figure D1: Mp Loss for Beam Set B

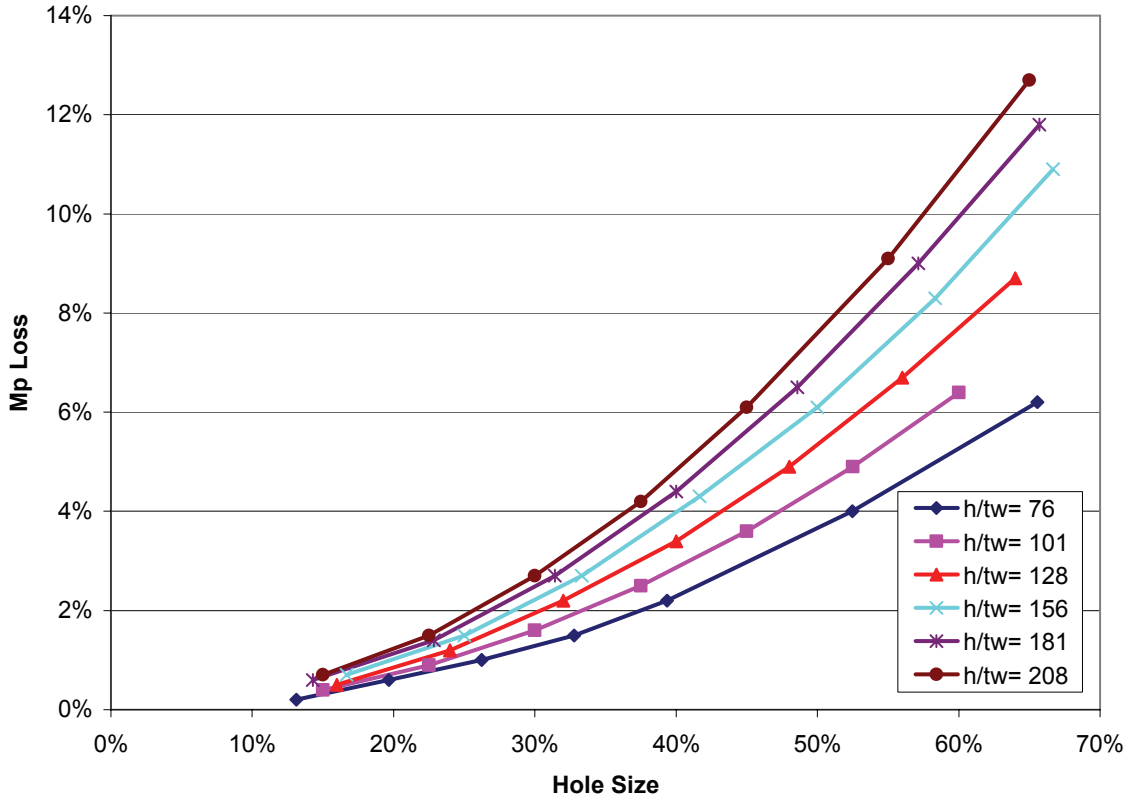

Figure D2: Mp Loss for Beam Set C

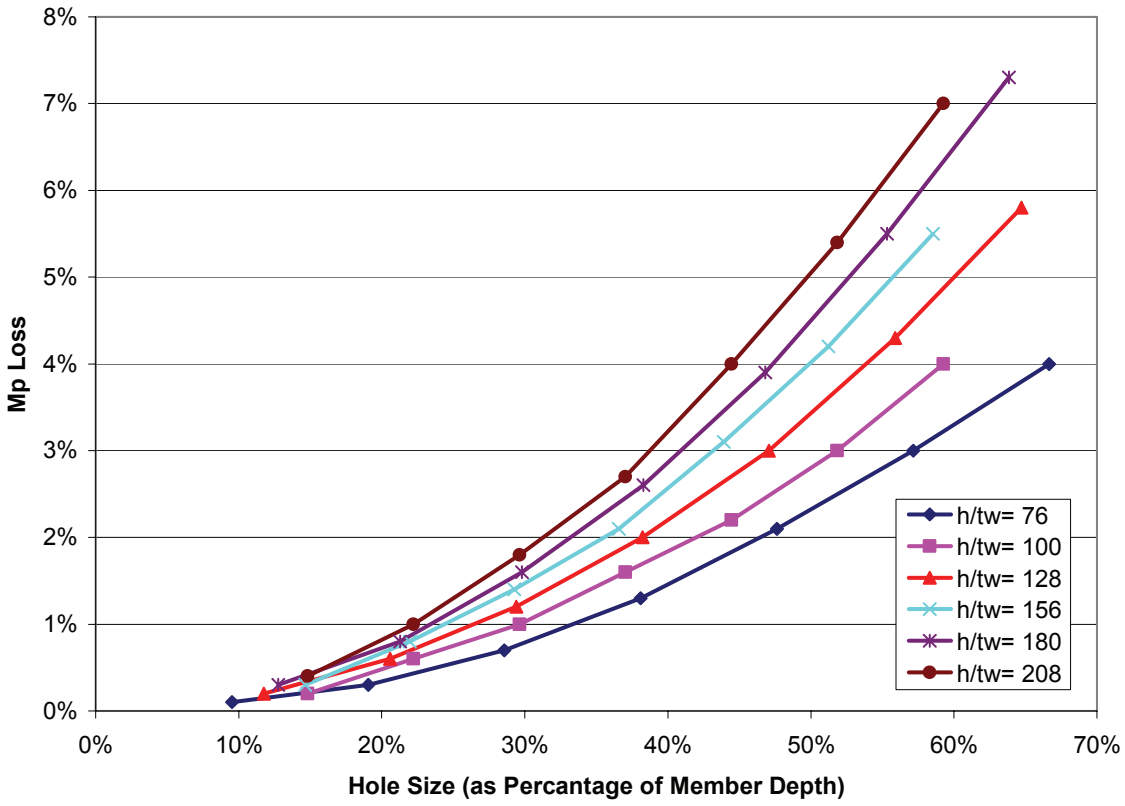

VITA

Aaron Michael Finley

Candidate for the Degree of

Master of Science

Thesis: EFFECTS OF CORROSION AND VEHICULAR IMPACT DAMAGE ON STRESS DISTRIBUTIONS IN STEEL BRIDGE BEAMS

Major Field: Civil Engineering

Biographical:

Personal Data: Born in Winfield, Kansas on August 25, 1981, the son of Rex and Nancy Finley. Married Chanda Hockersmith on July 23, 2005.

Education: Graduated from Winfield High School, Winfield, Kansas, in May 1999; received Bachelor of Science degree in Civil Engineering from Oklahoma State University, Stillwater, Oklahoma, in May 2004. Completed the requirements for the Master of Science degree with a major in Civil Engineering at Oklahoma State University in July, 2006.

Experience: Employed as carpenter during summers in high school; Field Engineer intern with Martin K. Eby Construction, summer 2002; Engineering intern with Kansas Department of Transportation, summer 2003; Engineering intern with Cobb Engineering, summer 2004; Employed by Oklahoma State University, Department of Civil Engineering as a graduate research assistant, 2004-2005.

Professional Memberships: American Society of Civil Engineers

Name: Aaron Finley Date of Degree: July, 2006

Institution: Oklahoma State University Location: Stillwater, Oklahoma

Title of Study: EFFECTS OF CORROSION AND VEHICULAR IMPACT DAMAGE ON ULTIMATE CAPACITY OF STEEL BRIDGE BEAMS

Pages in Study: 132 Candidate for the Degree of Master of Science

Major Field: Civil Engineering

Scope and Method of Study: The purpose of this study was to use finite element analysis to model steel bridge beams subjected to damage commonly associated with corrosion or vehicular impact. Advanced finite element analysis software was used to investigate the buckling capacity of beams with thinned flanges or with holes in the web. The software was also used to investigate flexural stress distributions in beams with holes in the web, the remaining capacity of beams which had geometric distortion as a result of vehicular impact, and flexural stress distributions in remaining bridge beams with one beam removed. Computer-generated flexural stress distributions were also compared to distributions generated by hand calculation methods.

Findings and Conclusions: Introducing web holes has no significant impact on the buckling capacity of beams. Web holes are more detrimental to ultimate moment capacity than they are to buckling capacity. However, there is a direct relationship between flange thinning and reduction in buckling capacity. Web holes cause significant changes in the flexural stress distribution through beams. The ability to predict the magnitude and location of maximum flexural stress depends on parameters such as hole size and h/t_w ratio of the beam. Depending on the value of these parameters, the maximum flexural stress may be predicted by traditional elastic beam theory or by the Vierendeel method. Preliminary tests showed that impact damage can reduce the yield capacity of beams by up to 20% and the post-buckling capacity by up to 35%. Preliminary tests also showed that in a standard four-girder bridge, it may be possible to remove an exterior beam from service while allowing one lane of traffic on the opposite side of the bridge without dangerously elevating flexural stress levels.

ADVISOR'S APPROVAL: Dr. Charles M. Bowen